



**TAINÁH MARTINS RESENDE SANTOS**

**EMPREGO DE COMPLEXOS DE VANÁDIO PARA  
MANIPULAR A AUTOFAGIA: CÁLCULOS QUÂNTICOS E  
DESENVOLVIMENTO DE PARÂMETROS DE CAMPO DE  
FORÇA**

**LAVRAS – MG  
2023**

**TAINÁH MARTINS RESENDE SANTOS**

**EMPREGO DE COMPLEXOS DE VANÁDIO PARA MANIPULAR A AUTOFAGIA:  
CÁLCULOS QUÂNTICOS E DESENVOLVIMENTO DE PARÂMETROS DE CAMPO  
DE FORÇA**

Tese apresentada à Universidade Federal de Lavras, como parte das exigências do Programa de Pós-Graduação em Agroquímica, área de concentração em Química Computacional, para a obtenção do título de Doutora.

Prof. Dr. Teodorico de Castro Ramalho  
Orientador  
Profa. Dra. Elaine Fontes Ferreira da Cunha  
Corientadora

**LAVRAS – MG  
2023**

**Ficha catalográfica elaborada pelo Sistema de Geração de Ficha Catalográfica da Biblioteca Universitária da UFLA, com dados informados pelo(a) próprio(a) autor(a).**

Santos, Taináh Martins Resende.

Emprego de complexos de vanádio para manipular a autofagia: cálculos quânticos e desenvolvimento de parâmetros de campo de força / Taináh Martins Resende Santos. - 2023.

166 p. : il.

Orientador(a): Teodorico de Castro Ramalho.

Coorientador(a): Elaine Fontes Ferreira da Cunha.

Tese (doutorado) - Universidade Federal de Lavras, 2023.

Bibliografia.

1. Complexos de vanádio. 2. Campo de força AMBER. 3. Autofagia. I. Ramalho, Teodorico de Castro. II. da Cunha, Elaine Fontes Ferreira. III. Título.

**TAINÁH MARTINS RESENDE SANTOS**

**EMPREGO DE COMPLEXOS DE VANÁDIO PARA MANIPULAR A AUTOFAGIA:  
CÁLCULOS QUÂNTICOS E DESENVOLVIMENTO DE PARÂMETROS DE CAMPO  
DE FORÇA**

**USING OF VANADIUM COMPLEXES TO MANIPULATE AUTOPHAGY:  
QUANTUM CALCULATIONS AND DEVELOPMENT OF FORCE FIELD  
PARAMETERS**

Tese apresentada à Universidade Federal de Lavras,  
como parte das exigências do Programa de Pós-  
Graduação em Agroquímica, área de concentração em  
Química Computacional, para a obtenção do título de  
Doutora.

APROVADA em 16 de fevereiro de 2023.

Prof. Dr. Gerd Bruno da Rocha – UFPB

Prof. Dr. Willian Ricardo Rocha – UFMG

Profa. Dra. Paula Homem-de-Mello – UFABC

Prof. Dr. Luciano Tavares da Costa – UFF



Prof. Dr. Teodorico de Castro Ramalho  
Orientador  
Profa. Dra. Elaine Fontes Ferreira da Cunha  
Corientadora

**LAVRAS – MG  
2023**

*À minha família, por ter batalhado junto a mim todos os dias.*

*A vocês, Papai, Mamãe e Irmão, todo meu amor e eterna gratidão!*

DEDICO.

## **AGRADECIMENTOS**

À Deus e à Nossa Senhora Aparecida, pelo dom da vida e do saber.

Ao meu pai, Sebastião Martins Santos, por nunca medir esforços para cada pedido meu e sempre acreditar no meu potencial. Seus esforços não foram em vão, eis aqui mais uma das provas.

À minha mãe, Aparecida Assunção Resende, pelas orações diárias e por toda força que sempre me passou. Pelas broncas, ensinamentos e carinhos que a cada dia me apresentava de forma diferente. A mulher que me tornei é, com certeza, espelho seu.

Ao meu irmão, Luiz Fernando Resende Santos, pelo apoio de sempre, por servir como exemplo em inúmeras ocasiões e por todo regalo.

À vó Nini (*in memoriam*), pelas suas incansáveis rezas pelas milhares de provas, tanto da faculdade quanto da vida. Obrigada por todo ensinamento. Minha eterna saudade!

Ao meu tio Eustáquio (*in memoriam*), pelo companheirismo de sempre e por nunca ter medido esforços para nos ajudar. O senhor foi nota mil. Saudade grande!

A todos os meus tios, primos e amigos, pelo companheirismo e pela força de sempre.

Aos meus amigos de Oliveira, Alfenas e Lavras, sem vocês eu certamente não conseguiria.

À minha amiga e companheira de laboratório, Camila Assis Tavares, por sempre me ajudar sem nunca hesitar, por toda paciência e, principalmente, pelos bons momentos compartilhados durante o Mestrado e Doutorado.

Ao meu orientador, Prof. Dr. Teodorico de Castro Ramalho, pela paciência, excelente orientação e as belas discussões sobre Ciência. O senhor é, certamente, um grande exemplo de pessoa e cientista!

À minha coorientadora, Profa. Elaine Fontes Ferreira da Cunha, por toda parceria durante o Doutorado, paciência, gentileza e atenção nos momentos que precisei.

Agradeço aos membros da banca, os Professores Gerd, Willian, Paula e Luciano, por terem aceitado com satisfação participar deste momento tão importante na minha carreira acadêmica/científica e, também, por colaborarem com este trabalho.

À agência de fomento pelo auxílio financeiro durante a pesquisa. O presente trabalho foi realizado com apoio da Coordenação de Aperfeiçoamento de Pessoal de Nível Superior – Brasil (CAPES) – Código de Financiamento 001.

À Universidade Federal de Lavras (UFLA) e aos professores que tive ao longo da minha formação.

A todos os professores que tive ao longo da vida, principalmente aqueles que me inspiraram e continuam me inspirando para um dia, quem sabe, me tornar uma excelente professora como eles.

A todos que, direta ou indiretamente, contribuem para que o meu amor pela Ciência continue se engrandecendo. A cada dia que passa tenho mais orgulho de fazer parte de uma comunidade científica que busca fazer uma Ciência boa e de qualidade. Felizmente, tenho muitos exemplos a seguir.

A todos, agradeço de coração!

*“Some things are simple but hard to do.”*

*(Albert Einstein)*

## RESUMO

A modulação da autofagia tem se apresentado como uma estratégia muito útil no combate ao câncer. Nesse sentido, sabe-se que complexos de vanádio (CV) são capazes tanto de inibir quanto de induzir a autofagia em células cancerosas. Neste trabalho, foram utilizados dois complexos de vanádio. O primeiro, [VO(oda)(phen)], possui comprovada eficiência em inibir a autofagia em células do câncer de pâncreas. Já o segundo, [VO(bpy)<sub>2</sub>Cl], é conhecido por possuir a capacidade de induzir a autofagia em células do câncer de mama triplo-negativo. Neste contexto, simulações de Dinâmica Molecular (DM) são excelentes estratégias para investigar a interação de complexos metálicos e seus alvos biológicos. Entretanto, simulações desse tipo são fortemente dependentes da escolha adequada do campo de força (FF, do inglês *Force Field*). FFs gerais não são eficientes para descrever as propriedades de complexos metálicos. Além disso, ainda não foram relatados na literatura FFs específicos para os CVs, alvos deste estudo. Sendo assim, esta tese apresenta uma investigação dividida em três partes: desenvolvimento, validação e aplicação. Portanto, inicialmente é proposto o desenvolvimento de parâmetros de FF AMBER para os dois CVs, a partir de uma estrutura de mínima energia, obtida por cálculos de DFT com nível de teoria B3LYP/def2-TZVP mais ECP para o átomo de vanádio. A partir da geometria otimizada, os cálculos da matriz hessiana e das cargas RESP foram realizados para fornecer as cargas de cada átomo, as constantes de força e os valores de equilíbrio. Os parâmetros de Lennard-Jones para todos os átomos, exceto para o vanádio, foram atribuídos de acordo com o GAFF. Simulações de DM no vácuo foram realizadas para validar os FFs desenvolvidos. A partir de análises estruturais, foi possível encontrar valores com apreciáveis acordos entre os dados experimentais e a referência quântica. A partir dos FFs desenvolvidos e validados, foi possível investigar as interações entre os CVs e as proteínas PI3K e ULK1, cruciais para o maquinário autofágico. Análises de RMSD, ligações de hidrogênio e RMSF foram realizadas. Além disso, apresentamos como os CVs agem para inibir/induzir a autofagia e sugerimos como seria possível modificar as atuações dos complexos para que a modulação da autofagia ocorra. Em linhas gerais, nossos achados encorajam novas parametrizações de complexos metálicos com significativas importâncias biológicas, bem como permitem contribuir para a elucidação do complexo processo de autofagia.

**Palavras-chave:** Autofagia. Modulação. Complexos de Vanádio. Campo de Força AMBER. Dinâmica Molecular.

## ABSTRACT

The modulation of autophagy has been presented as a very useful strategy in anticancer treatments. In this sense, it is known that vanadium complexes (VCs) are capable of both inhibiting and inducing autophagy in cancer cells. In this work, two vanadium complexes were used. The first compound, [VO(oda)(phen)], has proven efficiency in inhibiting autophagy in pancreatic cancer cells. The second, [VO(bpy)<sub>2</sub>Cl], is known for having the ability to induce autophagy in triple-negative breast cancer cells. In this context, Molecular Dynamics (MD) simulations are excellent strategies to investigate the interaction between metallic complexes and their biological targets. However, simulations of this type are heavily dependent on the proper choice of the force field (FF). General FFs are not efficient to describe the properties of metallic complexes. Furthermore, specific FFs for the VCs targeted by this study have not yet been reported in the literature. That way, this thesis presents an investigation divided into three parts: development, validation, and application. Therefore, initially it is proposed the development of AMBER FF parameters for the two VCs, from a minimum energy structure, obtained by DFT calculations using B3LYP/def2-TZVP level of theory plus ECP for the vanadium atom. From the optimized geometry, the calculations of the Hessian matrix and the RESP charges were performed to provide the charges of each atom, the force constants and the equilibrium values. Lennard-Jones parameters for all atoms except vanadium were assigned according to GAFF. Vacuum MD simulations were performed to validate the developed FFs. Structural analyses allowed to find values with appreciable agreements between the experimental data and the quantum reference. From the developed and validated FFs, it was possible to investigate the interactions between the VCs and the PI3K and ULK1 proteins, crucial for the autophagic machinery. RMSD, hydrogen bonds, and RMSF analyses were performed. In addition, we present how the VCs act to inhibit/induce autophagy and suggest how it would be possible to modify the actions of the complexes so that autophagy modulation occurs. From a general perspective, our findings encourage new parameterizations of metallic complexes with significant biological importance, as well as allow to contribute to the elucidation of the complex process of autophagy.

**Keywords:** Autophagy. Modulation. Vanadium Complexes. AMBER Force Field. Molecular Dynamics.

## SUMÁRIO

<b>PARTE I .....</b>	<b>13</b>
<b>1. INTRODUÇÃO E JUSTIFICATIVA.....</b>	<b>14</b>
<b>2. OBJETIVOS.....</b>	<b>17</b>
<b>2.1. Objetivo geral .....</b>	<b>17</b>
<b>2.2. Objetivos específicos .....</b>	<b>17</b>
<b>3. REFERENCIAL TEÓRICO .....</b>	<b>18</b>
<b>3.1. Câncer .....</b>	<b>18</b>
3.1.1. Câncer de Mama Triplo-Negativo .....	19
3.1.2. Câncer de Pâncreas .....	20
<b>3.2. Autofagia .....</b>	<b>21</b>
3.2.1. A manipulação da autofagia no tratamento do câncer .....	22
<b>3.3. Complexos de Vanádio .....</b>	<b>25</b>
3.3.1. Complexos de vanádio em manipulações de autofagia e câncer .....	26
<b>3.4. Abordagem Teórica .....</b>	<b>28</b>
3.4.1. Métodos teóricos fundamentados em Mecânica Molecular.....	28
3.4.1.1. <i>Dinâmica Molecular Clássica</i> .....	29
3.4.1.2. <i>Campos de força</i> .....	31
3.4.1.3. <i>Docking</i> .....	35
3.4.2. Métodos teóricos fundamentados em Mecânica Quântica .....	36
3.4.2.1. <i>A Teoria do Funcional de Densidade</i> .....	37

<b>REFERÊNCIAS.....</b>	40
<b>PARTE II .....</b>	46
<b>ARTIGO 1.....</b>	47
<b>Evaluation of autophagy inhibition to combat cancer: (vanadium complex)–protein interactions, parameterization, and validation of a new force field .....</b>	47
<b>ARTIGO 2.....</b>	109
<b>Vanadium complex as a potential modulator of the autophagic mechanism through proteins PI3K and ULK1: development, validation and biological implications of a specific force field for [VO(bpy)<sub>2</sub>Cl] .....</b>	109
<b>ANEXO .....</b>	164

## **PARTE I**

## 1. INTRODUÇÃO E JUSTIFICATIVA

Segundo estimativa mais recente, o câncer matou quase 10,0 milhões de pessoas no ano de 2020 e houve cerca de 19,3 milhões de novos casos em todo o mundo. Além disso, estima-se que até o ano de 2040, a carga global de câncer deve atingir cerca de 28,4 milhões de casos, resultando em um aumento de 47% em relação ao ano de 2020. A partir desses dados, fica evidente a necessidade de alcançar melhores formas de tratamento e a cura desta doença (SUNG *et al.*, 2021).

Dentre os vários tipos de cânceres existentes, o câncer de mama e o câncer de pâncreas apresentam estimativas preocupantes (INCA, 2021). No que diz respeito ao câncer de mama, pode-se ainda destacar, dentre os quatro subtipos desse câncer, o subtipo conhecido como câncer de mama triplo-negativo (USCANGAPERALES; SANTUÁRIO-FACIO; ORTIZ-LÓPEZ, 2016).

A quimioterapia é o tratamento mais utilizados nesses tipos de cânceres. Entretanto, sabe-se que a quimioterapia afeta, além das células cancerosas, as células saudáveis do corpo, acarretando efeitos colaterais indesejáveis, assim como uma queda na qualidade de vida do paciente (MBUGUA *et al.*, 2020).

Nesse sentido, o fato de tanto o câncer de mama triplo-negativo quanto o câncer de pâncreas não apresentarem uma forma de tratamento específica, torna-se extremamente relevante a busca por terapias que sejam cada vez mais direcionadas para cada tipo de câncer de forma específica (PEDDI; ELLIS; MA, 2012; CAO *et al.*, 2019; CONROY *et al.*, 2011; HOSEIN; BREKKEN; MAITRA, 2020).

Diante deste cenário, a autofagia tem se mostrado como um campo crescente na ciência, principalmente por ter sido recentemente destacada pelo reconhecimento das contribuições do Dr. Yoshinori Ohsumi, ganhador do prêmio Nobel de Medicina ou Fisiologia em 2016 (LEVINE; KLIONSKY, 2017).

A autofagia consiste em um mecanismo conservativo de reciclagem celular, onde materiais como organelas danificadas, proteínas malformadas etc., são levadas ao lisossomo para que a degradação dos materiais danificados ocorra (DIKIC; ELAZAR, 2018). A via de sinalização da autofagia é composta pelas proteínas PI3K/Akt/mTOR (KONDO *et al.*, 2005).

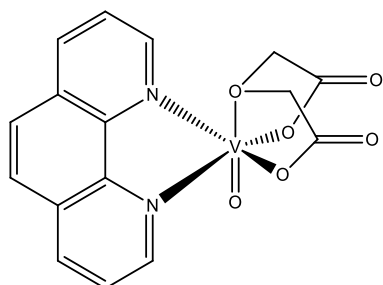
Após ocorrer a sinalização, a proteína responsável por fazer com que a autofagia ocorra é a proteína ULK1 (KALEAĞASIOĞLU; ALI; BERGER, 2020).

A autofagia possui consideráveis vantagens em comparação à quimioterapia. Uma dessas vantagens é o fato de a autofagia atuar diretamente nas células doentes, como sugere sua própria definição, o que difere da quimioterapia que afeta também células saudáveis (MBUGUA *et al.*, 2020). Outra vantagem consiste no fato dos processos autofágicos poderem atuar nas diferentes etapas no avanço do câncer, pois, como se sabe, o tratamento anticâncer depende de muitos fatores, dentre eles, o estágio da doença. Nesse sentido, a modulação da autofagia, ou seja, a inibição ou indução, pode ser vista como uma nova possibilidade de tratamento contra o câncer (KOCAK *et al.*, 2021).

É importante salientar que, a autofagia é um processo que ocorre de forma natural no corpo a partir de, por exemplo, falta de nutrientes, infecção por patógenos e outros estresses ambientais. Nesse sentido, a partir da possibilidade de manipulação da autofagia é que se torna possível obter melhores formas de tratamento. Em outras palavras, manipular a autofagia, ora induzindo-a, ora inibindo-a, pode favorecer diversos tratamentos anticâncer (MISHRA; AMMANATHAN; MANJITHAYA, 2018).

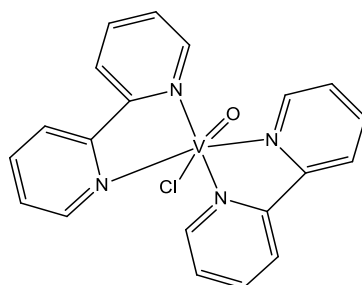
Neste contexto, complexos de vanádio se destacam por serem capazes tanto de induzir processos de autofagia quanto de inibir (EL-SHAFETY; ELSHERBINY, 2019; SUTRADHAR *et al.*, 2019; KOWALSKI *et al.*, 2019; HUANG *et al.*, 2018; KOWALSKI *et al.*, 2017; MACHADO *et al.*, 2017; WALKER *et al.*, 2012; WU *et al.*, 2014). Neste trabalho, foram utilizados dois complexos de vanádio que possuem comprovada eficiência em inibir o processo autofágico em células do câncer de pâncreas (Figura 1.1), além de induzir autofagia em células do câncer de mama triplo-negativo (Figura 1.2).

**Figura 1.1** – Complexo de vanádio 1 (CV1),  
[VO(oda)(phen)].



Fonte: KOWALSKI *et al.*, 2017.

**Figura 1.2** – Complexo de vanádio 2 (CV2),  
[VO(byp)<sub>2</sub>Cl].



Fonte: EL-SHAFETY; ELSHERBINY, 2019.

A atuação de complexos de vanádio em tratamentos anticâncer, por intermédio de processos autofágicos, mostra, por si só, a evidente relevância deste tipo de estudo. Dessa forma, entender como ocorre a indução/inibição da autofagia a nível molecular, isto é, quais as interações entre os alvos moleculares e os complexos de vanádio, pode ser entendido como um estudo que fornece importantes contribuições para área. Nesse sentido, simulações de *Docking* e de Dinâmica Molecular Clássica (DM) podem auxiliar neste tipo de investigação.

Levando em consideração o âmbito teórico deste trabalho, é de extrema importância que os cálculos aqui desenvolvidos sejam executados da maneira mais eficiente possível. Diante disso, para que sejam obtidos resultados satisfatórios, é preciso que o campo de força utilizado nas simulações de DM seja eficiente para descrever os complexos de vanádio.

Sabe-se que parâmetros de campos de força para compostos inorgânicos são escassos e muitas vezes não estão representados por campos de força padrão. Além disso, campos de força gerais apresentam um número reduzido de tipos atômicos, impossibilitando a descrição de um número variado de compostos (LOPES *et al.*, 2006).

No que diz respeito à parametrização de complexos de vanádio, ainda não foi relatado na literatura o desenvolvimento de parâmetros de campos de força específicos para esses tipos de compostos. Além disso, fazer uso de um campo de força geral pode não fornecer resultados satisfatórios, além de resultar em estruturas não realistas (PRANDI *et al.*, 2016; TAVARES *et al.*, 2023). Diante disso, fica evidente a necessidade de desenvolver parâmetros de campos de força específicos para os complexos de vanádios, alvos deste estudo.

A partir do exposto, o objetivo deste trabalho consistiu no desenvolvimento e validação de parâmetros de campo de força (FF) AMBER específicos para cada um dos dois complexos de vanádio (Figura 1.1 e Figura 1.2). Na sequência, este trabalho buscou o entendimento, através de docking e DM, de quais as interações presentes entre os complexos de vanádio e as proteínas PI3K (responsável por iniciar a via de sinalização) e ULK1 (responsável por ativar ou não a autofagia).

Neste estudo, o FF desenvolvido tratou-se do campo de força AMBER, para ser, posteriormente, utilizado no software de mesmo nome (AMBER). Este interesse fundamenta-se no fato de que a metodologia para a parametrização de um FF AMBER já é conhecida e bem clara (PEREIRA, 2020; PRANDI *et al.*, 2016), permitindo a replicação em diversos outros

complexos metálicos, e, além disso, o FF AMBER também é conhecido por sua eficiência com biomoléculas (CORNELL *et al.*, 1995).

## 2. OBJETIVOS

### 2.1. Objetivo geral

O objetivo geral do trabalho consistiu no desenvolvimento e validação de parâmetros de campo de força AMBER para dois complexos de vanádio, [VO(oda)(phen)] (CV1) e [VO(byp)<sub>2</sub>Cl] (CV2), partindo de uma estrutura minimizada com mecânica quântica (DFT). Além disso, este trabalho investigou as interações entre os complexos de vanádio e importantes alvos moleculares do mecanismo autófágico, isto é, as proteínas PI3K e ULK1.

### 2.2. Objetivos específicos

Para que o objetivo geral fosse alcançado, algumas etapas foram realizadas, a saber:

1. Desenvolvimento do FF AMBER para o complexo CV1;
2. Validação da parametrização realizada para o CV1;
3. Simulação de docking entre CV1 e a proteína PI3K;
4. Simulação de DM entre CV1 e a proteína PI3K;
5. Análise e interpretação dos dados obtidos a partir das etapas anteriores (1-4);
6. Desenvolvimento do FF AMBER para o complexo CV2;
7. Validação da parametrização realizada para o complexo CV2;
8. Simulação de docking entre CV2 e a proteína PI3K;
9. Simulação de docking entre CV2 e a proteína ULK1;
10. Simulação de DM entre CV2 e a proteína PI3K;
11. Simulação de DM entre CV2 e a proteína ULK1;
12. Análise e interpretação dos dados obtidos a partir das etapas anteriores (6-11).

### 3. REFERENCIAL TEÓRICO

#### 3.1. Câncer

Segundo a Organização Mundial da Saúde (2021), câncer trata-se de um termo genérico para doenças nas quais células anormais se dividem sem controle e podem afetar qualquer parte do corpo humano. A maioria dos tipos de células cancerígenas forma um nódulo ou massa chamada *tumor*. No entanto, nem todos os tumores são cânceres. Um tumor que não é câncer é chamado de *benigno*, já um tumor cancerígeno é chamado de *maligno*. O processo em que as células anormais se espalham para outros órgãos é chamado de metástase. Essa, por sua vez, é uma das principais causas de mortes por câncer (WHO, 2021).

O câncer é considerado um grande problema de saúde pública em todo o mundo e se encontra entre as principais causas de mortes prematuras na maioria dos países, isto é, mortes antes dos 70 anos de idade. As causas de aumentos constantes de casos podem ser atribuídas, em partes, ao sedentarismo, alimentação inadequada, má qualidade de vida, dentre outras causas (BRAY *et al.*, 2018).

A mais recente estimativa mundial, ano 2020, aponta que ocorreram no mundo cerca de 19,3 milhões de novos casos e quase 10,0 milhões de óbitos por câncer (SUNG *et al.*, 2021). No Brasil, foi realizado um estudo pelo Instituto Nacional de Câncer José Alencar Gomes da Silva (INCA), que apresenta a estimativa para cada ano do triênio 2020-2022, apontando que ocorrerão cerca de 625 mil novos casos de câncer no país (INCA, 2019).

Existem muitos tipos de câncer, onde cada um se denomina a partir de sua origem. Alguns deles são: câncer de pulmão; câncer de mama; câncer de próstata; câncer de pâncreas; câncer de estômago; câncer de fígado; dentre outros (WHO, 2021).

O câncer de mama é uma doença que afeta, principalmente, as mulheres e é caracterizado por vários subtipos. Devido a isso, a doença pode evoluir de diferentes maneiras, o que dificulta as formas de tratamento (INCA, 2021). Além disso, outro tipo de câncer, o câncer de pâncreas, também possui uma forma difícil de detecção, além de um comportamento agressivo. Nesse sentido, o câncer de pâncreas apresenta alta taxa de mortalidade, devido, principalmente, ao diagnóstico tardio (INCA, 2021).

### 3.1.1. Câncer de Mama Triplo-Negativo

O câncer é uma das doenças mais temidas em todo o mundo. Ele não se caracteriza como uma única doença e, sim, como um conjunto de diversas enfermidades que tem ações diferentes, localizações diferentes e tratamentos diferentes. O câncer de mama é um bom exemplo dessa diferença, pois ele ainda se divide em quatro subtipos: os cânceres luminais A e B, o câncer HER2 positivo e o triplo-negativo (USCANGA-PERALES; SANTUÁRIO-FACIO; ORTIZ-LÓPEZ, 2016).

O câncer de mama é considerado a principal causa de morte relacionada a neoplasias em mulheres. Estima-se cerca de 2,3 milhões de novos casos de câncer de mama feminino, que corresponde a 11,7% dos casos de câncer em todo o mundo, e quase de 685 mil óbitos no ano de 2020, correspondendo a 6,9% das mortes relacionadas ao câncer no mundo todo. Além disso, um número que se aproxima de 15% a 20% do total de pacientes com câncer de mama pode ser classificado como triplo-negativos (SUNG *et al.*, 2021; LEE *et al.*, 2019).

Sabe-se que, no procedimento para diagnóstico de câncer de mama, é necessário avaliar se a doença apresenta três biomarcadores (proteínas), isto é, três moléculas conhecidas como receptor de estrogênio, receptor de progesterona e receptor HER2. Nenhum desses três receptores estão presentes neste tipo de câncer de mama, por isso é chamado de “câncer de mama triplo-negativo” (TNBC, do inglês *Triple-Negative Breast Cancer*) (KALIMUTHO *et al.*, 2015).

Diante disso, os remédios desenvolvidos para tratar o câncer de mama têm como alvo esses três receptores (estrogênio, progesterona e HER2), sendo o câncer de mama triplo-negativo dando negativo para a presença dessas três moléculas, qualquer tratamento com os remédios já desenvolvidos seria ineficaz (CAO *et al.*, 2019).

Neste cenário, esse subtipo de câncer de mama que, em geral, se forma nas células dos ductos por onde passa o leite materno, possui uma alta taxa de mortalidade, visto que ainda não se dispõe de uma terapia-alvo, isto é, ainda não foi desenvolvido um tratamento específico e direcionado para esse tipo de câncer. Como a quimioterapia age atacando as células que se dividem rapidamente, ela é o tratamento mais efetivo nesta doença (PEDDI; ELLIS; MA, 2012; CAO *et al.*, 2019).

### 3.1.2. Câncer de Pâncreas

O câncer de pâncreas, também conhecido como adenocarcinoma ductal pancreático (PDAC), está entre os cânceres mais letais devido à natureza agressiva do tumor, diagnóstico tardio e efeitos terapêuticos limitados por quimioterapia. As razões para o mau prognóstico se atribuem, também, à falta de triagem, à alta probabilidade de doença metastática oculta, à falta de sintomas precoces e à falta de estratégias eficazes de rastreamento (KLEEFF *et al.*, 2016; CHIARAVALLI; RENI; O'REILLY, 2017; TULI *et al.*, 2020).

Os sintomas do câncer de pâncreas são, geralmente, inespecíficos, o que dificulta a detecção da doença, além de conduzir os pacientes a descobrirem a doença já em estágios avançados. A quimioterapia citotóxica, neste tipo de câncer, é o tratamento mais convencional considerando casos avançados ou metastáticos do PDAC, além de fornecer apenas meses de sobrevida em geral (VON HOFF *et al.*, 2013; HO; JAFFEE; ZHENG, 2020).

Estima-se que, no ano de 2020, foram realizados cerca de 496 mil diagnósticos de câncer de pâncreas, que corresponde a 2,6% dos casos de câncer em todo o mundo. Além disso, aproximadamente 466 mil mortes foram relatadas, totalizando 4,7% das mortes relacionadas ao câncer no mundo todo. Como é possível notar, o câncer de pâncreas é responsável por quase tantas mortes (466.000) quanto por casos (496.000). Além disso, estimativas apontam que o câncer de pâncreas ultrapassará o câncer de mama como a terceira principal causa de morte por câncer em 2025 (SUNG *et al.*, 2021).

Cerca de mais da metade dos pacientes diagnosticados com câncer de pâncreas apresentam a doença localmente avançada ou metastática logo quando descobrem o tumor, sendo os principais locais de metástase o fígado e os pulmões. Esse cenário dificulta a indução da regressão da doença, além de dificultar o prolongamento da vida do paciente e do alívio dos sintomas (CHIARAVALLI; RENI; O'REILLY, 2017).

Os tratamentos mais atuais são baseados em 5-fluorouracil ou gencitabina. Entretanto, esses fármacos oferecem apenas um breve tempo de sobrevivência no intervalo de meses no cenário paliativo. Apesar dos avanços na área, pode-se dizer que não existe uma terapêutica direcionada para o adenocarcinoma ductal pancreático, o que conduz ao tratamento tradicional, isto é, a quimioterapia (CONROY *et al.*, 2011; HOSEIN; BREKKEN; MAITRA, 2020).

### 3.2. Autofagia

Diante do exposto, é possível compreender que tanto o câncer de mama triplo-negativo quanto o câncer de pâncreas, não apresentam terapias direcionadas. Em muitas das vezes, ambos utilizam do tratamento mais tradicional e generalizado, a quimioterapia. No entanto, sabe-se que a quimioterapia resulta em sérios efeitos colaterais, além de não ser o tratamento mais eficaz, levando em consideração as taxas de mortalidades das duas doenças (MBUGUA *et al.*, 2020; SUNG *et al.*, 2021). Sendo assim, novas estratégias de combate são necessárias e, neste caso, processos autofágicos podem ser bons aliados na luta contra o câncer.

A autofagia consiste em um mecanismo conservativo de reciclagem celular, onde materiais como, por exemplo, organelas danificadas, proteínas malformadas, etc., são levadas ao lisossomo para que a degradação dos materiais danificados ocorra. Ela possui três tipos mais conhecidos, macroautofagia, microautofagia e autofagia mediada por chaperonas (CMA). As divisões de tipos de autofagia se diferem, basicamente, pela forma como o material danificado é entregue ao lisossomo para ser degradado (BOYA; REGGIORI; CODOGNO, 2013; DIKIC; ELAZAR, 2018).

A macroautofagia, que se trata da própria autofagia, se inicia quando conteúdos indevidos no citosol, como, por exemplo, proteínas desestruturadas, organelas danificadas, dentre outros materiais, são englobadas por uma membrana chamada de fagóforo. Quando esse fagóforo se alonga, é formado o autofagossomo que, posteriormente se fundirá ao lisossomo para formar o autolisossomo. É neste momento que o material capturado é degradado pelas enzimas hidrolases presentes no lisossomo. Em outras palavras, através da autofagia (ou macroautofagia), as células são capazes de fazer, por exemplo, a reciclagem de proteínas, lipídios, aminoácidos, ácidos graxos, etc. (ABDRAKHMANYAN; GOGVADZE; ZHIVOTOVSKY, 2020).

A microautofagia se difere na forma com que essas proteínas malformadas, organelas danificadas, são entregues ao lisossomo. De forma simplificada, esses materiais indevidos não passam pela formação do autofagossomo, eles são incorporados diretamente ao lisossomo para que sua degradação aconteça. Por fim, a autofagia mediada por chaperonas (CMA), é uma via que contém chaperonas específicas que permitem a condução de determinadas proteínas para o lisossomo por interação com o receptor LAMP-2A (ABDRAKHMANYAN; GOGVADZE; ZHIVOTOVSKY, 2020).

A autofagia pode ainda ser dividida entre *seletiva* e *não seletiva*. Antes, pensava-se que a autofagia induzida pela privação de nutrientes agia de forma *não seletiva* sequestrando e degradando o material citoplasmático. Entretanto, está cada vez mais sendo reconhecido que a autofagia é um processo *seletivo*, onde um englobamento direcionado dos materiais citoplasmáticos ocorre (KAUR; DEBNATH, 2015).

Segundo Carmona-Gutierrez e colaboradores (2020), a autofagia pode possuir uma relação direta com a doença da COVID-19 (*Coronavirus Disease 2019*). A questão levantada é sobre se a manipulação da autofagia pode ser benéfica para o combate contra a doença. Embora essa questão ainda não possa ser respondida com total clareza, devida à necessidade de mais estudos, especula-se que a indução de autofagia possa neutralizar a infecção pelo vírus da COVID-19 em diferentes níveis (CARMONA-GUTIERREZ *et al.*, 2020).

O mecanismo de atuação da autofagia trata-se de um processo de muita complexidade. A via de sinalização da autofagia, PI3K/Akt/mTOR, se inicia com as proteínas PI3K e Akt que são responsáveis por regular positivamente a proteína mTOR. A proteína mTOR regula negativamente a proteína ULK1 que, por sua vez, inibe todo o processo de autofagia (KALEAĞASIOĞLU; ALI; BERGER, 2020).

Entende-se que investigações envolvendo a proteína PI3K são muito importantes para a compreensão de processos autófágicos, principalmente pelo fato desta proteína estar no início da via de sinalização da autofagia. Além disso, é preciso ressaltar também a importância de outro alvo molecular, a proteína ULK1, responsável por iniciar de fato o maquinário autófágico (KALEAĞASIOĞLU; ALI; BERGER, 2020). Diante disso, a possibilidade de manipular, por meio de agentes terapêuticos, a via e proteínas envolvidas na autofagia, é uma estratégia bem-vinda na luta contra o câncer (NAM, 2021).

### 3.2.1. A manipulação da autofagia no tratamento do câncer

Sabe-se que a autofagia, quando relacionada ao câncer, possui um comportamento dual, ou seja, ela pode tanto ajudar às células cancerígenas a não se formarem quanto ajudar as células cancerosas, já formadas, a sobreviverem. Essa dualidade no comportamento da autofagia já dividiu inúmeras opiniões. No entanto, hoje em dia, está claro que a possibilidade de manipulação da autofagia de tanto induzir quanto inibir (por meio de vias, proteínas, fármacos,

etc.) é uma realidade que carrega tamanha importância para os tratamentos contra o câncer (NAZIO *et al.*, 2019).

Sabe-se que a autofagia é um processo que ocorre de forma natural no corpo humano. No entanto, uma vez que esse processo autofágico está factível a falhas, um possível cenário, não favorável, começa a se formar. Em outras palavras, a desregulação da autofagia pode favorecer o surgimento de diversas doenças, entre elas, o câncer (ONORATI *et al.*, 2018; KOCAK *et al.*, 2021).

Do ponto de vista da autofagia atuando na tumorigênese, sabe-se que ela tem a função de não permitir que as células tumorosas se formem de fato. Isto é, quando a transição da célula normal para uma célula com tumor está prestes a acontecer, a autofagia atua no intuito de impedir este processo. Sendo assim, pode-se dizer que a reciclagem que o processo autofágico proporciona é extremamente importante para limpar a célula e prevenir contra possibilidade do tumor se formar (BISHOP; BRADSHAW, 2018).

Por outro lado, uma vez que a autofagia não consiga conter a tumorigênese e o tumor se instale nas células, a atuação da autofagia começa a se desenhar de forma diferente. Depois de já instalado e espalhado, a autofagia começa a atuar a favor do câncer, pois as células cancerosas localizadas nas áreas centrais do tumor são pouco vascularizadas, de modo que a ocorrência de autofagia lhes permite sobreviver nessas condições de baixo teor de nutrientes e de baixo oxigênio (KOCAK *et al.*, 2021).

Além disso, nesse estágio da doença, a autofagia pode dificultar os tratamentos contra o câncer. Isto porque na situação de um quimioterápico atuar para destruir as células tumorosas, a autofagia pode contribuir para que o câncer fique resistente àquele remédio (quimiorresistência). Em outras palavras, os quimioterápicos, que geram danos às células cancerosas, são responsáveis por induzir a autofagia que, por sua vez, pode anular todo o trabalho feito pelas drogas (YUN; LEE, 2018).

Para desenvolver um tratamento eficaz para o câncer, é preciso identificar quais moléculas regulam positivamente (induzindo) ou negativamente (inibindo) a autofagia contra o tumor. Além disso, cabe aos cientistas e médicos especializados no assunto, saberem quando induzir ou quando inibir o processo de autofagia (BISHOP; BRADSHAW, 2018).

Diante do exposto, entende-se que o conceito de autofagia para o câncer depende de alguns fatores como, por exemplo, o estágio em que o câncer se encontra. Entretanto, uma consideração indiscutível é que a autofagia, para prevenção contra o câncer e diversas outras doenças, é um processo essencial. Além disso, a possibilidade de manipulação do processo autofágico é uma grande aliada no combate ao câncer (MISHRA; AMMANATHAN; MANJITHAYA, 2018).

É importante salientar, que a autofagia possui apreciáveis vantagens em comparação aos tradicionais processos quimioterápicos. Como ela é um processo de autodegradação, a autofagia atua diretamente nas células doentes, evitando possíveis efeitos colaterais. Já a quimioterapia, além de atuar nas células cancerosas, atua também em células saudáveis responsáveis por inúmeros processos importantes no corpo humano, acarretando efeitos colaterais indesejados e queda da qualidade de vida do paciente (MBUGUA *et al.*, 2020).

Um estudo liderado por Cassidy e colegas de trabalho (2020), analisou o papel dual da autofagia em células cancerosas em camundongos. Um dos objetivos dos autores foi conciliar as duas funções da autofagia na supressão e progressão de tumores. De maneira geral, o grupo concluiu que a inibição da autofagia em camundongos acelerou a formação espontânea do câncer. Uma vez instalado o câncer, o papel promotor de tumor da autofagia fez com que ocorresse uma maior incidência de tumores em comparação com camundongos que não tiveram a autofagia reativada. Em outras palavras, na carcinogênese, a indução da autofagia é bem-vinda, já em estágios mais avançados da doença, é sugestiva a inibição da autofagia (CASSIDY *et al.*, 2020).

Neste contexto, nota-se a relevante atuação dos moduladores de autofagia, isto é, agentes que possuem as funções de ativar ou desativar os processos autofágicos. O grande interesse que tem surgido nos últimos anos a respeito da atuação da autofagia no câncer, tem motivado a descoberta de medicamentos que possuem a capacidade de modular a autofagia. Sendo assim, diversas empresas de biotecnologia têm dedicado seus esforços para desenvolver moduladores de autofagia para tratar diversas doenças (DOLGIN, 2019; KOCAK *et al.*, 2021). Algumas dessas empresas estão destacas na Tabela 3.1.

**Tabela 3.1 – Algumas empresas de biotecnologia que desenvolvem moduladores de autofagia; estratégia de modulação; e descrição da ação.**

Nome da empresa	Estratégia	Descrição
Biophagy	Ativação/Inibição	Descoberta usando métodos de alto conteúdo para identificar moduladores farmacêuticos de autofagia.
Deciphera Pharmaceuticals	Inibição	Inibidor ULK1-ULK2 para tratamento de câncer.
Nanna Therapeutics	Ativação	Concentra-se nas mitocôndrias, visando doenças relacionadas à idade, incluindo doenças neurodegenerativas, inflamatórias, cardíacas e metabólicas, bem como muitos cânceres.
Sprint Bioscience	Inibição	Inibidor PIK3C3/VPS34 direcionado ao câncer.
Vescor Therapeutics	Ativação	Alvos não divulgados no câncer.

Fonte: KOCAK *et al.*, 2021.

Outro detalhe digno de nota, é o fato de que toda a investigação sobre a manipulação da autofagia possui muitas vantagens, entretanto, duas se destacam. Além dos moduladores atuarem como ferramentas para estudar e melhor compreender o maquinário da autofagia, essas moléculas podem ter também um grande potencial terapêutico (MISHRA; AMMANATHAN; MANJITHAYA, 2018).

Diante do exposto, fica clara a importância de se estudar moléculas que são capazes de manipular a autofagia, ora inibindo-a, ora induzindo-a. Dessa forma, complexos de vanádio têm sido destacados por serem capazes de atuarem nos processos autófágicos, alguns ativando a autofagia, outros desativando o processo.

### 3.3. Complexos de Vanádio

Uma reconhecida atenção tem sido dada aos complexos vanádio nos últimos anos por, principalmente, apresentarem uma ampla variedade de ações em química medicinal. As aplicações dos complexos de vanádio que têm recebido maiores destaque nos últimos tempos, são aquelas acerca de tratamentos de diabetes e certos tipos de cânceres (PESSOA *et al.*, 2021; UGONE *et al.*, 2020).

Complexos a base do metal vanádio possuem a capacidade de explorar a relação estrutura-atividade, por exemplo, através de sua geometria octaédrica, que possui a capacidade

de melhor se ajustar ao sítio ativo de proteínas quinases. Além disso, o papel anticancerígeno de complexos de vanádio é algo notável (KOWALSKI *et al.*, 2019).

Neste cenário, diversos estudos na literatura a respeito da manipulação da autofagia têm sugerido que complexos metálicos, possuindo como átomo central o vanádio (elemento do grupo 5 da tabela periódica), apresentam resultados promissores em relação a terapias, incluindo terapias de câncer e leishmaniose (HUANG *et al.*, 2018; KOWALSKI *et al.*, 2017; MACHADO *et al.*, 2017; WALKER *et al.*, 2012; WU *et al.*, 2014).

### 3.3.1. Complexos de vanádio em manipulações de autofagia e câncer

Como mencionado, nos últimos tempos, complexos de vanádio têm sido aplicados na manipulação de processos autofágicos, tanto para induzir quanto para inibir de maneira útil e eficaz. Nesse sentido, dois desses relevantes trabalhos estão resumidos a seguir (EL-SHAFETY; ELSHERBINY, 2019; KOWALSKI *et al.*, 2017).

Em outubro de 2019, E. S. El-Shafey e E. S. Elsherbiny apresentaram suas investigações a respeito da ação antitumoral do complexo de vanádio,  $[VO(bpy)_2Cl]$ <sup>1</sup>, no câncer de mama triplo-negativo (TNBC), indicando sua atividade citotóxica seletiva através de diferentes vias moleculares, dentre elas, a autofagia. A Microscopia Eletrônica de Transição (TEM) foi utilizada para examinar a estrutura fina dos autofagossomos (compartimentos autofágicos iniciais/precoces) e dos anfissomos e/ou autolisossomos (compartimentos autofágicos tardios). Os resultados informaram que o crescimento das células MDA-MB-231 (linha celular referente ao TNBC) foi suprimido após o tratamento com o complexo de vanádio de maneira dependente da dose.

A análise de TEM mostrou que havia numerosos vacúolos de membrana dupla, autofagossomos e autolisossomos, contendo materiais digeridos residuais do citoplasma. Além disso, outros resultados, obtidos por análise citométrica de fluxo de células MDA-MBA-231, demonstraram que a célula sem o tratamento com o complexo de vanádio possuía a presença de 29,1% de LC3 (proteína responsável por quantificar a autofagia). Já o tratamento envolvendo o complexo  $[VO(bpy)_2Cl]$  em diferentes concentrações de IC<sub>50</sub>, foram divididos entre grupos I, II e III (dose do complexo aumentada na ordem I < II < III), onde foi favorecido o aumento

---

<sup>1</sup> Complexo de vanádio estudado no Artigo 2 desta tese,  $[VO(bpy)_2Cl]$ .

do nível da proteína LC3 para 50,2%, 65,4% e 85,6%, respectivamente. Esses resultados permitiram inferir que a presença do complexo de vanádio mencionado, aumentou, de forma considerável, os níveis da proteína LC3, indicando uma indução no processo de autofagia (EL-SHAFEY; ELSHERBINY, 2019).

Outra importante investigação foi realizada por Kowalski e colaboradores em 2017, onde sete complexos de vanádio foram inicialmente estudados. Dentre os sete compostos investigados no trabalho (C1, C2, C3<sup>2</sup>, C4, C5, C6 e C7), foi realizada uma triagem de quais apresentavam citotoxicidade seletiva nas células de câncer de pâncreas. Apenas C3, C5 e C7 demonstraram citotoxicidade seletiva contra as células cancerosas. O motivo dessa citotoxicidade seletiva pode ser atribuída a diferentes mecanismos moleculares, dentre eles, a autofagia.

Para análise de autofagia, os complexos C3, C5 e C7, foram incubados com células contendo o tumor e a proteína LC3. Dessa forma, depois de algum tempo, foi medido o nível da proteína LC3 que, por sua vez, é responsável por quantificar autofagia. Através da análise Western Blot, foi observado que a proteína LC3 diminuiu nas células cancerosas tratadas com concentração seletiva de 1 µM dos compostos C3 e C5. Em contrapartida, o complexo C7 apresentou um aumento no nível da proteína. Neste contexto, pôde-se entender que os complexos de vanádio C3 e C5 inibiram a autofagia, ao passo que o complexo de vanádio C7 induziu a autofagia (KOWALSKI *et al.*, 2017).

Nota-se que os trabalhos citados anteriormente tratam-se de investigações puramente experimentais. As ciências experimentais representam de maneira elegante os eventos do dia a dia e reações relevantes no corpo humano. Em outras palavras, os experimentos em laboratórios possibilitam explorar minuciosamente a natureza do mundo real. Entretanto, em muitos cenários, os experimentos possuem custos altos com reagentes e aparelhos caros que tornam pesquisas de grande impacto muitas vezes inviáveis, além de metodologias envolvendo uma infinidade de possibilidades a serem testadas.

Diante disso, abordagens teóricas surgem como uma interessante alternativa para complementar as pesquisas experimentais. Nesse sentido, a química computacional contemporânea desempenha um papel de destaque cada vez maior, implicando em pesquisas científicas (de base e aplicadas) de forte impacto no entendimento da natureza do mundo real (LI; MERZ JR, 2017).

---

<sup>2</sup> Complexo de vanádio estudado no Artigo 1 desta tese, [VO(oda)(phen)].

### 3.4. Abordagem Teórica

Com o advento dos computadores modernos com elevada competência em desempenhar cálculos numéricos, a química computacional tem se revelado uma ferramenta poderosa na investigação de sistemas químicos, físicos e biológicos. Dessa forma, muitos cientistas recorrem a estudos teóricos para prever ou medir propriedades de interesse. Entre elas, destacam-se a estrutura molecular, análise conformacional, espectros vibracional e eletrônico, interações intermoleculares, reatividade química e mecanismos de reações químicas (PLIEGO JR., 2006; COSTA, 2014).

Os métodos que incorporam a Química Computacional baseiam-se em teorias que vão desde as de alta precisão, usualmente aplicáveis a sistemas menores, até as muito aproximadas, apropriadas para sistemas grandes, englobando abordagens em Mecânica Quântica e em Mecânica Molecular (MORGON, 2001).

As escolhas acerca dos tipos de abordagens teóricas se baseiam, em geral, em métodos fundamentados em Mecânica Molecular, onde é possível destacar métodos como as simulações de Dinâmica Molecular Clássica, Monte Carlo e *Docking*; além de métodos fundamentados em Mecânica Quântica como, por exemplo, semi-empíricos, *ab initio* e o método da Teoria do Funcional de Densidade. Tais abordagens vêm apresentando uma apreciável convergência com resultados experimentais, mesmo levando-se em conta os níveis de aproximações existentes.

#### 3.4.1. Métodos teóricos fundamentados em Mecânica Molecular

O número de átomos, de certa forma, norteia os estudos, influenciando consideravelmente a escolha da metodologia a ser empregada. Sistemas com enorme número de átomos, geralmente são tratados com Mecânica Clássica. Os métodos teóricos fundamentados em Mecânica Clássica são definidos pela Mecânica Molecular (MM). Neste método, os átomos são representados por esferas e os elétrons são generalizados em forma da carga de cada átomo (ANCONI, 2007).

Cálculos fundamentados em MM são conhecidos por não tratarem de forma explícita os elétrons nas moléculas. Além disso, são práticas menos demoradas e que permitem trabalhar com sistemas de elevada complexidade. Esses cálculos possuem seus fundamentos baseados

nas leis da Mecânica Clássica e são alternativas importantes na determinação de propriedades estruturais e parâmetros termodinâmicos de um sistema molecular sob investigação (PEREIRA, 2020).

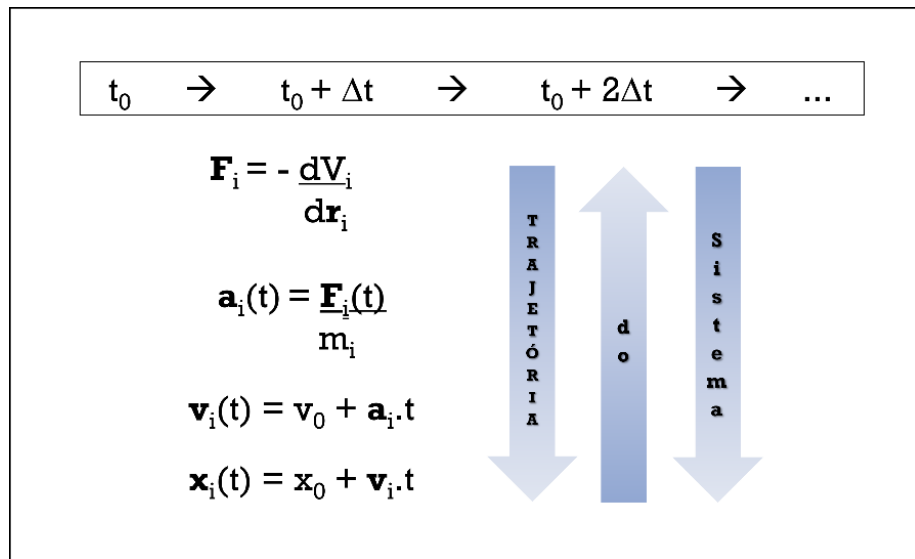
Dois métodos muito eficientes, fundamentados em Mecânica Molecular, são as simulações de Dinâmica Molecular Clássica (DM) e as simulações de ancoramento molecular, o *Docking*. Tais simulações se apresentam como umas das técnicas computacionais mais empregadas para o entendimento e previsão de propriedades, assim como estrutura e função de macromoléculas biológicas (NAQVIL *et al.*, 2018).

#### 3.4.1.1. Dinâmica Molecular Clássica

Pode-se dizer que a Dinâmica Molecular Clássica (DM), por definição, é um método teórico que estuda o comportamento das moléculas ao longo do tempo sob certas condições. Nesse sentido, as moléculas presentes em um determinado sistema são tratadas como um conjunto de partículas unidas por forças harmônicas ou elásticas. Dessa forma, simulações de DM não fornecem as ferramentas necessárias para se investigar formação e ruptura de ligações, interações entre orbitais, transferência de carga ou qualquer outro efeito eletrônico (BRAUN *et al.*, 2019; DE VIVO *et al.*, 2016; NAIR; MINERS, 2014).

Segundo este método de cálculo, as partículas presentes em um sistema se movimentam a partir de potenciais intermoleculares. Sendo assim, as equações de movimento Newtonianas formam o escopo do método (HOLLINGSWORTH; DROR, 2018). A Figura 3.1 ilustra um resumo básico do formalismo das simulações de DM.

**Figura 3.1 – Resumo básico do formalismo matemático de simulações de Dinâmica Molecular Clássica.**



Fonte: da autora (2023).

Na Figura 3.1,  $t_0$  representa um tempo inicial;  $t_0 + \Delta t$  significa um incremento de tempo, assim como  $t_0 + 2\Delta t$  indica um tempo posterior.  $\mathbf{F}_i$  representa a força atuando na partícula  $i$ ;  $m_i$  é a massa atômica;  $\mathbf{a}_i$  é a aceleração, assim como  $\mathbf{v}_i$  e  $\mathbf{x}_i$  correspondem, respectivamente, à velocidade e posição de uma determinada partícula;  $v_0$  é a velocidade inicial e  $x_0$  a posição inicial; a variável  $t$  representa o tempo;  $V_i$  é o potencial total dependente da posição da partícula, representada por  $\mathbf{r}_i$ .

O entendimento de como funcionam as simulações de DM (Figura 3.1) se inicia a partir do conhecimento de que os átomos estão dispostos com uma certa configuração inicial, que nos permite conhecer as posições e velocidades iniciais de todas as partículas em um instante de tempo  $t_0$ . Em um instante de tempo posterior  $t_0 + \Delta t$ , tem-se uma nova distribuição espacial que permite estimar novas forças resultantes em cada partícula. Em seguida, é possível obter a aceleração a partir da segunda lei de Newton que, por sua vez, permite obter a velocidade e, por fim, novas posições. Novamente, em um próximo instante  $t_0 + 2\Delta t$ , esse processo se repete, e assim sucessivamente, formando o que é chamado de trajetória do sistema (MARTÍNEZ; BORIN; SKAF, 2007).

O formalismo matemático das simulações de DM, isto é, as equações presentes na Figura 3.1, são resolvidas simultaneamente, gerando um grande conjunto de equações de movimento para cada partícula constituinte do sistema. Dessa forma, desenvolver todo esse

formalismo matemático sem ajuda de quaisquer recursos seria uma tarefa árdua. Em outras palavras, as equações Newtonianas que compõe o escopo do método de cálculo de DM, não podem ser resolvidas de forma analítica. Isso acontece devido à complexidade dos sistemas sob investigação que contam com elevados números de partículas interagentes (PEREIRA, 2020).

Diante do exposto, nota-se a necessidade de fazer uso de resoluções numéricas, ou seja, códigos de programação, que resolvam consecutivamente as equações de interesse. Esse tipo de resolução torna-se possível com a utilização de algoritmos específicos, nos quais a integração é feita em pequenos intervalos de tempo. Nesse sentido, os algoritmos mais utilizados para a integração dessas equações são o Verlet (VERLET, 1967) e Leap-Frog (HOCKNEY, 1970).

Em linhas gerais, pode-se dizer que a Dinâmica Molecular Clássica é um método teórico útil e sofisticado. Além disso, uma característica do método é o estabelecimento de forte concordância com estudos experimentais. Resultados obtidos de simulações de Dinâmica Molecular fornecem explicações detalhadas a nível microscópico de fenômenos observados experimentalmente. Em contrapartida, um dos maiores desafios para a realização de simulações de Dinâmica Molecular é a parametrização dos campos de força (MARTÍNEZ; BORIN; SKAF, 2007).

### *3.4.1.2. Campos de força*

Como mencionado, em Mecânica Molecular os átomos são considerados como esferas. Sendo assim, campos de força que atuam nas moléculas são responsáveis por descrever todo o sistema molecular de interesse. As forças atuantes nas partículas são descritas pelas funções de energia potencial que dizem respeito aos comprimentos de ligação, ângulos de ligação, ângulos diedros e interações entre átomos não ligados. Dessa forma, nos campos de força estão inclusos parâmetros que tentam descrever de maneira adequada a forma de ligação dos átomos (PEREIRA, 2016).

Sabe-se que a energia de uma molécula está diretamente relacionada com a posição e velocidade das partículas que a compõem, sendo a composição da energia total como:  $E_{total} = E_{cinética}(K) + E_{potencial}(V)$ . A energia potencial ( $V$ ) é a energia que descreve determinado sistema e pode ser expressa, de modo geral, como na equação (3.1), onde estão inclusos os somatórios da energia intramolecular e intermolecular, respectivamente.

$$V_{\text{Total}} = \sum V_{\text{Intra}} + \sum V_{\text{Inter}} \quad (3.1)$$

Nesse sentido, ao conjunto de parâmetros necessários para descrever todas as interações intramoleculares e intermoleculares dá-se o nome de *campo de força* (FF, do inglês *Force Field*). A eficiência dos campos de força depende, fortemente, da qualidade da parametrização realizada.

A etapa de escolha dos potenciais de interação intramoleculares e intermoleculares é uma das etapas mais importantes para a descrição eficaz dos sistemas sob investigação. Isso porque são esses potenciais que irão determinar as forças que atuam em cada partícula e, consequentemente, serão peças-chaves no desempenho do sistema e como ele irá evoluir ao longo do tempo para gerar as trajetórias para análise (MARTÍNEZ; BORIN; SKAF, 2007).

A energia potencial descrita de forma geral pela equação (3.1), pode ser melhor detalhada. Sendo assim, a equação (3.2) apresenta um potencial total ( $V_{\text{Total}}$ ) que descreve as forças atuantes sobre cada átomo, levando em consideração as contribuições intramoleculares (átomos ligados) e intermoleculares (átomos não ligados).

$$V_{\text{Total}} = V_L + V_A + V_D + V_{\text{LJ}} + V_C \quad (3.2)$$

Na equação (3.2), os termos ligados correspondem ao potencial de estiramento das ligações ( $V_L$ ), ao potencial de deformação angular ( $V_A$ ) e ao potencial referente aos ângulos diedros ( $V_D$ ). Já os termos não ligados são descritos pelo potencial de Lennard-Jones ( $V_{\text{LJ}}$ ) e o potencial de Coulomb ( $V_C$ ) (PEREIRA, 2020).

Além disso, os termos comentados podem ser descritos por suas respectivas equações. Por exemplo, os potenciais harmônicos  $V_L$  e  $V_A$ , referem-se, respectivamente, aos valores de energia de estiramentos das ligações e deformações angulares, cada um em relação aos devidos valores de equilíbrio. Esses potenciais obedecem à lei de Hooke e podem ser representados nas formas

$$V_L = \sum_{\text{ligações}} K_b(b - b_0)^2 \quad (3.3)$$

e

$$V_A = \sum_{\text{ângulos}} K_\theta(\theta - \theta_0)^2 \quad (3.4)$$

Em que  $b$  e  $\theta$  correspondem aos comprimentos e ângulos de ligação, respectivamente; além de  $b_0$  e  $\theta_0$  corresponderem aos valores de equilíbrio; por fim,  $K_b$  e  $K_\theta$  representam as constantes de força (PEREIRA, 2020).

Sabe-se que valores referentes à constante de força das ligações ( $K_b$ ) são, geralmente, altos. Isso sugere, de certa forma, que uma significativa quantidade de energia é requerida para esticar ou comprimir determinada ligação química (MONTICELLI; TIELEMAN, 2013).

O terceiro termo da equação (3.2) refere-se ao potencial de energia dos átomos para uma torção, onde geralmente é representado em termos de uma função periódica (cosseno), como

$$V_D = \frac{1}{2} \sum_{diedros} K_\phi [\cos(n\phi - \delta) + 1] \quad (3.5)$$

onde  $K_\phi$  representa à constante que define a altura da barreira de rotação; o número de mínimos está representado por  $n$ ; o ângulo diedro por  $\phi$ ; e  $\delta$  é o ângulo de fase.

Por fim, os termos referentes às interações intermoleculares (átomos não ligados), correspondem às interações de van der Waals ( $V_{LJ}$ ) e interações eletrostáticas ( $V_C$ ), e estão apresentadas nas equações (3.6) e (3.7), respectivamente.

$$V_{LJ} = \sum_{não\ ligados} 4\epsilon_{ij} \left[ \frac{\sigma^{12}}{r_{ij}^{12}} - \frac{\sigma^6}{r_{ij}^6} \right] \quad (3.6)$$

$$V_C = \sum_{não\ ligados} \left[ \frac{q_i q_j}{4\pi\epsilon_0 r_{ij}} \right] \quad (3.7)$$

Em (3.6) e (3.7), a distância entre os átomos  $i$  e  $j$  está representada por  $r_{ij}$ ; assim como a profundidade do poço de potencial está representada por  $\epsilon_{ij}$ ;  $\sigma$  corresponde à distância em que o potencial de Lennard-Jones ( $V_{LJ}$ ) é zero;  $q_i$  e  $q_j$  representam as cargas parciais atômicas; e, por fim,  $\epsilon_0$  representa a permissividade no vácuo (PEREIRA, 2020).

Por fim, vale comentar que as funções potenciais descritas pelas equações (3.3), (3.4), (3.5), (3.6) e (3.7), são representações de um campo de força amplamente conhecido, o campo de força AMBER (CASE *et al.*, 2010).

Conforme exposto nas equações anteriores, para descrever cada interação, tanto intramolecular quanto intermolecular, necessita-se obter os valores de equilíbrio e as constantes

de força para todas as ligações, ângulos e diedros. Através de campos de força tradicionais como, por exemplo, AMBER (WANG *et al.*, 2004), CHARMM (WANG *et al.*, 2006), OPLS (JORGENSEN; MAXWELL; TIRADO-RIVES, 1996) e GROMOS (OOSTENBRINK *et al.*, 2004), é possível obter essas informações para um grande conjunto de sistemas já parametrizados.

Além da metodologia teórica para obter os valores de equilíbrio que compõem os campos de força, técnicas experimentais como cristalografia de raios-X e Ressonância Magnética Nuclear (RMN), também podem fornecer essas informações. Além disso, técnicas de infravermelho e Raman podem ser utilizadas para fornecer as informações das constantes de força (PEREIRA, 2020).

Outro detalhe digno de nota, é que os potenciais que formam os campos de força são, geralmente, parametrizados para um sistema específico. Assim, torna-se possivelmente equivocada a transferibilidade entre campos de força devido, principalmente, às peculiaridades de cada sistema interagente (MARTÍNEZ; BORIN; SKAF, 2007).

É preciso muito cuidado ao lidar com campos de força considerados gerais, porque em muitos casos, esses campos de força gerais não reproduzem de forma eficiente os dados de interesse. Nesse sentido, fazer uso de um campo de força geral em uma simulação de DM, contendo moléculas altamente conjugadas e metais de transição, pode ser considerado um equívoco, pois simulações assim podem não reproduzir, de forma satisfatória, os modos de vibração, além de poderem resultar em estruturas não realísticas (PRANDI *et al.*, 2016; TAVARES *et al.*, 2023).

Sabe-se que os metais de transição possuem suas peculiaridades como, por exemplo, orbitais *d* em suas camadas de valência, além de uma variedade de estados de oxidação. Seus diversos estados de oxidação podem favorecer sistemas altamente carregados, que devem ser descritos com precisão nas simulações. Por conta disso, os cálculos quânticos ainda são as principais formas de se obter parâmetros (GONZÁLEZ, 2011; LI; MERZ JR., 2017).

Parâmetros de campos de força para centros metálicos são altamente escassos. Neste cenário, existe uma grande dificuldade em achar tais parâmetros que descrevam sistemas contendo metais de transição. Essa pode ser uma das maiores limitações em se trabalhar com simulações de Dinâmica Molecular (PEREIRA, 2020).

### 3.4.1.3. Docking

O método de cálculo denominado como “*docking*”, é uma técnica muito importante na modelagem estrutural de biomoléculas. Outros termos também são comumente utilizados como, por exemplo, “acoplamento” ou “ancoramento”. O objetivo das simulações de *docking* consiste, basicamente, na avaliação das interações energéticas de algumas orientações de uma molécula em relação à outra, em busca de interações que resultem em baixa energia. Em outras palavras, o ancoramento molecular pode ser entendido como uma otimização que tem como objetivo encontrar a interação do ligante com a biomolécula que possuam a menor energia (BASTOS, 2006).

O processo de reconhecimento molecular da biomolécula com um ligante, geralmente descrito como receptor-ligante, é dirigido por uma combinação de efeitos entálpicos e entrópicos. Nesse sentido, esses efeitos podem ser estimados segundo a energia livre de ligação de Gibbs ( $\Delta G_{\text{lig}}$ ) que, por sua vez, está diretamente relacionada à constante de dissociação  $K_i$ , na forma

$$\Delta G_{\text{lig}} = \Delta H - T\Delta S = RT\ln K_i \quad , \quad (3.8)$$

Em que  $\Delta H$  representa a variação de entalpia,  $T$  a temperatura,  $\Delta S$  a variação de entropia e  $R$  a constante universal dos gases. Nota-se um sinal contrário na equação acima (positivo), isso se deve ao fato de que a constante medida,  $K_i$ , é uma constante de dissociação (MAGALHÃES; BARBOSA; DARDENNE, 2007).

A função de desempenho do ancoramento (*Docking Scoring Function*),  $E_{\text{score}}$ , pode ser definida pela equação

$$E_{\text{score}} = E_{\text{inter}} + E_{\text{intra}} \quad , \quad (3.9)$$

em que  $E_{\text{inter}}$  representa a energia de interação do ligante com a proteína e  $E_{\text{intra}}$  representa a energia interna do ligante (THOMSEN; CHRISTENSEN, 2006).

Em outras palavras, simulações de *docking* receptor-ligante consistem em investigações sobre os modos de interações de uma pequena molécula ligante na região de ligação de um alvo molecular, além de medir a afinidade entre o ligante e o receptor em questão. De modo geral, esse alvo molecular, que pode ser, por exemplo, uma proteína, está relacionado à alguma doença

a qual se deseja desenvolver um tratamento (MAGALHÃES; BARBOSA; DARDENNE, 2007).

Vale salientar, que no desenvolver do reconhecimento molecular, as moléculas interagentes (receptor-ligante) sofrem mudanças conformacionais. Além disso, o complexo e dinâmico processo de reconhecimento molecular é constituído por etapas que envolvem um significativo número de interações intermoleculares entre o ligante e o receptor (MAGALHÃES; BARBOSA; DARDENNE, 2007).

Entender os mecanismos de reconhecimento molecular receptor-ligante é um dos aspectos mais importantes para o sucesso na descoberta e planejamento de novos fármacos, além de ser um dos principais desafios da biologia molecular (ROCHA, 2010).

Os estudos sobre os processos de reconhecimento molecular receptor-ligante são, em grande parte, motivados pelas possibilidades de redução de tempo de cálculo, além de custos apreciavelmente mais baixos em comparação com custos de técnicas laboratoriais para o desenvolvimento de novas drogas (MAGALHÃES; BARBOSA; DARDENNE, 2007).

### 3.4.2. Métodos teóricos fundamentados em Mecânica Quântica

A mecânica quântica (MQ) é um método teórico de cálculo que possui seu formalismo fundamentado, especialmente, em matemática e física. Este método é protagonizado pelo conceito de função de onda e apresenta-se como uma poderosa ferramenta de trabalho para estudos de sistemas químicos (ANCONI, 2007).

Modelos quanto-mecânicos são extremamente eficientes e capazes de conectar interfaces do mundo microscópico e macroscópico. Em outras palavras, a MQ proporciona o contato mais próximo com a estrutura da matéria, peça fundamental de estudos da ciência química (SANTOS, 2017).

Devida a grande complexidade de conceitos e formalismo da mecânica quântica, foi necessária a utilização de uma quantidade razoável de métodos e aproximações para, assim, tornar-se possível estender as implicações da teoria quântica para átomos que fossem diferentes do hidrogênio e até mesmo para moléculas (ANCONI, 2007).

A década de 1930 é bastante conhecida por datar os primeiros estudos de aplicação da mecânica quântica moderna, com os trabalhos de Erwin Schrödinger e Paul Dirac. A famosa equação de Schrödinger, exposta na equação (3.10), fornece o entendimento de um estado particular para cada ente presente em um sistema, considerando o comportamento onda-partícula dos elétrons e a descrição da energia mecânica como sendo a soma da energia cinética e potencial (GRIFFITHS, 2011).

$$\left[ -\frac{\hbar^2}{2m} \nabla^2 + V \right] \Psi(r, t) = i\hbar \frac{\partial \Psi}{\partial t} (r, t) \quad (3.10)$$

$$\nabla^2 = \frac{\partial^2}{\partial x^2} + \frac{\partial^2}{\partial y^2} + \frac{\partial^2}{\partial z^2} \quad (3.11)$$

A equação (3.10) representa uma equação diferencial da função de onda ( $\Psi$ ) dependente da posição e do tempo, onde  $\hbar$  (lê-se, “h cortado”) é a constante de Planck (h) dividida por  $2\pi$ , m é a massa do elétron,  $\nabla$  é o operador Laplaciano das posições x, y e z (descrito na equação (3.11)), V é a energia potencial e  $i$  o número imaginário. A Equação de Schrödinger pode ser simplificada através de recursos matemáticos, onde se faz uso da técnica de separação de variáveis (GRIFFITHS, 2011).

Em abordagens teóricas é preciso uma grande atenção no tamanho do sistema a ser estudado. Isso porque, como já mencionado, o aumento no número de átomos faz com que as equações se tornem mais complexas, uma vez que envolvem as diversas interações entre cada ente presente no sistema (PEREIRA, 2016).

Neste sentido, para conhecer o comportamento de um estado particular ou de um sistema em um todo, é importante utilizar aproximações que melhor descrevem a função de onda ( $\Psi$ ). Em virtude da tamanha dificuldade no trato de sistemas com elevado número de átomos, tais aproximações tornam-se imprescindíveis. Um método teórico que recebe grande atenção da comunidade científica por fornecer bons valores, é o método da Teoria do Funcional de Densidade – DFT.

#### *3.4.2.1. A Teoria do Funcional de Densidade*

O método da Teoria do Funcional de Densidade (DFT, do inglês *Density Functional Theory*), vem se tornando, nos últimos tempos, uma importante metodologia para investigar a

estrutura eletrônica de sistemas químicos. Situações que antes eram abordadas pelo viés de métodos *ab initio*, passaram a poder serem tratados mediante DFT, o que em determinadas ocasiões, apresenta uma melhor convergência com resultados experimentais. Este método de cálculo se destaca por fornecer uma considerável precisão química, mesmo se tratando de sistemas com tamanhos significativos (DUARTE; ROCHA, 2007).

Este método surgiu, inicialmente, pela proposta de Thomas e Fermi (FERMI, 1928; THOMAS, 1926) de descrever a energia em termos da densidade de partículas. A abordagem estatística foi utilizada por Thomas e Fermi para aproximar a distribuição de um gás de elétrons e desenvolver o funcional de energia.

Logo em seguida, Dirac propôs incluir no modelo Thomas-Fermi um termo referente a energia de troca para um gás de elétrons. Este funcional ficou então conhecido como o funcional de energia ( $E$ ) de Thomas-Fermi-Dirac (TFD). Contudo, apenas em 1964, com os trabalhos de Kohn e Hohenberg (HOHENBERG; KOHN, 1964), é que foi demonstrado que as propriedades do estado fundamental de um sistema de partículas são funcionais de densidade (DUARTE; ROCHA, 2007). Dessa forma, o fator chave no método DFT é a densidade eletrônica (equação (3.12)) que descreve a probabilidade de se encontrar um elétron no ponto  $\vec{r}$  (PEREIRA, 2016).

$$\rho(\vec{r}) = |\Psi(\vec{r})|^2 \quad (3.12)$$

A equação (3.13) representa um dos teoremas de Hohenberg-Kohn que demonstra a existência de um único funcional tal que a  $E_{elec}$  é a energia eletrônica exata. Além disso, no intuito de resolver a energia pelo método DFT, Kohn e Shan propuseram que o funcional tem a forma descrita pela equação (3.14).

$$E[\rho(r)] = E_{elec} \quad (3.13)$$

$$E[\rho(r)] = T_e[\rho(r)] + V_{ne}[\rho(r)] + V_{ee}[\rho(r)] + E_{xc}[\rho(r)] \quad (3.14)$$

Como nota,  $T_e$  refere-se à energia cinética do elétron,  $V_{ne}$  à energia potencial de atração núcleo-elétron,  $V_{ee}$  à energia potencial de repulsão elétron-elétron e  $E_{xc}$  refere-se ao funcional de troca e correlação, sendo usualmente descrito como uma soma de dois componentes, um de troca e outro de correlação.

Como pode ser observado na equação (3.14), a energia de troca e correlação é definida como um funcional de densidade eletrônica ( $E_{xc}[\rho(r)]$ ), onde, a partir da presença deste

funcional, é que o método DFT se difere dos demais métodos *ab initio*. Além disso, grande parte da motivação em desenvolver este método de cálculo teórico, está nas propostas de novos funcionais de troca-correlação mais precisos e algoritmos eficientes de integração numérica (ROCHA, 2010).

Em linhas gerais, a essência do método DFT consiste em obter propriedades do estado fundamental das moléculas, por meio da densidade eletrônica. Além disso, dentre as muitas vantagens do método, destaca-se a implementação computacional eficiente da correlação eletrônica, permitindo uma descrição razoável de sistemas complexos (DUARTE; ROCHA, 2007).

## REFERÊNCIAS

- ABDRAKHMANNOV, A.; GOGVADZE, V.; ZHIVOTOVSKY, B. To eat or to die: deciphering selective forms of autophagy. **Trends in biochemical sciences**, v. 45, n. 4, p. 347-364, 2020.
- ÁLVAREZ, L. *et al.* Comparison of the coordination capabilities of thiodiacetate and oxydiacetate ligands through the X-ray characterization and DFT studies of [V(O)(tda)(phen)]·4H<sub>2</sub>O and [V(O)(oda)(phen)]·1.5 H<sub>2</sub>O. **Polyhedron**, v. 29, n. 16, p. 3028-3035, 2010.
- ANCONI, C. P. A. **Pseudo-polirotaxanos e tubos moleculares de a ciclodextrinas no âmbito das metodologias teóricas**. 2007. 196f. Tese (Doutorado em Química) - Instituto de Química, Universidade Federal de Minas Gerais, Belo Horizonte, 2007.
- BASTOS, D. **A estrutura do mycobacterium tuberculosis catalase-peroxidase e os mecanismos de ação da isoniazida: um estudo para novos ligantes**. 2006. 152f. Dissertação (Mestrado em Química) - Instituto de Química, Universidade de Brasília, Brasília, 2006.
- BISHOP, E.; BRADSHAW, T. D. Autophagy modulation: a prudent approach in cancer treatment? **Cancer chemotherapy and pharmacology**, v. 82, n. 6, p. 913-922, 2018.
- BOYA, P.; REGGIORI, F.; CODOGNO, P. Emerging regulation and functions of autophagy. **Nature cell biology**, v. 15, n. 7, p. 713-720, 2013.
- BRAUN, E. *et al.* Best practices for foundations in molecular simulations [Article v1. 0]. **Living journal of computational molecular science**, v. 1, n. 1, 2019.
- BRAY, F. *et al.* Global cancer statistics 2018: GLOBOCAN estimates of incidence and mortality worldwide for 36 cancers in 185 countries. **CA: a cancer journal for clinicians**, v. 68, n. 6, p. 394-424, 2018.
- CAO, W. *et al.* AMP-activated protein kinase: a potential therapeutic target for triple-negative breast cancer. **Breast Cancer Research**, v. 21, n. 1, p. 29, 2019.
- CARMONA-GUTIERREZ, D. *et al.* Digesting the crisis: autophagy and coronaviruses. **Microbial Cell**, v. 7, n. 5, p. 119, 2020.
- CASE, D. A. *et al.* AMBER 11, University of California São Francisco, CA, 2010.
- CASSIDY, L. D. *et al.* Temporal inhibition of autophagy reveals segmental reversal of ageing with increased cancer risk. **Nature communications**, v. 11, n. 1, p. 1-12, 2020.
- CHIARAVALLI, M.; RENI, M.; O'REILLY, E. M. Pancreatic ductal adenocarcinoma: State-of-the-art 2017 and new therapeutic strategies. **Cancer treatment reviews**, v. 60, p. 32-43, 2017.

CONROY, T. *et al.* FOLFIRINOX versus gemcitabine for metastatic pancreatic cancer. **New England Journal of Medicine**, v. 364, n. 19, p. 1817-1825, 2011.

COSTA, M. A. S. **Investigação Teórica do Processo de Inclusão do Fluconazol com Ciclodextrinas e Calixareno**. 2014. 26f. Monografia (Bacharelado em Química) – Departamento de Química, Universidade Federal de São João del-Rei, São João del-Rei, 2014.

DE VIVO, M. *et al.* Role of molecular dynamics and related methods in drug discovery. **Journal of medicinal chemistry**, v. 59, n. 9, p. 4035-4061, 2016.

DIKIC, I.; ELAZAR, Z. Mechanism and medical implications of mammalian autophagy. **Nature reviews Molecular cell biology**, v. 19, n. 6, p. 349-364, 2018.

DOLGIN, E. Anticancer autophagy inhibitors attract ‘resurgent’ interest. **Nat. Rev. Drug Discov.**, v. 18, p. 408-410, 2019.

DUARTE, H. A.; ROCHA, W. R. Teoria do Funcional de Densidade. In: MORGON, N H.; COUTINHO, K. (Ed). **Métodos de química teórica e modelagem molecular**. 539f. São Paulo: Livraria da Física, 2007.

EL-SHAFFEY, E. S.; ELSHERBINY, E. S. Possible selective cytotoxicity of vanadium complex on breast cancer cells involving pathophysiological pathways. **Anti-Cancer Agents in Medicinal Chemistry (Formerly Current Medicinal Chemistry-Anti-Cancer Agents)**, v. 19, n. 17, p. 2130-2139, 2019.

FERMI, E. Eine statistische Methode zur Bestimmung einiger Eigenschaften des Atoms und ihre Anwendung auf die Theorie des periodischen Systems der Elemente. **Zeitschrift für Physik**, v. 48, n. 1-2, p. 73-79, 1928.

GONZÁLEZ, M. A. Force fields and molecular dynamics simulations. **École thématique de la Société Française de la Neutronique**, v. 12, p. 169-200, 2011.

GRIFFITHS, D. J. **Mecânica Quântica**. 2 ed. Ed. Pearson Prentice Hall. São Paulo, 2011.

HO, W. J.; JAFFEE, E. M.; ZHENG, L. The tumour microenvironment in pancreatic cancer-clinical challenges and opportunities. **Nature Reviews Clinical Oncology**, p. 1-14, 2020.

HOHENBERG, P.; KOHN, W. Inhomogeneous electron gas. **Physical review**, v. 136, n. 3B, p. B864, 1964.

HOCKNEY, R. W. The potential calculation and some applications. **Methods Comput. Phys.**, v. 9, p. 136, 1970.

HOLLINGSWORTH, Scott A.; DROR, Ron O. Molecular dynamics simulation for all. **Neuron**, v. 99, n. 6, p. 1129-1143, 2018.

HOSEIN, A. N.; BREKKEN, R. A.; MAITRA, A. Pancreatic cancer stroma: an update on therapeutic targeting strategies. **Nature Reviews Gastroenterology & Hepatology**, p. 1-19, 2020.

HUANG, Y. *et al.* Vanadium (IV)-chlorodipicolinate alleviates hepatic lipid accumulation by inducing autophagy via the LKB1/AMPK signaling pathway in vitro and in vivo. **Journal of inorganic biochemistry**, v. 183, p. 66-76, 2018.

INSTITUTO NACIONAL DE CÂNCER - INCA, (18 de julho de 2022). **Câncer de pâncreas**. Disponível em: <https://www.inca.gov.br/tipos-de-cancer/cancer-de-pancreas>. Acesso em: 05 de dezembro de 2022.

INSTITUTO NACIONAL DE CÂNCER - INCA, (26 de setembro de 2022). **Câncer de mama**. Disponível em: <https://www.inca.gov.br/tipos-de-cancer/cancer-de-mama>. Acesso em: 05 de dezembro de 2022.

INSTITUTO NACIONAL DE CÂNCER - INCA. **Estimativa | 2020 - Incidência de Câncer no Brasil**. Ministério da Saúde: Instituto Nacional de Câncer José Alencar Gomes da Silva. Rio de Janeiro: INCA, 2019. Disponível em: <https://www.inca.gov.br/sites/ufu.sti.inca.local/files//media/document//estimativa-2020-incidencia-de-cancer-no-brasil.pdf>. Acesso em: 05 de dezembro de 2022.

JORGENSEN, W. L.; MAXWELL, D. S.; TIRADO-RIVES, J. Development and testing of the OPLS all-atom force field on conformational energetics and properties of organic liquids. **Journal of the American Chemical Society**, v. 118, n. 45, p. 11225-11236, 1996.

KALEAĞASIOĞLU, F.; ALI, D. M.; BERGER, M. R. Multiple facets of autophagy and the emerging role of alkylphosphocholines as autophagy modulators. **Frontiers in pharmacology**, v. 11, p. 547, 2020.

KALIMUTHO, M. *et al.* Targeted therapies for triple-negative breast cancer: combating a stubborn disease. **Trends in pharmacological sciences**, v. 36, n. 12, p. 822-846, 2015.

KAUR, J.; DEBNATH, J. Autophagy at the crossroads of catabolism and anabolism. **Nature reviews Molecular cell biology**, v. 16, n. 8, p. 461-472, 2015.

KAUR, N. *et al.* Spin Inversion Phenomenon and Two-State Reactivity Mechanism for Direct Benzene Hydroxylation by V4O10 Cluster. **Journal of Physical Chemistry A**, v. 120, n. 48, p. 9588-9597, 2016.

KAUR, N.; GUPTA, S.; GOEL, N. Enantioselective synthesis of sulfoxide using an SBA-15 supported vanadia catalyst: a computational elucidation using a QM/MM approach. **Physical Chemistry Chemical Physics**, v. 19, n. 36, p. 25059-25070, 2017.

KLEEFF, J. *et al.* Pancreatic cancer. **Nature Reviews Disease Primers**, v. 2, n. 1, p. 1-22, 2016.

KOCAK, M. *et al.* Targeting autophagy in disease: established and new strategies. **Autophagy**, p. 1-23, 2021.

KONDO, Y. *et al.* The role of autophagy in cancer development and response to therapy. **Nature Reviews Cancer**, v. 5, n. 9, p. 726-734, 2005.

KOWALSKI, S. *et al.* Selective cytotoxicity of vanadium complexes on human pancreatic ductal adenocarcinoma cell line by inducing necroptosis, apoptosis and mitotic catastrophe process. **Oncotarget**, v. 8, n. 36, p. 60324, 2017.

KOWALSKI, S. *et al.* New oxidovanadium (IV) coordination complex containing 2-methylnitrilotriacetate ligands induces cell cycle arrest and autophagy in human pancreatic ductal adenocarcinoma cell lines. **International journal of molecular sciences**, v. 20, n. 2, p. 261, 2019.

LEE, KL. *et al.* Triple-negative breast cancer: Current understanding and future therapeutic breakthrough targeting cancer stemness. **Cancers**, v. 11, n. 9, p. 1334, 2019.

LEVINE, B.; KLIONSKY, D. J. Autophagy wins the 2016 Nobel Prize in Physiology or Medicine: Breakthroughs in baker's yeast fuel advances in biomedical research. **Proceedings of the National Academy of Sciences**, v. 114, n. 2, p. 201-205, 2017.

LI, P.; MERZ JR, K. M. Metal ion modeling using classical mechanics. **Chemical reviews**, v. 117, n. 3, p. 1564-1686, 2017.

LOPES, J. F. *et al.* Monte Carlo simulation of cisplatin molecule in aqueous solution. **The Journal of Physical Chemistry B**, v. 110, n. 24, p. 12047-12054, 2006.

MACHADO, P. A. *et al.* VOSalophen: a vanadium complex with a stilbene derivative - induction of apoptosis, autophagy, and efficiency in experimental cutaneous leishmaniasis. **Journal of Biological Inorganic Chemistry**, v. 22, n. 6, p. 929-939, 2017.

MAGALHÃES, C. S.; BARBOSA, H. J. C.; DARDELINE, L. E. Métodos de Docking Receptor-Ligante para o Desenho Racional de Compostos Bioativos. In: MORGON, N H.; COUTINHO, K. (Ed). **Métodos de química teórica e modelagem molecular**. 539f. São Paulo: Livraria da Física, 2007.

MARTÍNEZ, L.; BORIN, I. A.; SKAF M. S. Fundamentos de Simulação por Dinâmica Molecular. In: MORGON, N H.; COUTINHO, K. (Ed). **Métodos de química teórica e modelagem molecular**. 539f. São Paulo: Livraria da Física, 2007.

MBUGUA, S. N. *et al.* Beyond DNA-targeting in Cancer Chemotherapy. Emerging Frontiers-A Review. **Current topics in medicinal chemistry**, 2020.

MISHRA, P.; AMMANATHAN, V.; MANJITHAYA, R. Chemical biology strategies to study autophagy. **Frontiers in cell and developmental biology**, v. 6, p. 160, 2018.

MONTICELLI, L.; TIELEMAN, D. P. Force fields for classical molecular dynamics. In: Biomolecular simulations. **Springer**, p. 197-213, 2013.

MORGON, N. H. Computação em química teórica: informações técnicas. **Química nova**, v. 24, n. 5, p. 676-682, 2001.

NAIR, P. C.; MINERS, J. O. Molecular dynamics simulations: from structure function relationships to drug discovery. **In silico pharmacology**, v. 2, n. 1, p. 1-4, 2014.

NAM, H. J. Autophagy Modulators in Cancer: Focus on Cancer Treatment. **Life**, v. 11, n. 8, p. 839, 2021.

NAQVI, A. A. T. *et al.* Advancements in docking and molecular dynamics simulations towards ligand-receptor interactions and structure-function relationships. **Current topics in medicinal chemistry**, v. 18, n. 20, p. 1755-1768, 2018.

NAZIO, F. *et al.* Autophagy and cancer stem cells: molecular mechanisms and therapeutic applications. **Cell Death & Differentiation**, v. 26, n. 4, p. 690-702, 2019.

ONORATI, A. V. *et al.* Targeting autophagy in cancer. **Cancer**, v. 124, n. 16, p. 3307-3318, 2018.

OOSTENBRINK, C. *et al.* A biomolecular force field based on the free enthalpy of hydration and solvation: the GROMOS force-field parameter sets 53A5 and 53A6. **Journal of computational chemistry**, v. 25, n. 13, p. 1656-1676, 2004.

PEDDI, P. F.; ELLIS, M. J.; MA, C. Molecular basis of triple negative breast cancer and implications for therapy. **International journal of breast cancer**, v. 2012, 2012.

PEREIRA, R. A. **Estudo teórico de compostos de inclusão dos herbicidas 2,4-D e Dicamba em b-Ciclodextrina**. 2016. 102f. Tese (Doutorado em Química) - Departamento de Química, Universidade Federal de Lavras, Lavras, 2016.

PEREIRA, A. F. **Development and biological application of a quantum mechanically derived force field: the case of a platinum (II) complex**. 2020. 100f. Dissertação (Mestrado em Agroquímica)- Departamento de Química, Universidade Federal de Lavras, Lavras, 2020.

PESSOA, J. C. *et al.* Binding of vanadium ions and complexes to proteins and enzymes in aqueous solution. **Coordination Chemistry Reviews**, v. 449, p. 214192, 2021.

PLIEGO JR, J. R. Modelos contínuos do solvente: fundamentos. **Química Nova**, v. 29, n. 3, p. 535-542, 2006.

PRANDI, I. G. *et al.* Combining classical molecular dynamics and quantum mechanical methods for the description of electronic excitations: The case of carotenoids. **Journal of computational chemistry**, v. 37, n. 11, p. 981-991, 2016.

ROCHA, M. V. J. **Análise do modo de ação biocida de compostos organoestânicos: ensaios a partir de modelos**. 2010. 114f. Dissertação (Mestrado em Agroquímica) - Departamento de Química, Universidade Federal de Lavras, Lavras, 2010.

SANTOS, T. M. R. **Investigação Teórica do Composto de Inclusão formado entre b-Ciclodextrina e o Anticonvulsivante Benzaldeído Semicarbazona**. 2017. 87f. Monografia (Licenciatura em Química) - Departamento de Química, Universidade Federal de Lavras, Lavras, 2017.

SUNG, H. *et al.* Global cancer statistics 2020: GLOBOCAN estimates of incidence and mortality worldwide for 36 cancers in 185 countries. **CA: a cancer journal for clinicians**, v. 71, n. 3, p. 209-249, 2021.

SUTRADHAR, M. *et al.* Antiproliferative activity of heterometallic sodium and potassiumdioxidovanadium (V) polymers. **Journal of inorganic biochemistry**, v. 200, p. 110811, 2019.

TAVARES, C. A. *et al.* Molecular Dynamics-Assisted Interaction of Vanadium Complex-AMPK: From Force Field Development to Biological Application for Alzheimer's Treatment. **The Journal of Physical Chemistry B**, v. 127, n. 2, p. 495-504, 2023.

THOMAS, L. H. The calculation of atomic fields. In: **Mathematical Proceedings of the Cambridge Philosophical Society**. Cambridge University Press, p. 542-548, 1926.

THOMSEN, R.; CHRISTENSEN, M. H. **MolDock: a new technique for high-accuracy molecular docking**. *Journal of medicinal chemistry*, v. 49, n. 11, p. 3315-3321, 2006.

TULI, R. *et al.* Duration of therapy for locally advanced pancreatic cancer: Does it matter? **Cancer Medicine**, v. 9, n. 13, p. 4572-4580, 2020.

UGONE, V. *et al.* ESI-MS Study of the Interaction of Potential Oxidovanadium (IV) Drugs and Amavadin with Model Proteins. **Inorganic chemistry**, v. 59, n. 14, p. 9739-9755, 2020.

USCANGA-PERALES, G. I.; SANTUARIO-FACIO, S. K.; ORTIZ-LÓPEZ, R. Triple negative breast cancer: Deciphering the biology and heterogeneity. **Medicina universitaria**, v. 18, n. 71, p. 105-114, 2016.

VERLET, L. Computer "experiments" on classical fluids. I. Thermodynamical properties of Lennard-Jones molecules. **Physical review**, v. 159, n. 1, p. 98, 1967.

VON HOFF, D. D. *et al.* Increased survival in pancreatic cancer with nab-paclitaxel plus gemcitabine. **New England Journal of Medicine**, v. 369, n. 18, p. 1691-1703, 2013.

WALKER, C. L. *et al.* Systemic bisperoxovanadium activates Akt/mTOR, reduces autophagy, and enhances recovery following cervical spinal cord injury. **PLoS One**, v. 7, n. 1, 2012.

WANG, J. *et al.* Development and testing of a general amber force field. **Journal of computational chemistry**, v. 25, n. 9, p. 1157-1174, 2004.

WANG, J. *et al.* Automatic atom type and bond type perception in molecular mechanical calculations. **Journal of molecular graphics and modelling**, v. 25, n. 2, p. 247-260, 2006.

WORLD HEALTH ORGANIZATION (WHO). **Cancer**. 03 February 2022. Disponível em: <https://www.who.int/en/news-room/fact-sheets/detail/cancer>. Acesso em: 05 de dezembro de 2022.

WU, Y. *et al.* Sodium orthovanadate inhibits growth of human hepatocellular carcinoma cells in vitro and in an orthotopic model in vivo. **Cancer letters**, v. 351, n. 1, p. 108-116, 2014.

YUN, C. W.; LEE, S. H. The roles of autophagy in cancer. **International journal of molecular sciences**, v. 19, n. 11, p. 3466, 2018.

## **PARTE II**

## ARTIGO 1

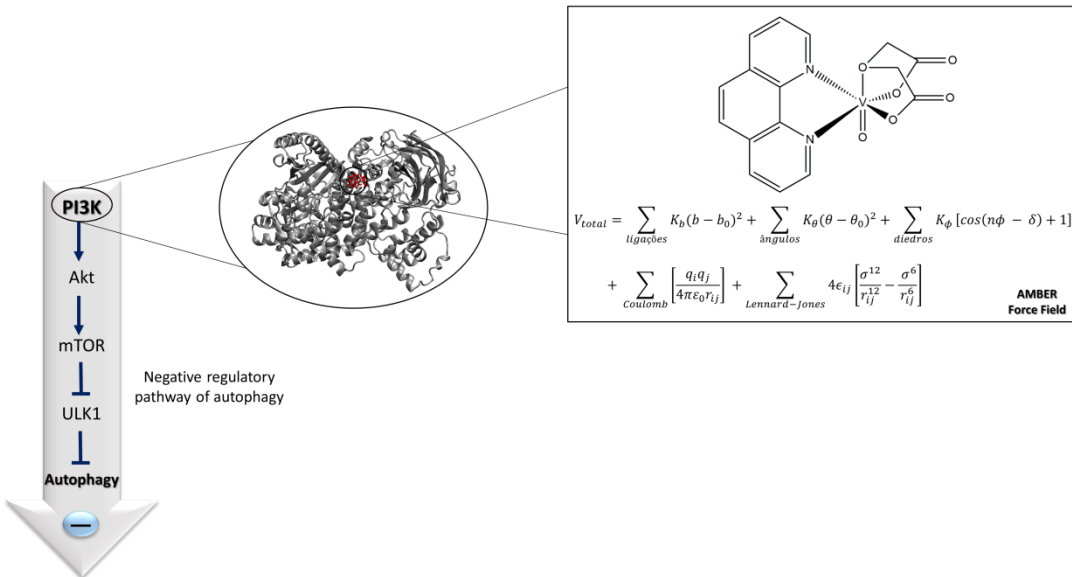
### Evaluation of autophagy inhibition to combat cancer: (vanadium complex)–protein interactions, parameterization, and validation of a new force field

#### Abstract

Autophagy has drawn attention from the scientific community, mainly because of its significant advantages over chemotherapeutic processes. One of these advantages is its direct action on cancer cells, avoiding possible side effects, unlike chemotherapy, which reaches tumor cells and affects healthy cells in the body, leading to a great loss in the quality of life of patients. In this way, it is known that vanadium complex (VC) [VO(oda)(phen)] has proven inhibition effect on autophagy process in pancreatic cancer cells. Keeping that in mind, Molecular Dynamics (MD) simulations can be considered excellent strategies to investigate the interaction of metal complexes and their biological targets. However, simulations of this type are strongly dependent on the appropriate choice of force field (FF). Therefore, this work proposes the development of AMBER FF parameters for VC, having a minimum energy structure as a starting point, obtained through DFT calculations with B3LYP/def2-TZVP level of theory plus ECP for the vanadium atom. An MD simulation in vacuum was performed to validate the developed FF. From the structural analyses, satisfying values of VC bond lengths and angles were obtained, where a good agreement with the experimental data and the quantum reference was found. The RMSD analysis showed an average of only 0.3%. Finally, we performed docking and MD (120 ns) simulations with explicit solvent between VC and PI3K. Overall, our findings encourage new parameterizations of metal complexes with significant biological applications, as well as allow to contribute to the elucidation of the complex process of autophagy.

**Keywords:** AMBER force field; vanadium complex; molecular dynamics; docking; autophagy.

## Graphical Abstract



### 1. Introduction

Without a doubt, COVID-19 (*Coronavirus Disease 2019*), caused by SARS-CoV-2 (*Severe Acute Respiratory Syndrome Coronavirus 2*), has taken the place of the dreaded disease of the century [1]. However, until recently, this prominent place was taken by cancer. According to the most recent estimate, cancer killed about 10.0 million people in the year 2020, in addition to a total of 19.3 million new cases [2,3].

Pancreatic cancer, also known as pancreatic ductal adenocarcinoma (PDAC), is among the most lethal cancers due to the aggressive nature of the tumor and late diagnosis [4-6]. It is estimated that in the year 2020, there were approximately 496,000 pancreatic cancer diagnoses and approximately 466,000 deaths were reported, amounting to 4.7% of cancer-related deaths worldwide [2].

The most up-to-date treatments are based on 5-fluorouracil or gemcitabine. However, these drugs offer only a brief survival period within months in the palliative care scenario [7]. Despite advances in the field, it can be said that there is no targeted therapy for pancreatic ductal adenocarcinoma, which leads to traditional treatments such as chemotherapy [8]. Nevertheless, despite aiming at eliminating cancer cells, chemotherapeutic processes end up also damaging

perfectly healthy cells and tissues, which induces side effects, leading to a drastic decrease in the quality of life of patients [9].

The limited effectiveness of this type of treatment, in addition to the increasing prevalence of drug-resistant tumors are strong arguments for seeking new treatment strategies. Thus, one of the most important challenges of modern scientific research is the pursue of new compounds that affect important processes in the development, progression, and metastasis of tumors [10,11].

Keeping that in mind, the literature has increasingly highlighted an important process that can be a great ally in fighting cancer, which is the processes of autophagy [12]. Autophagy has shown itself to be a growing field in science, mainly because it has recently been highlighted by the recognition of the contributions of Dr. Yoshinori Ohsumi, 2016 Nobel Prize laureate in Medicine or Physiology [13].

Autophagy (or macroautophagy) consists of cell recycling mechanism, where materials, such as damaged organelles, malformed proteins, etc., are taken to the lysosome for the degradation of the damaged materials to occur [14-16]. Its process starts when undue contents in the cytosol are encompassed by a membrane known as phagophore [17]. When this phagophore elongates, the autophagosome is formed, which will later fuse with the lysosome to form the autolysosome. Then, the captured material is degraded by the hydrolase enzymes present in the lysosome [18-21].

The important PI3K/Akt/mTOR pathway is a signaling pathway of the autophagy process and begins with the PI3K and Akt proteins that are responsible for positively regulating the mTOR protein [22-24]. In this sense, by means of therapeutic agents, the possibility of manipulating the pathways and proteins involved in the autophagic process is a welcome strategy in the fight against cancer [25].

It is known that autophagy, when related to cancer, has a dual behavior, i.e., it can either help cancer cells not to form or help already-formed cancer cells to survive [26]. This duality has so far divided numerous opinions in the scientific community. While nowadays, it is possible to understand that the possibility of manipulating autophagy, either inducing or inhibiting it (by means of pathways, proteins, drugs, etc.), is an important reality for cancer

treatments [25], after all, as it is known, cancer is divided into stages and, therefore, the manipulation of autophagy can be a great advantage [27].

On this basis, vanadium complexes are usefully reported in the literature for acting in the autophagy processes [28-35]. In this work, a vanadium complex that has proofed efficiency in inhibiting the autophagic process in pancreatic cancer cells (Figure 1) was the object of study [31].

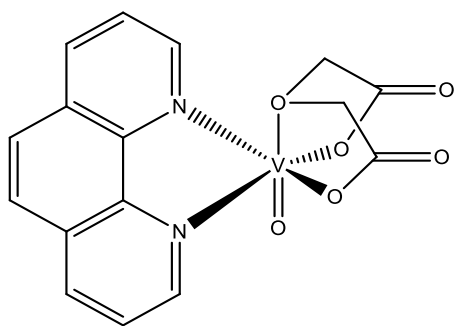


**Figure 1** – Vanadium complex (VC) under study,  $[\text{VO}(\text{oda})(\text{phen})]$ .

Understanding how the inhibition of autophagy occurs at the molecular level, i.e., what are the interactions between the molecular targets and the vanadium complex, can be perceived as a study that will provide important contributions to the field. In this sense, Classical Molecular Dynamics (MD) simulations can assist in this type of investigation.

However, MD simulations are strongly dependent on the proper choice of force fields, and it is also known that force field parameters for inorganic compounds are scarce and often not represented by standard force fields [36-39]. Furthermore, general force fields have a small number of atomic types, making it impossible to describe a wide-ranging number of compounds [40,41].

Regarding the parameterization of vanadium complexes, the development of specific force field parameters for this coordination environment of vanadium and specific type of complex (Figure 1) has not yet been reported in the literature. Moreover, making use of a general force field may not favor satisfactory results leading to unrealistic structures [42]. Thus, the need to develop specific force field parameters for the vanadium complex, the target of this study, is crucial.

Based on the above considerations, the goal of this work is divided into three parts: (i) To report the development of AMBER force field parameters, specific for the complex

[VO(oda)(phen)], from a minimum energy structure, obtained by quantum mechanics calculations (DFT). After that, (ii) to validate this new force field by implementing these new parameters to classical molecular dynamics simulations and comparing the post-calculation properties with experimental values [43] and the quantum reference (DFT). Finally, as mentioned previously, the manipulation of autophagy by therapeutic agents may be an excellent strategy to combat cancer [25]. Thus, the last goal is (iii) to investigate the types of interactions that occur between the vanadium complex and the protein responsible for initiating the autophagy signaling pathway (PI3K).

## 2. Computational details

### 2.1 QM calculations

The initial structure of the complex under study (Figure 1) was optimized through quantum mechanics calculations with B3LYP level of theory (exchange-correlation functional, used in Density Functional Theory - DFT) and the basis set def2-TZVP for ligand and LANL2DZ ECP for vanadium. This level of theory was successfully used and validated by Kaur and collaborators in purely theoretical investigations for vanadium complexes [44,45]. In this step, the *Gaussian 09* software [46] was used.

Furthermore, using the software ORCA 4.0 [47], relativistic effects on the vanadium complex were investigated with B3LYP/def2-TZVP level of theory through relativistic method ZORA. The ZORA-def2-TZVP basis set was successfully used for the vanadium metal by Cárdenas and co-workers recently [48].

Based on the lowest energy spatial arrangement found, the calculations of the non-polarizable RESP (Restrained Electrostatic Potential) partial atomic charges [49] and the Hessian matrix were performed with the same level of theory and software as the optimization calculation. This last calculation, based on the Seminario method [50], allowed the values of the force constants for the bonded terms to be obtained through the diagonalization of the Hessian matrix, using the Paratool plugin [51], available on the software VMD (Visual Molecular Dynamics) [52].

To validate the developed force field, an MD simulation was performed in vacuum ( $T = 300K$ ) using the AMBER 20 package [59], with a simulation time of 20 ns. The developed

parameters were validated through structural analysis of the bond lengths and bond angles of the complex, RMSD, and Bond Length Alternation (BLA) analysis. In addition, we investigated the symmetry of the molecule through the developed force field (FF). All results were compared with experimental values [43], quantum mechanics calculations and values obtained by GAFF. Regarding the MD performed using GAFF, there are no parameters for metals in this force field. Therefore, for the bonded terms involving the vanadium atom, the parameters developed and validated by us in this work were used.

## 2.2 Development of force field parameters

In classical Molecular Dynamics (MD) simulations, the force acting on each of the particles in the system is obtained by the contribution of each interaction with the other particles involved. Such forces are described by the potential energy functions of the structural contributions, bond lengths, bond angles, and dihedral angles, as well as interactions between non-bonded atoms [67].

Thus, potential energy ( $V$ ) is the energy that describes a given system and can be expressed, in general, as

$$\begin{aligned} V_{total} = & \sum_{bonds} K_b(b - b_0)^2 + \sum_{angles} K_\theta(\theta - \theta_0)^2 + \sum_{dihedrals} K_\phi [\cos(n\phi - \delta) + 1] \\ & + \sum_{Coulomb} \left[ \frac{q_i q_j}{4\pi\epsilon_0 r_{ij}} \right] + \sum_{Lennard-Jones} 4\epsilon_{ij} \left[ \frac{\sigma^{12}}{r_{ij}^{12}} - \frac{\sigma^6}{r_{ij}^6} \right] \end{aligned} \quad (1)$$

where  $K_b$ ,  $K_\theta$  and  $K_\phi$  are force constants;  $b$  and  $\theta$  correspond to the bond length and bond angle, respectively;  $b_0$  and  $\theta_0$  are the equilibrium values;  $n$  is the periodicity;  $\phi$  is the dihedral angle;  $\delta$  is the phase angle;  $r_{ij}$  is the distance between atoms  $i$  and  $j$ ;  $\epsilon$  is the depth of the potential well;  $\sigma$  is the distance at which the Lennard-Jones potential is zero;  $q_i$  and  $q_j$  are the charges of each atom; and  $\epsilon_0$  is the permittivity in vacuum. Equation (1) describes a typical force field, known as AMBER force field [68].

In general, the parameterization of intermolecular potentials ( $V_{Coulomb}$  and  $V_{Lennard-Jones}$ ) is a great challenge and, in addition, obtaining these parameters in particular may result in loss of precision of intramolecular parameters. Thus, it is important to inform that in this work the

parameterization of the intramolecular potentials was carried out, i.e., the parameters referring to the potentials  $V_{\text{bonds}}$ ,  $V_{\text{angles}}$  and  $V_{\text{dihedrals}}$ .

The force constants presented in equation (1), the equilibrium values, as well as the periodicity and the phase angle values were obtained by calculating the Hessian matrix (Subsection 2.1). To collect the data provided by the diagonalization of the Hessian matrix, the *Paratool* plugin [51], available in VMD software [52], was used. In this step the atomic types (Atom Types) were defined.

Regarding MD simulations in AMBER, it is necessary to define the Atom Types with only two characters. In this work, the characters used were letters and numbers (Figure 2). In addition, for the values of the bond length ( $K_b$ ) and bond angle ( $K_\theta$ ) constants that were equivalent (i.e., mirrored), an arithmetic average was performed to consider the symmetry of the molecule. An example of symmetric bonds is the V1-O2 and V1-O5 bonds, and an example of angles that are symmetric is the N1-V1-O2 and N2-V1-O5 angles.

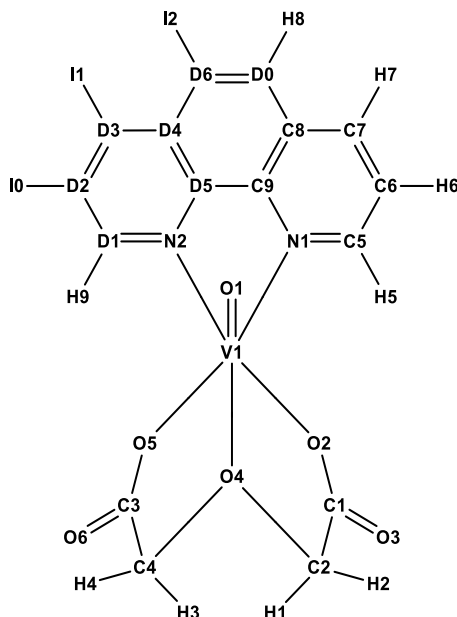


**Figure 2** – Atom types assigned to the vanadium complex (VC). Image generated using software *ChemDraw Ultra 12.0* [69].

Next, to obtain the Lennard-Jones potentials,  $\sigma$  and  $\epsilon$ , it was necessary to search the literature for GAFF (General AMBER Force Field) data regarding these two parameters. Thus, based on the investigation conducted by Wang and collaborators [70], it was possible to collect the parameters  $\sigma$  and  $\epsilon$  for all the vanadium complex atoms, except for the vanadium metal. The

van der Waals parameters for the vanadium atom were obtained based on a study of Šebesta and collaborators [71], since the parameterization of GAFF [70] was done targeting organic molecules.

Finally, obtaining the Coulomb interaction parameters of the vanadium complex,  $q_i$  and  $q_j$ , was performed by calculating the non-polarizable RESP partial atomic charges (Subsection 2.1). For this calculation, the same functional and basis function used in the optimization calculation was adopted.

The final layout of the topology file, according to Figure 2 and containing all the information described in this section, can be found in the Supporting Information (SI) file made available by the authors (Section S2). The values corresponding to the RESP charges are also found in the SI (Table S4).

### 2.3 PI3K protein treatment

The Protein Data Bank (PDB) database provides crystallographic structures of several proteins, including PI3K (code 3QJZ [53]; resolution = 2.90 Å). However, there are absent residues in the crystal of the molecule, which could lead, in a way, to inaccurate results in its analyses. Thus, we performed a treatment of the PI3K protein so that the missing residues are described within the PDB of the molecule, providing more reliable results.

To generate the protein model that contains all the original and the missing residues, the SWISS-MODEL platform [54] was used. After that, it was necessary to evaluate the model generated by the platform. Thus, we performed an alignment between the protein generated by SWISS-MODEL after completing the missing residues and the original protein (code 3QJZ [53]), using the “LovoAlign” protein structural alignment package [55]. From the aligned protein, we calculate its RMSD with relation to the original protein. The overlap between the two proteins (complete/aligned and original) is available in the Supporting Information file (Figure S1, Section S3).

## 2.4 Molecular Docking Calculations

Using the MolDock algorithm, present in the Molegro Virtual Docker (MVD) software [56], VC was docked within the human PI3K protein. The binding site considered for the docking study was the same used by Gurumoorthy and collaborators [57], where it was shown that the phenanthroline (*phen*) ligand promotes an interaction with the Arg839 residue of PI3K. Such interaction was evaluated in this study.

After further investigation to evaluate the best parameters for the best performance of docking with VC, a binding site within a restricted simulation space of 10 Å was considered. In addition, residues within a radius of 12 Å were considered flexible. At the end of the docking simulation of the complex on the protein, 100 poses were generated. Of these 100 poses (conformations and orientations of the VC), the pose that showed the lowest energy of interaction and indicated an interaction with residue Arg839 was chosen as the starting point for the next step, the Molecular Dynamics simulation.

## 2.5 Molecular Dynamics Simulations

The three preparation steps for Molecular Dynamics (MD) simulation, plus the last production step, were performed using PMEMD software [58], included in the AMBER 20 package [59].

As previous commented, the simulations were divided into four steps, namely: minimization, heating, equilibrium, and production. To perform the four steps, the force field "leaprc.ff14SB" was used to simulate the protein [60,61]. On the other hand, to simulate the vanadium complex, the force field developed and validated in this work was used. Furthermore, the simulations were carried out with explicit solvation which incorporated a cubic TIP3P water box [62]. Water molecules were added within a radius of 25 Å from the protein to the edge of the simulation box. Nine counterions ( $\text{Na}^+$ ) were added to neutralize the system. To counterbalance the charges of the amino acids in the protein, the neutral pH was considered, and the program *leap* was used. All four steps were performed considering the work of Arba *et al.* [60] and Farrokhzadeh *et al.* [61].

The first step (minimization) was performed to remove the bad contacts between the atoms, and to prepare the system for the heating step. This simulation was divided into two steps, the

first simulation (min1) performed with a system restriction of 500.0 kcal/mol and the second simulation (min2) performed without restriction. Both steps were performed at constant volume with 500 cycles of steepest descent and 5500 cycles of conjugate gradient methods.

In the next step, the system was heated gradually from 0 to 100 K (heat1), 100 to 200 K (heat2), and 200 to 300 K (heat3), each step being performed at 50 ps with a time step of 0.0005 ps and a constraint with a force constant of 5 kcal/mol. The system was then equilibrated at 300 K. For this third step, the simulations were divided into three parts, the first two steps (eq1 and eq2) being performed both at 50 ps with a force constant of 5 and 3 kcal/mol, respectively. Finally, the third equilibration step (eq3) was performed without restriction and with a time of 100 ps. In total, the heating step was performed at 150 ps and the equilibration step at 200 ps.

The MD simulation is finally performed in the production step, where a simulation time of 120 ns was considered in NPT ensemble without any restraint. All bonds involving hydrogen atoms were constrained using the SHAKE algorithm [63] with 2 fs integration time step. The particle-mesh Ewald algorithm method was used to treat long-range electrostatics interactions [64] of a periodic box with a non-bonding cutoff distance of 10.0 Å. In addition, the simulations were carried out using the Berendsen barostat and the Langevin thermostat [65] with a collision frequency of 1.0 ps<sup>-1</sup>.

The analyses of the trajectories of all simulation steps were performed with the CPPTRAJ module [66] and Visual Molecular Dynamics (VMD) software [52].

### **3. Results and Discussion**

#### **3.1 Static Calculations**

Computational modeling of drug-target systems is commonly performed to determine the likely mechanism of action. In this context, Molecular Dynamics (MD) simulations play a prominent role in this type of approach, providing further information about the structural properties and thermodynamic parameters of molecular systems [72].

Nevertheless, one of the biggest challenges in performing MD simulations to investigate the behavior of ligands with their molecular targets is to use a force field that satisfactorily reproduces the properties of interest [73]. In the case of metal complexes, the difficulty increases significantly [68,85].

In the *HyperChem 7.0* software [74], it is possible to find the AMBER force field available for the vanadium complex (VC) under study. In addition, the UFF (Universal Force Field) is also available for the target complex of this study in the software *Gaussian 09*. The result containing the relative errors of some bond lengths and bond angles are available in Table S1.

In general, metal atoms that occupy lower periods in the periodic table (sixth period onwards), have more pronounced relativistic effects. On the other hand, atoms that occupy the initial periods of the periodic table have a theoretical basis of study very well established by non-relativistic quantum mechanics [75]. Thus, the vanadium atom, which is located in period 4 of the periodic table, does not have such expressive relativistic effects. Even so, we performed calculations in the *ORCA* software [47], where the relativistic method ZORA is available, and a comparison of the previously mentioned data with calculations performed in the Gaussian 09 software was conducted [46].

Thus, Table S2 presents some values of VC bond lengths and bond angles, where three comparisons were made. The first is the comparison of the experimental values with the values obtained by the quantum calculation with B3LYP/def2-TZVP with ECP level of theory, where the role of the Effective Core Potential (ECP) is to modify the basis function so that relativistic effects on the vanadium atom are considered.

The second comparison was made between the experimental data and the data derived from the quantum-mechanical calculation obtained by the same functional and basis set, but without ECP and with the relativistic method ZORA, which, in turn, modifies the Hamiltonian of the Schrödinger equation to consider relativistic effects. Finally, the last comparison (Table S2, fourth column) concerns the comparison between the two quantum mechanics calculations previously mentioned, namely: B3LYP/def2-TZVP with ECP and B3LYP/def2-TZVP with ZORA.

It can be seen from Table S2 that the relative errors are low in all three comparisons. Furthermore, the low relative error originated from [ECP/ZORA] comparison shows that the level of theory used in this work to obtain the lower energy spatial arrangement of the vanadium complex is as effective as the relativistic method ZORA, thus validating the use of the B3LYP/def2-TZVP level of theory with ECP for vanadium. In other words, the lower energy geometry of the vanadium complex obtained by optimization with ZORA is appreciably equivalent to the result of optimization with ECP.

### **3.2 Dynamics Calculations: validation of FF parameters**

After the entire AMBER force field parameter development step (Subsection 2.2), efforts were directed towards validating the performed parameterization. To this end, a Molecular Dynamics (MD) simulation was performed in AMBER 20 simulation package [59]. The simulation was performed in vacuum with a total time of 20 ns, with the temperature equal to 300 K and a time interval of 1 fs. In order to ensure that the system undergoing the simulation has reached equilibrium, only the last 10 ns were considered for further analysis.

In general, the analyses performed in this work to validate the developed force field, called here as "New\_FF", were structural analyses with comparisons between the bond lengths and angles, obtained by different methods, namely: data obtained by X-ray crystallography [43]; DFT calculations with B3LYP functional and def2-TZVP and LANL2DZ ECP basis sets for vanadium; MD simulation with the new force field developed in this study; and, finally, an MD simulation with GAFF force field, under the same conditions as the previous MD. In addition, analyses of RMSD, BLA, geometry and symmetry of the molecule were performed. All the mentioned analyses are described in the following topic.

#### **3.2.1 Analysis of structural properties**

The first step to validate the parameterization performed in this work was to analyze the deviation of the spatial coordinate set of the complex in the simulation according to the coordinate set of the optimized geometry with DFT. This analysis was obtained by calculating the RMSD (*root mean square deviation*) [76] that provides the information of the difference between the predicted value (quantum reference) and the calculated value (MD with New\_FF).

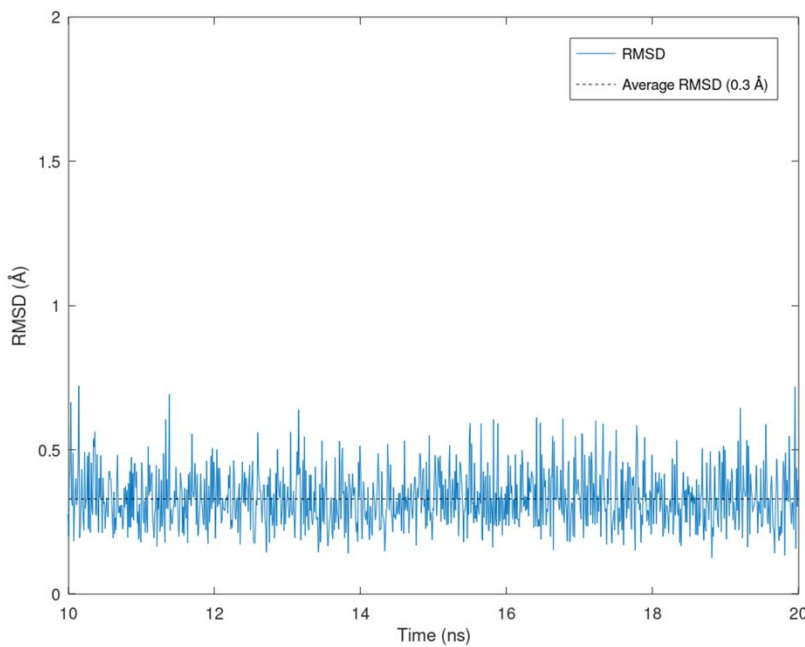


**Figure 3** – RMSD values ( $\text{\AA}$ ) versus time (ns) of MD simulation performed in vacuum at 300 K.

Based on the graph shown in Figure 3, it is possible to see a very good agreement between the two overlapping geometries. Subtracting the largest RMSD value from the smallest value, it is possible to find an oscillation amplitude of approximately 0.6  $\text{\AA}$ . Furthermore, the average of the values of the last 10 ns is  $0.3 \text{ \AA} \pm 0.003 \text{ \AA}$ . From these results, it can be clearly seen that the geometry provided by the force field parameter set proposed in this work is quite similar to the geometry obtained by quantum mechanics calculation.

The fact that the MD simulation was performed in vacuum enriches the good results obtained after the RMSD calculation since the complex is totally free to oscillate, i.e., there are no other molecules restricting its motion in the surroundings. In this sense, even oscillating freely, the VC presents a low and stable conformational variation throughout the simulation.

Furthermore, as a mean of comparison, we carried out an RMSD calculation between the MD coordinates with GAFF and the quantum reference (Figure S4). The average of the RMSD values was equal to 0.4  $\text{\AA}$ , which suggests that the performance of GAFF to describe the geometry of the VC, from the general point of view, was satisfactory. In addition, we also performed the calculation of the mean deviation for the bonds and angles of New\_FF and GAFF, both with respect to the DFT values (Table S6).

In the work reported by Álvarez and collaborators [43], the geometries obtained by DFT calculations and X-ray crystallography indicated that the vanadium metal and the other atoms connected to it have a distorted octahedral geometry. On this basis, a distorted octahedral is observed in Figure 4(a), where the spatial arrangement was obtained after a quantum mechanical (DFT) calculation. The same can be observed in Figure 4(b), where a slightly more distorted octahedral geometry was obtained from the MD simulation performed with the new set of force field parameters (New\_FF). The ideal octahedral geometry cannot be found since the angles around the vanadium metal do not have  $90^\circ$ . In addition, as a mean of comparison, the geometry obtained with GAFF is shown in Figure 4(c).

Moreover, it is also mentioned in the literature that the oxydiacetate ligand (oda - which corresponds to the atoms O2, O4 and O5 in Figure 4) adopts the *fac* arrangement and the central oxygen atom in the ligand (in our reference, oxygen O4) displays a *trans* geometry with respect to the vanadyl group (V1=O1) [43,77]. The geometry obtained by mean of the parameterization proposed in this work also reproduces this spatial arrangement.

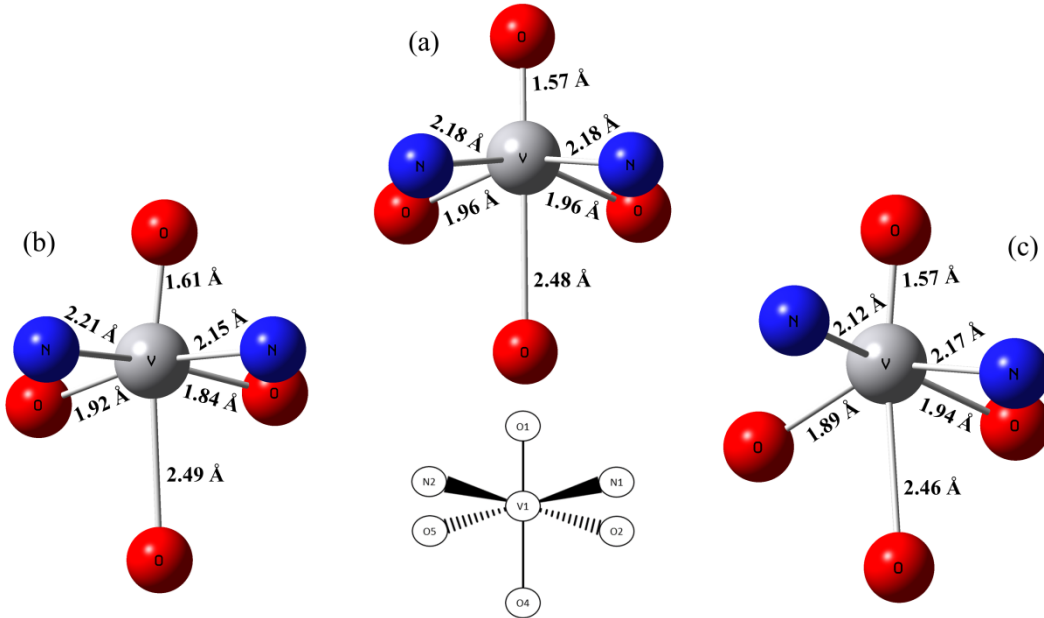


**Figure 4** – Distorted octahedral geometries of the VC obtained by (a) DFT calculation, (b) MD with New\_FF, and (c) MD with GAFF. The remaining atoms in the complex were deleted.

GAFF (General AMBER Force Field) is a force field often used in MD simulations, with success in many cases [70,78-80]. Howbeit, the developers of this useful force field aimed at organic molecules, which makes it difficult to apply to metal complexes [68,70]. Still, this work used GAFF parameters in an MD simulation in vacuum ( $T = 300$  K) with a total simulation

time of 20 ns [68]. The obtained results were confronted with experimental values [43] (Table 1).

**Table 1** – Bond lengths (Å) and angles (°) selected for the VC. Experimental values and average values obtained from the MD simulation with the GAFF force field.

Bond Lengths	Exp.	DFT	GAFF	Bond Lengths	Exp.	DFT	GAFF
<b>V1-O1</b>	1.59	1.57	1.56	<b>O3-C1</b>	1.22	1.22	1.21
<b>V1-O2</b>	1.97	1.96	1.91	<b>O4-C2</b>	1.43	1.43	1.46
<b>V1-O4</b>	2.30	2.48	2.46	<b>C1-C2</b>	1.51	1.53	1.51
<b>V1-N1</b>	2.11	2.18	2.18	<b>O5-C3</b>	1.28	1.30	1.33
<b>O2-C1</b>	1.28	1.30	1.33	<b>N1-C5</b>	1.32	1.32	1.39
Angles	Exp.	DFT	GAFF	Angles	Exp.	DFT	GAFF
<b>V1-O4-C2</b>	108.55	107.49	102.91	<b>O2-V1-O4</b>	76.02	72.85	71.10
<b>V1-N1-C5</b>	127.87	126.03	127.89	<b>O2-V1-O5</b>	90.93	98.65	105.45
<b>V1-O2-C1</b>	123.36	128.63	129.27	<b>O2-V1-N1</b>	90.78	87.36	82.26
<b>O1-V1-O2</b>	101.32	105.02	107.66	<b>O2-C1-O3</b>	124.34	125.83	121.70
<b>O1-V1-O4</b>	176.10	176.53	165.36	<b>C2-O4-C4</b>	114.77	116.68	114.82
<b>O1-V1-N1</b>	101.90	99.22	94.46	<b>N1-C5-C6</b>	122.08	122.01	119.28

From Table 1, the relative errors were calculated by considering equation (2). For example, for the O4-C2 bond and the O2-V1-O4 angle, the relative error values correspond to 2.1% and 6.5%, respectively.

$$\% = \frac{\text{calculated value} - \text{experimental value}}{\text{experimental value}} \times 100 \quad (2)$$

The vanadium complex under study in this work is comprised of 42 bonds and 80 angles. For each bond and angle, a percentage of relative error was obtained. Thus, the arithmetic mean of the module of values was obtained.

About 80.9% of the VC bond values, obtained from the MD simulation with the GAFF force field, varied in a relative error range of 0% to 11%. More precisely, the mean relative error of the comparison between the experimental and GAFF values was exactly 5.7%, with an average standard deviation of 0.001%.

The analysis of the bond angles was conducted in an analogous way. The average variation of the relative error of the comparison between the experimental values and the values obtained

by GAFF was equal to 2.7%. In other words, the relative error ranged around almost three percent, with an average standard deviation of 0.128%. Furthermore, it can be concluded that 81.2% (which corresponds to 65 angles out of 80) ranged between 0% and 4%.

The MD simulation with the implemented GAFF force field allowed the confirmation that GAFF is not a suitable force field to describe the vanadium complex under investigation. Indeed, its purpose is to describe organic molecules, however, the VC has two organic ligands, which makes the investigation of its applicability in our system valid.

It is important to highlight that GAFF is an excellent force field, however, it is usually applied to simulate organic molecules. In this sense, for the special case of [VO(oda)(phen)], the use of a specific force field to describe this metallic complex, such as New\_FF, is an advantage compared to general AMBER force field.

The proper choice of force field to use in Molecular Dynamics simulations is a crucial step for successful calculations and results. As mentioned previously, GAFF force field is not a suitable choice to describe the VC. Moreover, automatic force fields and those available in software Hyperchem 7.0 and Gaussian (AMBER and UFF, respectively) are not efficient to describe the molecule under study in this work. It is clear then that force fields that do not describe the system satisfactorily should be avoided.

Taking this into consideration, it is evident the need to develop a specific force field for the complex [VO(oda)(phen)], the focus of this work. After our efforts were directed towards the parameterization of the complex, validation was performed through an MD simulation in vacuum with the new implemented force field (New\_FF). Table 2 gathers some values of bond lengths and bond angles obtained from three methods, namely: X-ray crystallography (Exp.) [43]; quantum mechanical (DFT) calculations; and MD simulation with the new force field (New\_FF).

**Table 2** – Bond lengths (Å) and angles (°) selected for the VC. Experimental values, quantum reference values, and average values obtained from the MD simulation with New\_FF.

Bond Lengths	Exp.	DFT	New_FF	Bond Lengths	Exp.	DFT	New_FF
<b>V1-O1</b>	1.59	1.57	1.56	<b>O3-C1</b>	1.22	1.22	1.21
<b>V1-O2</b>	1.97	1.96	1.91	<b>O4-C2</b>	1.43	1.43	1.44
<b>V1-O4</b>	2.30	2.48	2.48	<b>C1-C2</b>	1.51	1.53	1.53
<b>V1-N1</b>	2.11	2.18	2.19	<b>O5-C3</b>	1.28	1.30	1.29
<b>O2-C1</b>	1.28	1.30	1.29	<b>N1-C5</b>	1.32	1.32	1.34
Angles	Exp.	DFT	New_FF	Angles	Exp.	DFT	New_FF
<b>V1-O4-C2</b>	108.55	107.49	101.86	<b>O2-V1-O4</b>	76.02	72.85	74.06
<b>V1-N1-C5</b>	127.87	126.03	129.23	<b>O2-V1-O5</b>	90.93	98.65	101.45
<b>V1-O2-C1</b>	123.36	128.63	127.10	<b>O2-V1-N1</b>	90.78	87.36	84.57
<b>O1-V1-O2</b>	101.32	105.02	106.58	<b>O2-C1-O3</b>	124.34	125.83	123.55
<b>O1-V1-O4</b>	176.10	176.53	172.14	<b>C2-O4-C4</b>	114.77	116.68	117.77
<b>O1-V1-N1</b>	101.90	99.22	94.77	<b>N1-C5-C6</b>	122.08	122.01	121.96

Analogously to the analyses performed in the comparison between the experimental values and the MD values with the GAFF force field, the analyses of the three comparisons of the data in Table 2 were made. The comparisons conducted were the experimental values with the New\_FF values (*Exp/MD*); values from the quantum reference (DFT) with the New\_FF values (*QM/MD*); and finally, the comparison between the experimental values and the DFT values (*Exp/QM*).

Regarding to the 42 VC bonds, we could conclude that 80.9% of the values of the relative errors of the *Exp/MD* comparison ranged between 0% and 10%. Although this seems like a wide range, the average of the values is only 4.8%, i.e., most of the relative errors oscillate around this value. In addition, the mean standard deviation was 0.001%.

The average relative error of the *QM/MD* comparison was 0.6%, showing an excellent agreement between the MD simulation with New\_FF and the quantum reference calculation (DFT). The variation of the latter comparison was between 0% and 2% for all bonds in the VC, where precisely 20 bonds had average relative error of 0%, 18 bonds with 1% and 4 bonds with 2%, totalizing the 42 bonds present in the molecule.

It is worth mentioning that the calculation of the relative error for the *QM/MD* comparison considered the value of the quantum reference as the truest value. Thus, in equation (2), instead

of the experimental value, the value obtained by the quantum mechanics calculation (DFT) was considered. The relative errors of the other comparisons (*Exp/MD* and *Exp/QM*) were obtained according to equation (2).

The comparison between the experimental data and the quantum reference (*Exp/QM*) values was performed to investigate whether the choice of the level of theory for the DFT calculations was a good choice. The range of variation for 34 bonds (representing 80.9% of the total bonds) was between 0% and 10%, however, the average of the values is only between 4.4%.

It is worth noting that the results obtained by comparing the New\_FF with the experimental values (*Exp/MD*) showed great similarity with the comparison of the DFT values and the experimental ones (*Exp/QM*). In other words, our proposed new force field had errors in the same range as the errors that the quantum structure presented. Moreover, this is explicit by looking at the average relative error of the *QM/MD* comparison, where the relative error values merely ranged around 0.6%.

The same analyses were performed for the set of 80 angles of the [VO(oda)(phen)] complex. Results of the first comparison (*Exp/MD*) provide a range of relative errors from 0% to 3% for 81.2% of the total angles of the molecule. The average relative errors were 2.0% and the mean standard deviation was 0.153%.

The comparison of the results between the quantum reference values and the New\_FF values (*QM/MD*), provided an average of a mere 1.4% and range of variation for 78.7% of the bonds (63 angles) from 0% to 2%. The *Exp/QM* comparison, on the other hand, indicates a range between 0% and 2% for 66 angles (82.5%), with an average error of 1.3%.

Remarkably low values are shown in the comparisons of the angles of the MD using the New\_FF with the experimental and quantum reference values. Strictly speaking, the force field developed by us shows excellent agreements, with the average relative errors of the bond angles for *Exp/MD* and *QM/MD* comparisons being 2.0% and 1.4%, respectively.

In references [77] and [81], the authors synthesized a few vanadium complexes, among them, the complexes  $[V(O)(oda)(H_2O)_2]$  **1**,  $[V(O)(oda)(N-N)].H_2O$  (N-N = bipy, **4**; phen, **5**). Complex **1** provides experimental values of some structural parameters and parameters of the molecule with *fac* arrangement, obtained after a DFT calculation (B3LYP/LANL2DZ level of

theory). Moreover, after X-ray analysis, the authors showed that system **4** obtained two independent molecules and that such molecules show little difference between each other.

Although complex **5** is identical to the complex under study in this work, the authors reported that the crystal quality was poor, making it impossible to represent the complex in detail. Even so, based on comparisons with the other complexes, especially complex **4**, the authors were able to extract important information about complex **5**. Thus, the information obtained from the analysis of the three complexes mentioned above were useful for our work.

Based on the parameters presented in Table 2, especially regarding the *Exp/MD* comparison, some bond lengths and bond angles showed relative errors greater than 3%. Therefore, these parameters are discussed below.

The V1-O4 bond (2.48 Å), obtained by New\_FF, was overestimated compared to its respective experimental value (2.30 Å), providing a relative error of 8.0%. However, in [77] this bond is also overestimated. This occurs both for complex **1** ([V(O)(oda)(H<sub>2</sub>O)<sub>2</sub>]) in its *fac* arrangement (2.44 Å) and for complex **4** ([V(O)(oda)(bpy)]], which has great similarity with the system under study in this work ([VO(oda)(phen)]) in the two molecules found, with values of 2.32 Å and 2.33 Å, respectively.

Additionally, when comparing the obtained value of the V1-O4 bond with the New\_FF (2.48 Å) and the quantum reference (2.48 Å), a relative error of 0.04% is found. As commented earlier, the comparison between the experimental and DFT (*Exp/QM*) data provided excellent agreement, which allows us to validate the obtained value of the V1-O4 bond (2.48 Å) based on the value obtained by the quantum reference.

The V1-O2 bond (1.91 Å) was underestimated by New\_FF compared to the experimental value (1.97 Å). However, in [77] the *fac* arrangement of complex **1**, similar to the *fac* arrangement of the VC under study in this work, shows the value for the V1-O2 bond of 1.92 Å, which provides a small relative error (0.5%) compared to the value given by New\_FF.

Finally, the V1-N1 bond showed an experimental value of 2.11 Å, while the MD simulation with the new force field provided a higher value of 2.19 Å. This led to a relative error of almost four percent (3.8%). In spite of that, looking at the bias of the *QM/MD* comparison, a relative error of 0.46% was found, since the quantum reference value for this bond was 2.18 Å. This understanding is acceptable, mainly because the validation of New\_FF in this study is done

based on two references, experimental values and values coming from quantum mechanics (DFT) calculations.

From the point of view of the bond angle analysis, it is already expected that the angle values will oscillate more compared to the bond length values. This is expected because the angle force constants ( $K_\theta$ ) are smaller than the bond force constants ( $K_b$ ) (see Section S2). Thus, the angular deformations are larger than the bond stretches. For this reason, angles in Table 2 with relative errors above 5% are discussed below.

Regarding the O1-V1-O2 bond angle, the new force field showed a higher value ( $106.58^\circ$ ) compared to the respective experimental value ( $101.32^\circ$ ). This angle also shows overestimated values in [77], with the complex  $[V(O)(oda)(H_2O)_2]$  showing *fac* arrangement and experimental values of  $106.95^\circ$  and  $108.30^\circ$ , respectively. Furthermore, the relative error of the QM/MD comparison for this angle was 1.5%, where the quantum reference value was  $105.02^\circ$ .

For the angle O2-V1-N1, the MD simulation with the new force field provided a value of  $84.57^\circ$ . The experimental value, on the other hand, was exactly  $90.78^\circ$ . Although suggesting a somewhat high difference, the quantum reference value ( $87.36^\circ$ ) was close to the New\_FF value, yielding a relative error of 3.2%.

The experimental value of the O2-V1-O5 bond angle, obtained by X-ray crystallography, was  $90.93^\circ$ , a bit far from the value provided by New\_FF ( $101.45^\circ$ ). However, this value can be validated by comparing with the value ( $101.60^\circ$ ) provided in [77] of its analogous complex (**1**), where the *fac* arrangement was found (spatial arrangement equivalent to that of VC). Moreover, in the comparison with the quantum reference (QM/MD) we found a relative error of only 2.8%.

The O1-V1-N1 bond angle has an experimental value of  $101.90^\circ$ . The force field developed in this work provided an underestimated value of  $94.77^\circ$  for this angle, but values of the similar complex (**4**)  $[V(O)(oda)(bipy)]$  [77] were also underestimated when compared to the experimental data. The DFT (quantum reference) value was  $99.22^\circ$ , giving a relative error of 4.5%. We consider this error acceptable, since angular deformations are more pronounced than bond stretches, as commented earlier.

Finally, the value of the V1-O4-C2 angle obtained by New\_FF, DFT, and the experimental value were  $101.86^\circ$ ,  $107.49^\circ$ , and  $108.55^\circ$ , respectively. The works cited do not comment on

this angle, however, an individual look at this angle does not portray the efficiency of the newly developed force field. Thus, the values of all the bond angles taken together provide the understanding that New\_FF can satisfactorily describe the set of bond angles of the vanadium complex [VO(oda)(phen)], the target system of this work.

By looking at Figure 2, it can be seen that there is a symmetry in the vanadium complex, where, for example, the V1-O2 and V1-O5 bonds are equivalent of each other, likewise the V1-N1-C9 and V1-N2-D5 angles are equivalent of each other. Some selected bond lengths and angles are gathered in Table S3, where a perfect symmetry between the experimental values is remarkable.

Regarding the values found after the MD simulation with New\_FF, excellent results are found, with differences only in the last decimal places. It is suggestive to remember that in each value of length and bond angle from the New\_FF has an associated standard deviation. Thus, it is understood that the new force field proposed in this work was able to efficiently reproduce the proposed symmetry in the vanadium complex.

In the system under study in this work, one of the vanadium atom ligands is phenanthroline, *phen*. This ligand is a bidentate heterocyclic organic compound, where three rings are connected to each other with alternating single and double bonds (Figure 2). Thus, it was included in the Supporting Information file an analysis of the Bond Length Alternation (BLA), Figure S5.

#### **4. Biomolecular study: (vanadium complex)–protein interactions**

A treatment with the PI3K protein was performed so that the missing residues were recovered. This procedure was performed using the SWISS-MODEL platform [54], as well as an alignment between the original protein and the one obtained through the “LovoAlign” program [55].

From this treatment, it was possible to recover 150 residues that were absent. The new number of residues, as well as those that were rescued, is available in the Supporting Information file, Table S5 (Section S3). In this work, we used the new numbering to identify the residues, since, from the molecular dynamic simulation, we found interactions between the VC and residues that were not described in the original protein file. However, the reader will

be able to make the equivalence with the original protein file by observing Table S5 in Section S3.

Even with the large number of new residues in the protein file, a RMSD of only 0.84 Å was obtained between the original protein and the complete, aligned protein. Supported by this value, as well as the good overlap observed between the two proteins (see Figure S1, in Section S3), it was possible to use the improved protein and perform more reliable docking and molecular dynamics simulations between the vanadium complex and PI3K biomolecule.

#### 4.1 Docking

Molecular docking simulations are well known for providing valuable information about the mechanism of action of a given ligand within a biomolecule, as well as providing remarkable relevance in the process of new drug discovery [82]. One important information that can be extracted from a docking calculation is the hydrogen bonds that a ligand performs with specific residues of the protein. The Molegro Virtual Docker (MVD) software [56] can be useful in evaluating such interactions.

In this context, as can be seen in Figure 5(b), four hydrogen bonds were indicated after docking simulation. The vanadium complex (VC) forms hydrogen bonds with the Arginine 697 (Arg697) and Lysine 526 (Lys526) residues of PI3K.

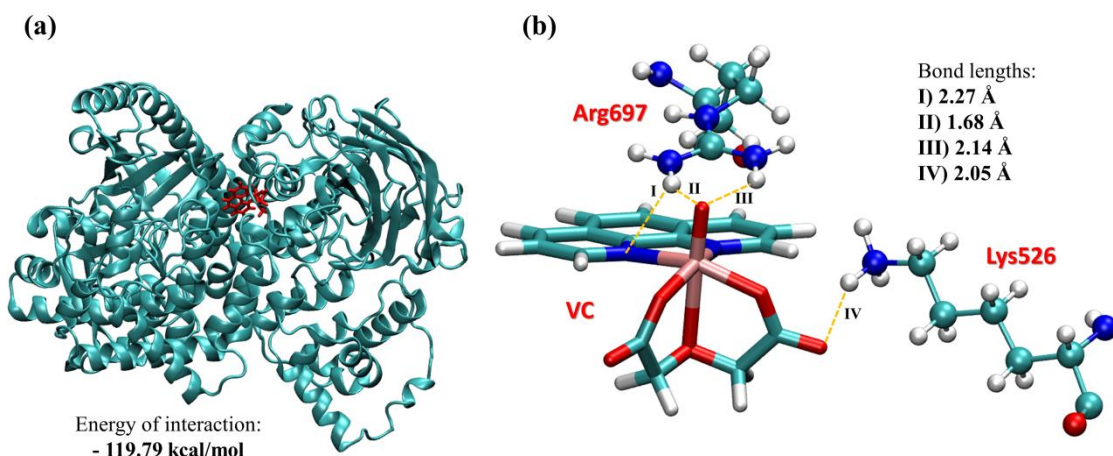


**Figure 5** - (a) Most favorable pose of the vanadium complex within the PI3K binding site and its energy of interaction. Complex in red. (b) Hydrogen bonds (in orange) formed between VC and residues Arg697 and Lys526. The bond lengths are pointed out.

The pose (conformation and orientation of the VC) shown in Figure 5(a) was chosen based on two criteria. The first criterion was guided by the choice of conformation and orientation of the complex within the protein. As mentioned earlier, it is known that the phenanthroline (phen) ligand, present in VC (Figure 1), exhibits interactions with the amino group of Arginine 839 [57] (Arginine 697 in our nomenclature). This information is reaffirmed by our docking study. By looking at Figure 5(b), it is possible to see that the nitrogen (N1 – Figure 2) of phenanthroline forms a hydrogen bond with the H of the amino group of the Arg697 residue (2.27 Å).

In addition, a second criterion was assigned from the energetic information that the interaction of the VC with the protein provides. The most favorable conformation and orientation (i.e., lower energy, therefore more stable) indicates better accommodation of the ligand within the binding site of the protein.

The pose observed in Figure 5(a) shows an intermolecular interaction energy of -119.79 kcal/mol. Therefore, based on the reported energy value, we can suggest that the vanadium complex does indeed interact with this PI3K binding site with favorable energy and conformation. Thus, the configuration obtained after the docking calculation is useful to serve as a starting point for other simulations, such as Molecular Dynamics simulations.

In general, it is important to note that, although docking studies provide important information at the molecular level of ligand-protein interactions, this type of study is not performed over time. In other words, investigations of this type provide information about a certain instant of time, which suggests to us that further investigations, over time, would be necessary.

## **4.2 Molecular Dynamics**

### **4.2.1 RMSD Analysis**

As previously stated, the best pose found in the molecular docking study was used to perform the MD step with explicit solvent. The RMSD calculation was performed considering the docking structure as coordinate reference. In this way, it was possible to observe the behavior of the protein and the complex over the course of 120 ns simulation (Figure 6).

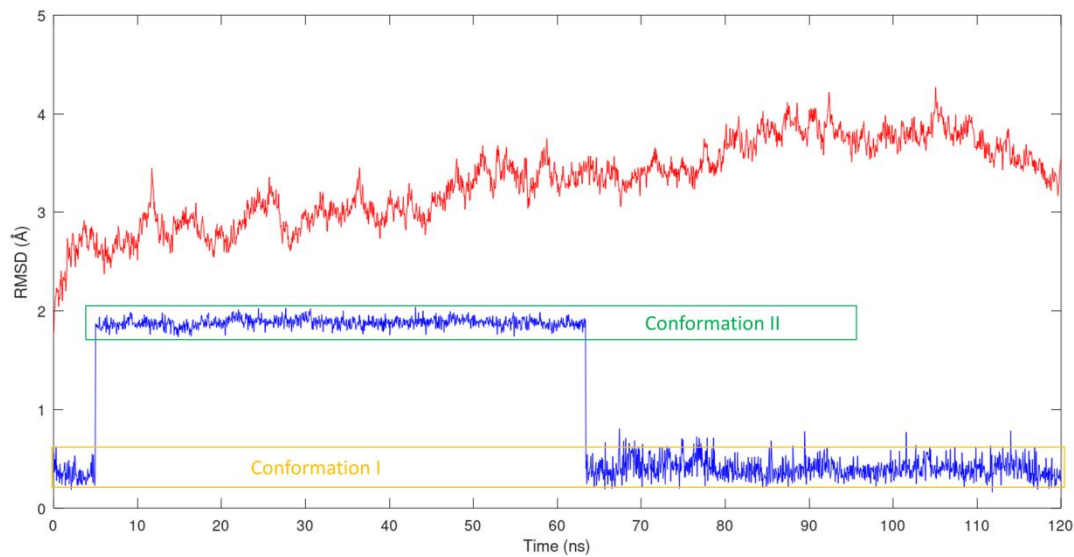


**Figure 6** - RMSD analysis of the evolution of VC (in blue) and PI3K (in red) during 120 ns of simulation. The docking structure was used as coordinate reference for the calculation.

The RMSD showed a low standard deviation value indicated throughout the simulation, only 0.74 Å, i.e., the complex had an oscillation smaller than 1 Å. In addition, the MD simulation revealed that the vanadium complex has two conformations, which can oscillate during the simulation time, being conformation I with values below 1 Å (highlighted in orange in Figure 6) and conformation II with values above 1 Å (highlighted in green in Figure 6).

In Figure S2, we present the two conformations obtained after the MD simulation. As can be seen, the difference occurs with the oxydiacetate ligand (*oda*), where in conformation I, the O1 atom is away from the viewer and the O4 atom is towards the viewer. The opposite occurs with conformation II. The spatial arrangement of the other atoms of the *oda* ligand can be seen in Figure S2.

Regarding the protein, the average oscillation was 3.30 Å. Furthermore, the standard deviation value was only 0.42 Å. Since this is a simulation where the effect of the solvent and the thermal effect are taken into account [83], we considered the mean value of the oscillation to be low, especially the observed standard deviation value.

#### 4.2.2 Hydrogen Bonds Analysis

Using the VMD (Visual Molecular Dynamics) software [52], it was possible to identify hydrogen bonds (H-Bonds) between the vanadium complex and the PI3K protein during the MD simulation trajectory (120 ns). H-Bonds with cutoff radius of 3.5 Å and cutoff angle of 30° were considered.

The interaction reported in the docking study between residue Arg697 and the phenanthroline ligand (Arg697@N1), mentioned by Gurumoorthy *et al.* [57], was not reported in our MD simulation. In our best knowledge, we could not compare our MD results with the work [57] since they did not perform this simulation, only docking.

On the other hand, we found interactions between Arginine 697 and the O1 of the vanadium complex. Therefore, the two H-Bonds between O1 and the Arg697 residue found after the docking simulation (see Figure 5(b)), were also found in our MD simulation, as can be seen in Figure 7(a).

It is also noteworthy that in the docking study (Subsection 4.1), in addition to indicating an interaction with the amino acid Arg697, we have mentioned a new VC interaction with the residue Lys526 (see Figure 5(b)). We found this bond (Lys526@O6(I)) in the MD simulation as well, as it can be seen in Figure 7(b).

In addition to the above-mentioned residues, another residue stands out for having significant frequencies of occurrences throughout MD simulation, Glu350. Regarding conformations I and II, this residue presented a frequency of 71.29% and 57.88%, respectively. Thus, we tracked the main atoms of VC that performed interactions with this residue.

Two intermolecular interactions between VC and Glu350 can be highlighted, the first interaction being with the O6 atom (Glu350@O6(I)) and the second with the O2 atom (Glu350@O2(II)), Figure 7 (c) and (d), respectively. Other VC atoms also form H-Bonds with the amino acid Glu350 (as O1, O3 and O5), however, the predominant occurrence during the 120 ns is of the Glu350@O6(I) and Glu350@O2(II) interactions.

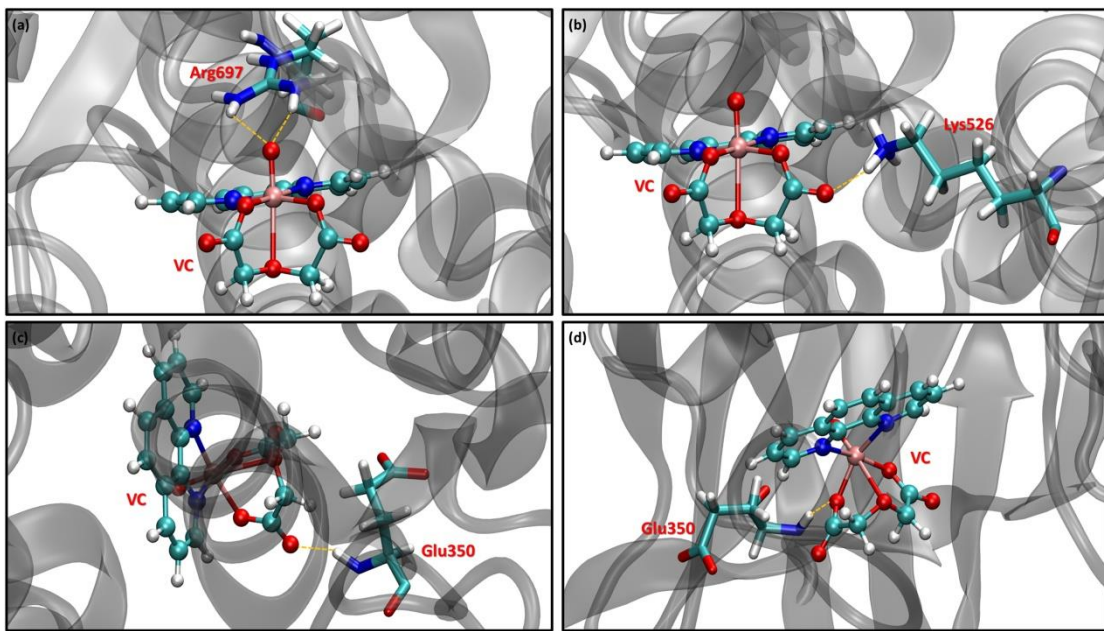


**Figure 7** - (a) Two H-Bonds Arg697@O1(I); (b) H-Bond Lys526@O6(I); (c) H-Bond Glu350@O6(I); and (d) H-Bond Glu350@O2(II). Hydrogen bonds in orange.

Through the analysis of Figure 7, it becomes interesting to observe that the vanadium complex always acts as an electron acceptor with respect to the PI3K protein residues. All pointed residues donate electrons from the N-H bond. In line with this, in all cases, the vanadium complex accepts electrons through the high electron affinity of the oxygen atoms in the complex.

The main hydrogen bonds, i.e., those involved in docking and MD simulations, as well as those that appeared more frequently, were described in the previous lines. However, we did find other H-Bonds. Although less frequent than those reported in Figure 7 (c) and (d), H-Bonds such as those shown in Figure S3 were detected after the MD simulation, namely: Asn829@O3(I) and Gln899@O1(II). On the other hand, H-Bonds with a minimum frequency of occurrence were not presented.

An important observation to make is the fact that H-Bonds such as Glu350@O6(I) (Figure 7(c)), Glu350@O2(II) (Figure 7(d)), Asn829@O3(I) (Figure S3(a)) and Gln899@O1(II) (Figure S3(b)), were found in residues that were not present in the original PI3K protein file. This reinforces the importance of the treatment performed with PI3K (Subsection 2.3), where we complete and align the protein before submitting it to the biomolecular study. The interactions cited would never have been observed if this previous treatment had not been carried out.

The combination of docking and MD simulations provides an elegant study of the interactions between a ligand and a molecular target. After the molecular docking calculation, it is suggestive to complement it with an MD simulation, due to the consideration of the effect of the solvent, as well as the thermal effect, allowing energy barriers to be overcome and thus new interactions to be pointed out [83].

In general, the atoms predominantly involved in hydrogen bonds were O1, O2, O3, O5, and O6. In addition, in a nutshell, we can also mention that the residue most involved in H-Bonds, in both conformations, was Glutamic Acid 350 (Glu350).

We suggest that the most stable conformation is conformation I. This conformation has x, y and z coordinates very close to the spatial coordinates of the docking structure (see Figure 6, where the RMSD was calculated with reference to the docking structure). Conformation II has an RMSD close to 2 Å, i.e., it moves further away from the reference. From our findings, conformation I is closer to quantum reference, and more importantly, the spatial arrangement observed in I is consistent with the crystallographic structure of the VC. Furthermore, the difference between conformation I and II was equal to 42,58 kcal/mol. Due conformation I being more favorable, it is possibly the biologically active one.

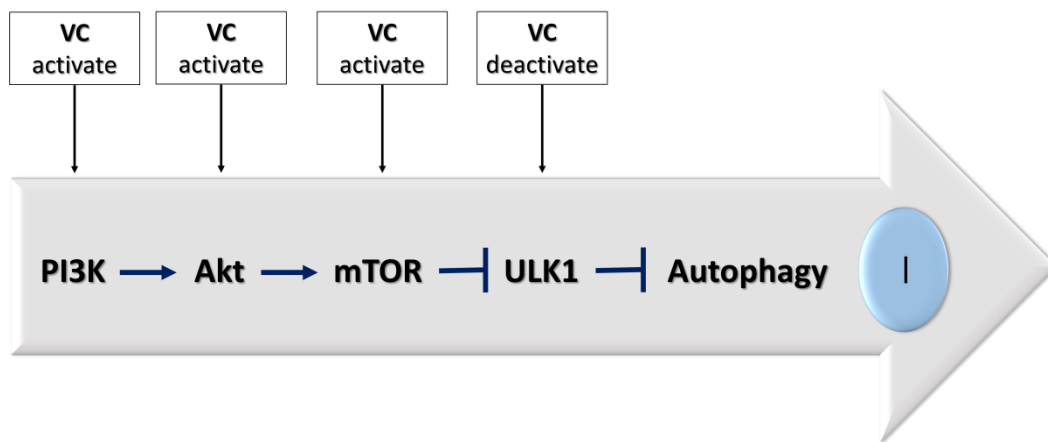
Now, an important question is, what causes the VC to remain in conformation I? At the beginning of the simulation, where the complex is in conformation I, it is observed that the residue Arg565 appears with high frequency (138%), while after the change to conformation II, this percentage decreased sharply (1.20%). The same scenario is observed with residues Lys526 (90%(I) - 2.14%(II)), Ser564 (71%(I) - 0%(II)), Arg697 (41%(I) – 2.48%(II)). Thus, our data point out that these residues are responsible for sustaining conformation I in the first moments of the simulation.

However, an important point is that, when returning from conformation II to conformation I (after 60 ns), the interactions with these residues are not restored. It is possible to attribute this to the fact that after more than half of the simulation had taken place (52.8%), the ligand moved slightly within the binding site. This can be confirmed by the fact that the interactions previously observed in conformation I (at the beginning of the simulation), are not the same observed in the second moment (i.e., after 60 ns of simulation). In this second moment of conformation I, the most accentuated interaction happened with residue Asn829. Thus, for this

moment, our findings put in evidence that the amino acid residue Asparagine 829 is responsible for sustaining the VC in conformation I.

#### 4.2.3 Analysis of autophagy inhibition through PI3K activation

The autophagy signaling pathway, PI3K/Akt/mTOR, is initiated by the PI3K and Akt proteins, which are responsible for positively regulating the mTOR protein. The mTOR negatively regulates the ULK1 protein, which in turn inhibits the entire autophagy process [84]. This can be understood more clearly through Scheme 1 presented below.



**Scheme 1** - Negative regulatory pathway of autophagy and performance of VC in interactions with each protein of the signaling pathway.

The vanadium complex (Figure 1) studied in this work is known for its ability to inhibit autophagy in pancreatic cancer cells [31]. Using this information and knowing the role of each protein in the autophagy signaling pathway (Scheme 1), it is possible to understand the action of VC against each of the proteins in the pathway.

For instance, the role of VC in interactions with the PI3K protein would be to activate this molecular target. By activating such protein, Akt will be activated, which in turn will activate mTOR, and the whole cascade will follow to inhibit autophagy. A different scenario would be seen in VC's actions with the ULK1 protein, where, in this case, the complex would have the role of deactivating the protein for autophagy inhibition to occur.

In this work, we sought to investigate the action of VC with the protein responsible for initiating the autophagy signaling process (PI3K). VC is able to inhibit autophagy, so its action

with respect to the PI3K protein is to activate this molecular target. Thus, our study could contribute to understanding how this activation occurs at the molecular level. For this purpose, the study of which hydrogen bonds occur during the MD simulation (previous topic), could be useful.

It was previously mentioned that the amino acids Arg565, Lys526, Ser564, Arg697 and Asn829 were responsible for sustaining the conformation I (more stable). Furthermore, the oxygen atoms of VC, with the exception of O4, were the most frequent in the intermolecular interactions. Based on this information, it is possible to suggest that the activation of PI3K occurs through these residues with the oxygens O1, O2, O3, O5 and O6.

Thus, to explore the manipulation of autophagy (due to its importance against cancer [25]), we can suggest that the opposite scenario, for instance, the deactivation of PI3K and thus induction of autophagy, can be achieved through modifications in the VC structure. However, it is important to emphasize that further studies are necessary for a better understanding of the manipulation of autophagy by therapeutic agents such as vanadium complexes. Thus, in the near future, efforts will be directed to a complete investigation of the autophagy signaling pathway.

## 5. Conclusions

In this work, we proposed three steps, the first being the development of the parameters; the second, validation of the new force field; and finally, a biomolecular study on protein-ligand interactions. The first part consisted of obtaining each parameter present in the potential energy equation that describes the AMBER force field. The second part focused on the validation of the developed parameter set. For this purpose, an MD simulation was performed in vacuum (300 K) with the new parameters implemented.

All our findings confirm the excellent performance of the AMBER force field parameters developed specifically for the vanadium complex under investigation in this work. From the structural analyses, it can be considered that New\_FF has been properly validated through comparisons with the experimental and quantum reference. Moreover, as comparative means, the difference in efficiency (when it comes to VC) between our force field and the widely used GAFF force field is clear.

In the last step of the work, we performed a study at the molecular level of the interactions between the vanadium complex and the PI3K biomolecule, a protein that is responsible for initiating the signaling of the autophagy process. This step consisted of two important types of molecular modeling simulations: docking simulations and classical molecular dynamics.

By performing the molecular docking simulation, the interaction between VC and the target protein was investigated. The interaction energy suggests that the VC interacts with PI3K at the considered binding site in a favorable and stable manner. Furthermore, our simulation demonstrated that the N1 of the phenanthroline ligand of VC forms a hydrogen bond with the amino group of the Arg839 (in our nomenclature: Arg697) residue of PI3K, as reported by the literature [57]. Therefore, the most stable conformation and orientation from the docking simulation was used as the starting point for the MD step.

The MD simulation provided an in-depth understanding over time of the VC behavior within PI3K, with a total simulation time of 120 ns. Through RMSD analysis, it can be observed that the vanadium complex has two conformations (I and II). In addition, a standard deviation of 0.74 Å and 0.42 Å was found for the VC and PI3K, respectively. After the execution of MD, new H-Bonds were pointed out, occurring predominantly with oxygen atoms of VC (O1, O2, O3, O5 and O6).

In order to contribute to the understanding of the mechanism of action of autophagy, we suggest that the H-Bonds between the PI3K protein and VC prevalent in the MD simulation are responsible for activating the protein, so that inhibition of autophagy occurs. Furthermore, we suggest that modifications in the VC structure, such as new bonds on oxygen atoms, would provide the opposite scenario, such as deactivation of PI3K as well as induction of autophagy. Future investigations of the autophagy signaling pathway may occur to complement the present work.

In general terms, this work fills the gap left by the absence of force field parameters for the vanadium complex [VO(oda)(phen)], which has great potential for applications in autophagy and, consequently, in anticancer treatments.

Thus, the authors acknowledge that this study contributes both to the theoretical perspective of developing force field parameters for metal complexes, and to the perspective of the biological applications, providing insights about the interactions between VC and PI3K,

allowing the contribution to the elucidation of the complex process of autophagy. If appropriate force field methods are used for large systems, in which *ab initio* calculations are highly computational-demanding, great advances can, in principle, be performed in designing proposing new vanadium complexes that are able, this time around, to induce autophagy. Moreover, the theoretical investigation developed here may serve as a starting point for other important work.

## **Declarations**

### **Ethics approval and consent to participate**

Not applicable.

### **Consent for publication**

All authors fully agree with the content of this work and are aware of the publication.

### **Availability of data and materials**

Along with the manuscript, the authors provide the Supporting Information file that was developed to assist in the results and discussion of the paper. In addition, we are available to send any files, if requested.

### **Competing interests**

The authors declare no conflict of interest.

### **Funding**

This work was carried out with the financial support of the Conselho Nacional de Desenvolvimento Científico e Tecnológico (CNPq, 307837/2014-9) and the Fundação de Amparo à Pesquisa do Estado de Minas Gerais (FAPEMIG, PPM-00831-15).

### **Acknowledgements**

The authors thank the Brazilian agencies CNPq, FAPEMIG and CAPES for the financial support.

## References

- [1] PHAM, Q. *et al.* Artificial intelligence (AI) and big data for coronavirus (COVID-19) pandemic: A survey on the state-of-the-arts. **Ieee Access**, v. 4, p. 1-19, 2020.
- [2] SUNG, H. *et al.* Global cancer statistics 2020: GLOBOCAN estimates of incidence and mortality worldwide for 36 cancers in 185 countries. **CA: a cancer journal for clinicians**, v. 71, n. 3, p. 209-249, 2021.
- [3] SHAH, U. A. Cancer and coronavirus disease 2019 (COVID-19)—facing the “C words”. **JAMA oncology**, v. 6, n. 9, p. 1330-1331, 2020.
- [4] GOLČIĆ, M. *et al.* Could fecal microbial transplantation offer a new potential in the treatment of metastatic pancreatic ductal adenocarcinoma?. **Medical Hypotheses**, v. 161, p. 110801, 2022.
- [5] GASIC, U. *et al.* Polyphenols as possible agents for pancreatic diseases. **Antioxidants**, v. 9, n. 6, p. 547, 2020.
- [6] CHENG, X.; ZHAO, G.; ZHAO, Y. Combination immunotherapy approaches for pancreatic cancer treatment. **Canadian Journal of Gastroenterology and Hepatology**, v. 2018, 2018.
- [7] HOSEIN, A. N.; BREKKEN, R. A.; MAITRA, A. Pancreatic cancer stroma: an update on therapeutic targeting strategies. **Nature Reviews Gastroenterology & Hepatology**, v. 17, n. 8, p. 487-505, 2020.
- [8] JIN, J.; TENG, C.; LI, T. Combination therapy versus gemcitabine monotherapy in the treatment of elderly pancreatic cancer: a meta-analysis of randomized controlled trials. **Drug design, development and therapy**, v. 12, p. 475, 2018.
- [9] PETRUCZYNIK, A. *et al.* Comparison of anticancer activity and HPLC-DAD determination of selected isoquinoline alkaloids from Thalictrum foetidum, Berberis sp. and Chelidonium majus extracts. **Molecules**, v. 24, n. 19, p. 3417, 2019.
- [10] HAQUE, A., BRAZEAU, D., AMIN, A. Perspectives on natural compounds in chemoprevention and treatment of cancer: an update with new promising compounds. **European Journal of Cancer**, v. 149, p. 165-183, 2021.
- [11] ZUO, W., KWOK, H. Development of marine-derived compounds for cancer therapy. **Marine Drugs**, v. 19, n. 6, p. 342, 2021.
- [12] SHENG, R.; QIN, Z. History and current status of autophagy research. In: **Autophagy: Biology and Diseases**. Springer, Singapore, p. 3-37, 2019.
- [13] FRAKE, R. A.; RUBINSZTEIN, D. Yoshinori Ohsumi's Nobel Prize for mechanisms of autophagy: from basic yeast biology to therapeutic potential. **Journal of the Royal College of Physicians of Edinburgh**, v. 46, n. 4, p. 228-233, 2016.
- [14] SHI, S. *et al.* Effects of tetrahedral DNA nanostructures on autophagy in chondrocytes. **Chemical Communications**, v. 54, n. 11, p. 1327-1330, 2018.
- [15] CZAJA, M. J. Function of autophagy in nonalcoholic fatty liver disease. **Digestive diseases and sciences**, v. 61, n. 5, p. 1304-1313, 2016.
- [16] SHI, Q. *et al.* Mechanisms of action of autophagy modulators dissected by quantitative systems pharmacology analysis. **International journal of molecular sciences**, v. 21, n. 8, p. 2855, 2020.
- [17] CAMPOS-BLÁZQUEZ, J. *et al.* Relationship Between ROS, Autophagy, and Cancer. 2022.
- [18] CUI, B.; YU, J. Autophagy: a new pathway for traditional Chinese medicine. **Journal of Asian natural products research**, v. 20, n. 1, p. 14-26, 2018.
- [19] XIAO, Z. *et al.* Autophagy promotion enhances the protective effect of Morroniside on human OA chondrocyte. **Bioscience, biotechnology, and biochemistry**, v. 84, n. 5, p. 989-996, 2020.

- [20] YANG, A.; HACHENEY, I.; WU, Y. Semisynthesis of autophagy protein LC3 conjugates. **Bioorganic & medicinal chemistry**, v. 25, n. 18, p. 4971-4976, 2017.
- [21] SUZUKI, H. *et al.* Structural biology of the core autophagy machinery. **Current opinion in structural biology**, v. 43, p. 10-17, 2017.
- [22] SU, R. *et al.* Particulate matter exposure induces the autophagy of macrophages via oxidative stress-mediated PI3K/AKT/mTOR pathway. **Chemosphere**, v. 167, p. 444-453, 2017.
- [23] LIN, C. *et al.* Honokiol induces autophagic cell death in malignant glioma through reactive oxygen species-mediated regulation of the p53/PI3K/Akt/mTOR signaling pathway. **Toxicology and Applied Pharmacology**, v. 304, p. 59-69, 2016.
- [24] LE SAGE, V. *et al.* Adapting the stress response: viral subversion of the mTOR signaling pathway. **Viruses**, v. 8, n. 6, p. 152, 2016.
- [25] DIKIC, I.; ELAZAR, Z. Mechanism and medical implications of mammalian autophagy. **Nature reviews Molecular cell biology**, v. 19, n. 6, p. 349-364, 2018.
- [26] AMARAVADI, R.; KIMMELMAN, A. C.; WHITE, E. Recent insights into the function of autophagy in cancer. **Genes & development**, v. 30, n. 17, p. 1913-1930, 2016.
- [27] KOCAK, M. *et al.* Targeting autophagy in disease: established and new strategies. **Autophagy**, p. 1-23, 2021.
- [28] EL-SHAFFEY, E. S.; ELSHERBINY, E. S. Possible selective cytotoxicity of vanadium complex on breast cancer cells involving pathophysiological pathways. **Anti-Cancer Agents in Medicinal Chemistry (Formerly Current Medicinal Chemistry-Anti-Cancer Agents)**, v. 19, n. 17, p. 2130-2139, 2019.
- [29] SUTRADHAR, M. *et al.* Antiproliferative activity of heterometallic sodium and potassium-dioxidovanadium (V) polymers. **Journal of inorganic biochemistry**, v. 200, p. 110811, 2019.
- [30] KOWALSKI, S. *et al.* New oxidovanadium (IV) coordination complex containing 2-methylnitrilotriacetate ligands induces cell cycle arrest and autophagy in human pancreatic ductal adenocarcinoma cell lines. **International journal of molecular sciences**, v. 20, n. 2, p. 261, 2019.
- [31] KOWALSKI, S. *et al.* Selective cytotoxicity of vanadium complexes on human pancreatic ductal adenocarcinoma cell line by inducing necroptosis, apoptosis and mitotic catastrophe process. **Oncotarget**, v. 8, n. 36, p. 60324, 2017.
- [32] HUANG, Y. *et al.* Vanadium (IV)-chlorodipicolinate alleviates hepatic lipid accumulation by inducing autophagy via the LKB1/AMPK signaling pathway in vitro and in vivo. **Journal of inorganic biochemistry**, v. 183, p. 66-76, 2018.
- [33] MACHADO, P A. *et al.* VOSalophen: a vanadium complex with a stilbene derivative—induction of apoptosis, autophagy, and efficiency in experimental cutaneous leishmaniasis. **JBIC Journal of Biological Inorganic Chemistry**, v. 22, n. 6, p. 929-939, 2017.
- [34] WALKER, C. L. *et al.* Systemic bisperoxovanadium activates Akt/mTOR, reduces autophagy, and enhances recovery following cervical spinal cord injury. **PLoS One**, v. 7, n. 1, p. e30012, 2012.
- [35] WU, Y. *et al.* Sodium orthovanadate inhibits growth of human hepatocellular carcinoma cells in vitro and in an orthotopic model in vivo. **Cancer letters**, v. 351, n. 1, p. 108-116, 2014.
- [36] LIN, F.; WANG, R. Systematic derivation of AMBER force field parameters applicable to zinc-containing systems. **Journal of chemical theory and computation**, v. 6, n. 6, p. 1852-1870, 2010.
- [37] KASHEFOLGHETA, S.; VERDE, A. V. Developing force fields when experimental data is sparse: AMBER/GAFF-compatible parameters for inorganic and alkyl oxoanions. **Physical Chemistry Chemical Physics**, v. 19, n. 31, p. 20593-20607, 2017.

- [38] ISLAM, M. *et al.* Interactions of hydrogen with the iron and iron carbide interfaces: a ReaxFF molecular dynamics study. **Physical Chemistry Chemical Physics**, v. 18, n. 2, p. 761-771, 2016.
- [39] ROGACKA, J. *et al.* Intermediate states approach for adsorption studies in flexible metal-organic frameworks. **Physical Chemistry Chemical Physics**, v. 21, n. 6, p. 3294-3303, 2019.
- [40] HU, L.; RYDE, U. Comparison of methods to obtain force-field parameters for metal sites. **Journal of Chemical Theory and Computation**, v. 7, n. 8, p. 2452-2463, 2011.
- [41] TAYLOR-EDINBYRD, K.; LI, T.; KUMAR, R. Effect of chemical structure of S-nitrosothiols on nitric oxide release mediated by the copper sites of a metal organic framework based environment. **Physical Chemistry Chemical Physics**, v. 19, n. 19, p. 11947-11959, 2017.
- [42] PRANDI, I. G. *et al.* Combining classical molecular dynamics and quantum mechanical methods for the description of electronic excitations: The case of carotenoids. **Journal of computational chemistry**, v. 37, n. 11, p. 981-991, 2016.
- [43] ÁLVAREZ, L. *et al.* Comparison of the coordination capabilities of thiodiacetate and oxydiacetate ligands through the X-ray characterization and DFT studies of [V (O)(tda)(phen)]·4H<sub>2</sub>O and [V (O)(oda)(phen)]·1.5 H<sub>2</sub>O. **Polyhedron**, v. 29, n. 16, p. 3028-3035, 2010.
- [44] KAUR, N. *et al.* Spin Inversion Phenomenon and Two-State Reactivity Mechanism for Direct Benzene Hydroxylation by V<sub>4</sub>O<sub>10</sub> Cluster. **Journal of Physical Chemistry A**, v. 120, n. 48, p. 9588-9597, 2016.
- [45] KAUR, N.; GUPTA, S.; GOEL, N. Enantioselective synthesis of sulfoxide using an SBA-15 supported vanadia catalyst: a computational elucidation using a QM/MM approach. **Physical Chemistry Chemical Physics**, v. 19, n. 36, p. 25059-25070, 2017.
- [46] FRISCH, M. J. *et al.* Gaussian 09, Revision E.01, Gaussian, Inc., Wallingford CT, 2013.
- [47] NEESE, F. Software update: the ORCA program system, version 4.0. **Wiley Interdisciplinary Reviews: Computational Molecular Science**, v. 8, n. 1, p. e1327, 2017.
- [48] CÁRDENAS, G. *et al.* A Force Field for a Manganese-Vanadium Water Oxidation Catalyst: Redox Potentials in Solution as Showcase. **Catalysts**, v. 11, n. 4, p. 493, 2021.
- [49] CORNELL, W. D. *et al.* Application of RESP charges to calculate conformational energies, hydrogen bond energies, and free energies of solvation. **Journal of the American Chemical Society**, v. 115, n. 21, p. 9620-9631, 2002.
- [50] SEMINARIO, J. M. Calculation of intramolecular force fields from second-derivative tensors. **International journal of quantum chemistry**, v. 60, n. 7, p. 1271-1277, 1996.
- [51] MAYNE, C. G. *et al.* Rapid parameterization of small molecules using the force field toolkit. **Journal of computational chemistry**, v. 34, n. 32, p. 2757-2770, 2013.
- [52] HUMPHREY, W.; DALKE, A.; SCHULTEN, K. VMD: visual molecular dynamics. **Journal of molecular graphics**, v. 14, n. 1, p. 33-38, 1996.
- [53] D'ANGELO, N. D. *et al.* Discovery and optimization of a series of benzothiazole phosphoinositide 3-kinase (PI3K)/mammalian target of rapamycin (mTOR) dual inhibitors. **Journal of medicinal chemistry**, v. 54, n. 6, p. 1789-1811, 2011.
- [54] WATERHOUSE, A. *et al.* SWISS-MODEL: homology modelling of protein structures and complexes. **Nucleic acids research**, v. 46, n. W1, p. W296-W303, 2018.
- [55] MARTÍNEZ, L.; ANDREANI, R.; MARTÍNEZ, J. M. Convergent algorithms for protein structural alignment. **BMC bioinformatics**, v. 8, n. 1, p. 1-15, 2007.
- [56] THOMSEN, R.; CHRISTENSEN, M. H. MolDock: a new technique for high-accuracy molecular docking. **Journal of medicinal chemistry**, v. 49, n. 11, p. 3315-3321, 2006.
- [57] GURUMOORTHY, P.; MAHENDIRAN, D.; RAHIMAN, A. K. Theoretical calculations, DNA interaction, topoisomerase I and phosphatidylinositol-3-kinase studies of water soluble mixed-ligand nickel (II) complexes. **Chimico-Biological Interactions**, v. 248, p. 21-35, 2016.

- [58] CASE, D. A. *et al.* The Amber biomolecular simulation programs. **Journal of computational chemistry**, v. 26, n. 16, p. 1668-1688, 2005.
- [59] CASE, D. A. *et al.* AMBER 2021, University of California, São Francisco, 2021.
- [60] ARBA, M.; SUFRIADIN, M.; TJAHJONO, D. H. Identification of Phosphatidylinositol 3-kinase δ (PI3Kδ) Inhibitor: Pharmacophore-based Virtual Screening and Molecular Dynamics Simulation. **Indonesian Journal of Chemistry**, v. 20, n. 5, p. 1070-1079, 2020.
- [61] FARROKHZADEH, A.; AKHER, F. B.; EGAN, T. J. Molecular Mechanism Exploration of Potent Fluorinated PI3K Inhibitors with a Triazine Scaffold: Unveiling the Unusual Synergistic Effect of Pyridine-to-Pyrimidine Ring Interconversion and CF<sub>3</sub> Defluorination. **The Journal of Physical Chemistry B**, v. 125, n. 36, p. 10072-10084, 2021.
- [62] JORGENSEN, W. L. *et al.* Comparison of simple potential functions for simulating liquid water. **The Journal of chemical physics**, v. 79, n. 2, p. 926-935, 1983.
- [63] RYCKAERT, J. P.; CICCOTTI, G.; BERENDSEN, H. J. C. Numerical integration of the cartesian equations of motion of a system with constraints: molecular dynamics of n-alkanes. **Journal of computational physics**, v. 23, n. 3, p. 327-341, 1977.
- [64] DARDEN, T.; YORK, D.; PEDERSEN, L. Particle mesh Ewald: An N· log (N) method for Ewald sums in large systems. **The Journal of chemical physics**, v. 98, n. 12, p. 10089-10092, 1993.
- [65] IZAGUIRRE, J. A. *et al.* Langevin stabilization of molecular dynamics. **The Journal of chemical physics**, v. 114, n. 5, p. 2090-2098, 2001.
- [66] ROE, D. R.; CHEATHAM III, T. E. PTraj and CPPtraj: software for processing and analysis of molecular dynamics trajectory data. **Journal of chemical theory and computation**, v. 9, n. 7, p. 3084-3095, 2013.
- [67] SALMASO, V.; MORO, S. Bridging molecular docking to molecular dynamics in exploring ligand-protein recognition process: an overview. **Frontiers in pharmacology**, v. 9, p. 923, 2018.
- [68] PEREIRA, A. F.; PRANDI, I. G.; RAMALHO, T. C. Parameterization and validation of a new force field for Pt (II) complexes of 2-(4'-amino-2'-hydroxyphenyl) benzothiazole. **International Journal of Quantum Chemistry**, v. 121, n. 6, p. e26525, 2021.
- [69] COUSINS, K. R. Computer review of ChemDraw Ultra 12.0. **Journal of the American Chemical Society**, v. 133, p. 8388-8388, 2011.
- [70] WANG, J. *et al.* Development and testing of a general amber force field. **Journal of computational chemistry**, v. 25, n. 9, p. 1157-1174, 2004.
- [71] SEBESTA, F. *et al.* Estimation of transition-metal empirical parameters for molecular mechanical force fields. **Journal of chemical theory and computation**, v. 12, n. 8, p. 3681-3688, 2016.
- [72] HOLLINGSWORTH, S. A.; DROR, R. O. Molecular dynamics simulation for all. **Neuron**, v. 99, n. 6, p. 1129-1143, 2018.
- [73] SANTOS, L. A.; PRANDI, I. G.; RAMALHO, T. C. Could quantum mechanical properties be reflected on classical molecular dynamics? The case of halogenated organic compounds of biological interest. **Frontiers in Chemistry**, v. 7, p. 848, 2019.
- [74] HYPERCHEM, Release 7.0 for Windows, Hypercube Inc. Gainesville FL USA, 2001.
- [75] PYPER, N. C. Relativity and the periodic table. **Philosophical Transactions of the Royal Society A**, v. 378, n. 2180, p. 20190305, 2020.
- [76] SARGSYAN, K.; GRAUFFEL, C.; LIM, C. How molecular size impacts RMSD applications in molecular dynamics simulations. **Journal of chemical theory and computation**, v. 13, n. 4, p. 1518-1524, 2017.
- [77] DEL RÍO, D. *et al.* Synthesis, molecular structure and properties of oxo-vanadium (IV) complexes containing the oxydiacetate ligand. **Dalton Transactions**, n. 9, p. 1813-1820, 2003.

- [78] SPRENGER, K., JAEGER, V., PFAENDTNER, J. The general AMBER force field (GAFF) can accurately predict thermodynamic and transport properties of many ionic liquids. **The Journal of Physical Chemistry B**, v. 119, n. 18, p. 5882-5895, 2015.
- [79] RABET, S., RAABE, G. Comparison of the GAFF, OPLSAA and CHARMM27 force field for the reproduction of the thermodynamics properties of furfural, 2-methylfuran, 2, 5-dimethylfuran and 5-hydroxymethylfurfural. **Fluid Phase Equilibria**, v. 554, p. 113331, 2022.
- [80] JÓJÁRT, B., MARTINEK, T. Performance of the general amber force field in modeling aqueous POPC membrane bilayers. **Journal of computational chemistry**, v. 28, n. 12, p. 2051-2058, 2007.
- [81] DEL RÍO, D. *et al.* Synthesis, antiapoptotic biological activity and structure of an oxovanadium (IV) complex with an OOO ligand donor set. **Inorganic Chemistry Communications**, v. 3, n. 1, p. 32-34, 2000.
- [82] NAQVI, A. A. T. *et al.* Advancements in docking and molecular dynamics simulations towards ligand-receptor interactions and structure-function relationships. **Current topics in medicinal chemistry**, v. 18, n. 20, p. 1755-1768, 2018.
- [83] ALONSO, H.; BLIZNYUK, A. A.; GREASY, J. E. Combining docking and molecular dynamic simulations in drug design. **Medicinal research reviews**, v. 26, n. 5, p. 531-568, 2006.
- [84] KALEAĞASIOĞLU, F.; A., D. M.; BERGER, M. R. Multiple facets of autophagy and the emerging role of alkylphosphocholines as autophagy modulators. **Frontiers in pharmacology**, v. 11, p. 547, 2020.
- [85] TAVARES, C. A. *et al.* Molecular Dynamics-Assisted Interaction of Vanadium Complex-AMPK: From Force Field Development to Biological Application for Alzheimer's Treatment. **The Journal of Physical Chemistry B**, v. 127, n. 2, p. 495-504, 2023.

## SUPPORTING INFORMATION

of

### Evaluation of autophagy inhibition to combat cancer: (vanadium complex)–protein interactions, parameterization, and validation of a new force field

#### Section S1

We performed the comparison between the experimental values and three levels of theory, namely: Molecular Mechanics (with the AMBER and UFF force field) and Quantum Mechanics (with B3LYP/def2-TZVP and LANL2DZ ECP for vanadium). The result containing the relative errors of some bond lengths and bond angles are available in Table S1.

It can clearly be seen that the available AMBER and UFF force fields fail when compared with the experimental values, while the comparison between the experimental and quantum data has appreciably lower relative errors (Table S1). High relative errors show how far away both the bond lengths and bond angles are from the experimental values, demonstrating that these two available force fields are not reliable to be used in MD simulations, as they do not reliably reproduce the structural parameters.

The relative errors presented in Tables S1 and S2 were obtained using the following equation.

$$\% = \frac{\text{calculated value} - \text{experimental value}}{\text{experimental value}} \times 100$$

**Table S1** – Comparative values of selected bond lengths and angles of the vanadium complex (VC), [VO(oda)(phen)]. Comparison between experimental values and three levels of theory: MM (with AMBER force field and UFF) and QM (B3LYP/def2-TZVP with ECP).

	Comparison (%) <i>[AMBER/Exp]</i>	Comparison (%) <i>[UFF/Exp]</i>	Comparison (%) <i>[B3LYP+ECP/Exp]</i>
V1 – O1	18.801	11.041	-1.136
V1 – O5	-8.105	0.963	-0.912
V1 – N2	-12.376	-1.470	3.461
V1 – O4	-16.630	-13.539	7.967
O5 – C3	-3.446	8.301	1.566
O6 – C3	0.903	3.366	-0.246

O4 – C4	-0.980	-1.120	0.140
O1 – V1 – O5	-18.246	-1.347	3.649
O5 – V1 – O2	44.346	82.675	8.517
O1 – V1 – N1	37.587	57.996	-2.644
O5 – V1 – N1	-61.030	-38.938	-2.227
O1 – V1 – N2	3.647	-12.551	-2.675
O5 – V1 – N2	-20.535	-1.229	-3.748
N1 – V1 – N2	1.557	1.715	-3.003
O1 – V1 – O4	-57.411	-44.139	0.249
O5 – V1 – O4	-11.507	7.909	-4.181
N2 – V1 – O4	71.418	109.161	2.980
O6 – C3 – O5	-3.788	-3.059	1.129
C4 – O4 – C2	1.228	-2.895	1.607

**Table S2** – Comparative values of selected bond lengths and angles of the vanadium complex. Comparison between experimental values and those obtained by quantum calculation with B3LYP/def2-TZVP+ECP (*[B3LYP+ECP/Exp]*) and B3LYP/def2-TZVP+ZORA (*[B3LYP+ZORA/Exp]*) levels of theory. Additional comparison of the values obtained by B3LYP/def2-TZVP+ECP and B3LYP/def2-TZVP+ZORA (*[ECP/ZORA]*).

	Comparison (%) <i>[B3LYP+ECP/Exp]</i>	Comparison (%) <i>[B3LYP+ZORA/Exp]</i>	Comparison (%) <i>[ECP/ZORA]</i>
V1 – O1	-1.136	-0.063	1.073
V1 – O5	-0.912	-0.659	0.255
V1 – N2	3.461	3.319	-0.138
V1 – O4	7.967	8.707	0.681
O5 – C3	1.566	1.723	0.154
O6 – C3	-0.246	-0.082	0.164
O4 – C4	0.140	0.420	0.279
O1 – V1 – O5	3.649	3.358	-0.281
O5 – V1 – O2	8.517	9.708	1.086
O1 – V1 – N1	-2.644	-2.034	0.622
O5 – V1 – N1	-2.227	-2.540	-0.321
O1 – V1 – N2	-2.675	-2.052	0.636
O5 – V1 – N2	-3.748	-4.466	-0.752
N1 – V1 – N2	-3.003	-3.034	-0.032
O1 – V1 – O4	0.249	-0.670	-0.924
O5 – V1 – O4	-4.181	-5.033	-0.898
N2 – V1 – O4	2.980	3.764	0.756
O6 – C3 – O5	1.129	1.154	0.025
C4 – O4 – C2	1.607	1.588	-0.019

**Table S3** – Selected bond lengths (Å) and bond angles (°). Bonds and angles on the left (first column) are equivalents of the bonds and angles on the right (fifth column).

Bonds	Exp.	DFT	New_FF	Bonds	Exp.	DFT	New_FF
Angles	Exp.	DFT	New_FF	Angles	Exp.	DFT	New_FF
<b>V1-O2</b>	1.974	1.956	1.912	<b>V1-O5</b>	1.974	1.956	1.914
<b>V1-N1</b>	2.109	2.182	2.189	<b>V1-N2</b>	2.109	2.182	2.183
<b>O3-C1</b>	1.218	1.215	1.214	<b>O6-C3</b>	1.218	1.215	1.214
<b>O4-C2</b>	1.428	1.430	1.438	<b>O4-C4</b>	1.428	1.430	1.437
<b>C8-C9</b>	1.406	1.408	1.432	<b>D4-D5</b>	1.406	1.408	1.433
<b>V1-O4-C2</b>	108.553	107.492	101.858	<b>V1-O4-C4</b>	108.553	107.463	101.962
<b>V1-N1-C9</b>	113.751	114.523	110.800	<b>V1-N2-D5</b>	113.751	114.521	111.043
<b>O3-C1-C2</b>	118.740	118.041	116.783	<b>O6-C3-C4</b>	118.740	118.049	117.024
<b>O4-C2-H1</b>	109.238	110.882	113.857	<b>O4-C4-H3</b>	109.238	110.895	113.751
<b>N1-C9-D5</b>	117.059	117.508	119.167	<b>C9-D5-N2</b>	117.059	117.507	119.191
<b>C6-C7-C8</b>	119.269	119.633	119.876	<b>D2-D3-D4</b>	119.269	119.633	119.871

## Section S2

Parameter file for the vanadium complex [VO(oda)(phen)]:

```

MASS
V1      50.94   0.0
O1      16.00   0.0
O2      16.00   0.0
O3      16.00   0.0
O4      16.00   0.0
C1      12.01   0.0
C2      12.01   0.0
H1      1.008   0.0
H2      1.008   0.0
O5      16.00   0.0
O6      16.00   0.0
C3      12.01   0.0
C4      12.01   0.0
H3      1.008   0.0
H4      1.008   0.0
N1      14.01   0.0
C5      12.01   0.0
H5      1.008   0.0
C6      12.01   0.0
H6      1.008   0.0

```

C7	12.01	0.0
H7	1.008	0.0
C8	12.01	0.0
C9	12.01	0.0
D0	12.01	0.0
H8	1.008	0.0
N2	14.01	0.0
D1	12.01	0.0
H9	1.008	0.0
D2	12.01	0.0
I0	1.008	0.0
D3	12.01	0.0
I1	1.008	0.0
D4	12.01	0.0
D5	12.01	0.0
D6	12.01	0.0
I2	1.008	0.0

## BONDS

V1	O1	570.466	1.5674
V1	O2	125.102	1.9559
V1	O5	125.102	1.9559
V1	O4	125.102	2.4801
V1	N1	75.380	2.1819
V1	N2	75.380	2.1819
O2	C1	481.548	1.2967
O3	C1	816.713	1.2153
O4	C2	295.047	1.4304
O4	C4	295.047	1.4304
C1	C2	239.237	1.5341
C2	H1	349.693	1.0907
C2	H2	345.592	1.0921
O5	C3	481.548	1.2967
O6	C3	816.713	1.2153
C3	C4	239.237	1.5341
C4	H3	349.693	1.0907
C4	H4	345.592	1.0921
N1	C5	478.336	1.3225
N1	C9	308.928	1.3529
C5	H5	374.227	1.0826
C5	C6	370.807	1.4026
C6	H6	376.826	1.0809
C6	C7	435.922	1.3745
C7	H7	370.763	1.0832
C7	C8	377.405	1.4085
C8	C9	301.199	1.4082
C8	D0	337.436	1.4315
C9	D5	250.369	1.4327
D0	H8	371.263	1.0828
D0	D6	473.841	1.3577
N2	D1	478.336	1.3225

N2	D5	308.928	1.3529
D1	H9	374.227	1.0826
D1	D2	370.807	1.4026
D2	I0	376.826	1.0809
D2	D3	435.922	1.3745
D3	I1	370.763	1.0832
D3	D4	377.405	1.4085
D4	D5	301.199	1.4082
D4	D6	337.436	1.4315
D6	I2	371.263	1.0828

## ANGLES

V1	O4	C2	20.129	107.49
V1	O4	C4	20.129	107.46
V1	O5	C3	20.129	128.62
V1	N1	C5	20.169	126.03
V1	N1	C9	13.867	114.52
V1	N2	D1	20.169	126.03
V1	N2	D5	13.867	114.52
V1	O2	C1	20.129	128.62
O1	V1	O2	20.129	105.02
O1	V1	O5	20.129	105.02
O1	V1	O4	20.129	176.53
O1	V1	N1	3.216	99.21
O1	V1	N2	3.216	99.21
O2	V1	O4	20.129	72.85
O2	V1	O5	20.129	98.65
O2	V1	N1	6.434	87.37
O4	V1	N1	6.434	83.51
O2	V1	N2	3.785	152.45
O2	C1	O3	46.963	125.83
O2	C1	C2	28.142	116.09
O3	C1	C2	41.689	118.05
O4	C2	C1	39.252	113.00
O4	C2	H1	18.355	110.89
O4	C2	H2	15.989	108.38
O4	C4	C3	39.252	113.00
O4	C4	H3	18.355	110.89
O4	C4	H4	15.989	108.38
C1	C2	H1	17.362	108.57
C1	C2	H2	18.733	108.09
C2	O4	C4	39.252	116.68
H1	C2	H2	8.278	107.76
O5	V1	O4	20.129	72.85
O5	V1	N1	3.785	152.45
O5	V1	N2	6.434	87.37
O4	V1	N2	6.434	83.52
O5	C3	O6	46.963	125.83
O5	C3	C4	28.142	116.09
O6	C3	C4	41.689	118.05
C3	C4	H3	17.362	108.57

C3	C4	H4	18.733	108.09
H3	C4	H4	8.278	107.76
N1	V1	N2	6.356	75.86
N1	C5	H5	27.908	116.21
N1	C5	C6	25.019	122.01
N1	C9	C8	21.013	122.60
N1	C9	D5	17.888	117.51
C5	N1	C9	22.316	119.33
C5	C6	H6	23.812	119.26
C5	C6	C7	24.514	119.40
H5	C5	C6	24.673	121.79
C6	C7	H7	23.665	120.76
C6	C7	C8	23.808	119.63
H6	C6	C7	23.605	121.34
C7	C8	C9	23.277	117.02
C7	C8	D0	27.227	123.96
H7	C7	C8	23.834	119.61
C8	C9	D5	19.899	119.89
C8	D0	H8	23.708	118.51
C8	D0	D6	22.765	121.09
C9	C8	D0	22.172	119.02
C9	D5	N2	17.888	117.51
C9	D5	D4	19.899	119.89
D0	D6	D4	22.765	121.09
D0	D6	I2	23.579	120.40
H8	D0	D6	23.579	120.40
N2	D1	H9	27.908	116.21
N2	D1	D2	25.019	122.01
N2	D5	D4	21.013	122.60
D1	N2	D5	22.316	119.33
D1	D2	I0	23.812	119.26
D1	D2	D3	24.514	119.40
H9	D1	D2	24.673	121.79
D2	D3	I1	23.665	120.76
D2	D3	D4	23.808	119.63
I0	D2	D3	23.605	121.34
D3	D4	D5	23.277	117.02
D3	D4	D6	27.227	123.96
I1	D3	D4	23.834	119.61
D4	D6	I2	23.708	118.51
D5	D4	D6	22.172	119.02

## DIHEDRALS

O1-V1-O2-C1	1	0.2285	349.22	4.000
O5-V1-O2-C1	1	0.2024	262.83	4.000
N1-V1-O2-C1	1	0.2126	250.38	4.000
N2-V1-O2-C1	1	0.1196	198.49	4.000
O1-V1-O5-C3	1	0.2285	349.22	4.000
O2-V1-O5-C3	1	0.2024	262.83	4.000
N1-V1-O5-C3	1	0.1196	198.49	4.000
N2-V1-O5-C3	1	0.2126	250.38	4.000

O1-V1-N1-C5	1	0.1403	261.01	4.000
O1-V1-N1-C9	1	0.1451	180.00	4.000
O2-V1-N1-C5	1	0.1092	203.74	4.000
O4-V1-N1-C5	1	0.1092	203.74	4.000
O2-V1-N1-C9	1	0.1000	340.29	4.000
O5-V1-N1-C5	1	0.1647	307.47	4.000
O5-V1-N1-C9	1	0.1552	236.51	4.000
N2-V1-N1-C5	1	0.0572	180.00	4.000
N2-V1-N1-C9	1	0.0360	180.00	4.000
O1-V1-N2-D1	1	0.1403	261.01	4.000
O1-V1-N2-D5	1	0.1451	180.00	4.000
O2-V1-N2-D1	1	0.1647	307.47	4.000
O2-V1-N2-D5	1	0.1552	236.51	4.000
O5-V1-N2-D1	1	0.1092	203.74	4.000
O4-V1-N2-D1	1	0.1092	203.74	4.000
O5-V1-N2-D5	1	0.1000	340.29	4.000
N1-V1-N2-D1	1	0.0573	180.00	4.000
N2-V1-N1-C5	1	0.0573	180.00	4.000
N1-V1-N2-D5	1	0.0360	180.00	4.000
N2-V1-N1-C9	1	0.0360	180.00	4.000
V1-O2-C1-O3	2	5.4000	180.00	2.000
V1-O2-C1-C2	2	5.4000	180.00	2.000
C4-O4-C2-C1	1	0.3830	0.00	-3.000
C4-O4-C2-C1	1	0.1000	180.00	2.000
C4-O4-C2-H1	3	1.1500	0.00	3.000
C4-O4-C2-H2	3	1.1500	0.00	3.000
C2-O4-C4-C3	1	0.3830	0.00	-3.000
C2-O4-C4-C3	1	0.1000	180.00	2.000
C2-O4-C4-H3	3	1.1500	0.00	3.000
C2-O4-C4-H4	3	1.1500	0.00	3.000
O2-C1-C2-O4	6	0.0000	180.00	2.000
O2-C1-C2-H1	1	0.8000	0.00	-1.000
O2-C1-C2-H1	1	0.0800	180.00	3.000
O2-C1-C2-H2	1	0.8000	0.00	-1.000
O2-C1-C2-H2	1	0.0800	180.00	3.000
O3-C1-C2-O4	6	0.0000	180.00	2.000
O3-C1-C2-H1	1	0.8000	0.00	-1.000
O3-C1-C2-H1	1	0.0800	180.00	3.000
O3-C1-C2-H2	1	0.8000	0.00	-1.000
O3-C1-C2-H2	1	0.0800	180.00	3.000
V1-O5-C3-O6	2	5.4000	180.00	2.000
V1-O5-C3-C4	2	5.4000	180.00	2.000
O5-C3-C4-O4	6	0.0000	180.00	2.000
O5-C3-C4-H3	1	0.8000	0.00	-1.000
O5-C3-C4-H3	1	0.0800	180.00	3.000
O5-C3-C4-H4	1	0.8000	0.00	-1.000
O5-C3-C4-H4	1	0.0800	180.00	3.000
O6-C3-C4-O4	6	0.0000	180.00	2.000
O6-C3-C4-H3	1	0.8000	0.00	-1.000
O6-C3-C4-H3	1	0.0800	180.00	3.000
O6-C3-C4-H4	1	0.8000	0.00	-1.000

O6-C3-C4-H4	1	0.0800	180.00	3.000
V1-N1-C5-H5	4	17.0000	180.00	2.000
V1-N1-C5-C6	4	17.0000	180.00	2.000
C9-N1-C5-H5	4	20.0000	180.00	2.000
C9-N1-C5-C6	4	20.0000	180.00	2.000
V1-N1-C9-C8	4	17.0000	180.00	2.000
V1-N1-C9-D5	4	17.0000	180.00	2.000
C5-N1-C9-C8	4	20.0000	180.00	2.000
C5-N1-C9-D5	4	20.0000	180.00	2.000
N1-C5-C6-H6	4	20.0000	180.00	2.000
N1-C5-C6-C7	4	20.0000	180.00	2.000
H5-C5-C6-H6	4	20.0000	180.00	2.000
H5-C5-C6-C7	4	20.0000	180.00	2.000
C5-C6-C7-H7	4	20.0000	180.00	2.000
C5-C6-C7-C8	4	20.0000	180.00	2.000
H6-C6-C7-H7	4	20.0000	180.00	2.000
H6-C6-C7-C8	4	20.0000	180.00	2.000
C6-C7-C8-C9	4	20.0000	180.00	2.000
C6-C7-C8-D0	4	20.0000	180.00	2.000
H7-C7-C8-C9	4	20.0000	180.00	2.000
H7-C7-C8-D0	4	20.0000	180.00	2.000
C7-C8-C9-N1	4	20.0000	180.00	2.000
C7-C8-C9-D5	4	20.0000	180.00	2.000
D0-C8-C9-N1	4	20.0000	180.00	2.000
D0-C8-C9-D5	4	20.0000	180.00	2.000
C7-C8-D0-H8	4	20.0000	180.00	2.000
C7-C8-D0-D6	4	20.0000	180.00	2.000
C9-C8-D0-H8	4	20.0000	180.00	2.000
C9-C8-D0-D6	4	20.0000	180.00	2.000
N1-C9-D5-N2	4	20.0000	180.00	2.000
N1-C9-D5-D4	4	20.0000	180.00	2.000
C8-C9-D5-N2	4	20.0000	180.00	2.000
C8-C9-D5-D4	4	20.0000	180.00	2.000
C8-D0-D6-D4	4	20.0000	180.00	2.000
C8-D0-D6-I2	4	20.0000	180.00	2.000
H8-D0-D6-D4	4	20.0000	180.00	2.000
H8-D0-D6-I2	4	20.0000	180.00	2.000
V1-N2-D1-H9	4	17.0000	180.00	2.000
V1-N2-D1-D2	4	17.0000	180.00	2.000
D5-N2-D1-H9	4	20.0000	180.00	2.000
D5-N2-D1-D2	4	20.0000	180.00	2.000
V1-N2-D5-C9	4	17.0000	180.00	2.000
V1-N2-D5-D4	4	17.0000	180.00	2.000
D1-N2-D5-C9	4	20.0000	180.00	2.000
D1-N2-D5-D4	4	20.0000	180.00	2.000
N2-D1-D2-I0	4	20.0000	180.00	2.000
N2-D1-D2-D3	4	20.0000	180.00	2.000
H9-D1-D2-I0	4	20.0000	180.00	2.000
H9-D1-D2-D3	4	20.0000	180.00	2.000
D1-D2-D3-I1	4	20.0000	180.00	2.000
D1-D2-D3-D4	4	20.0000	180.00	2.000

I0-D2-D3-I1	4	20.0000	180.00	2.000
I0-D2-D3-D4	4	20.0000	180.00	2.000
D2-D3-D4-D5	4	20.0000	180.00	2.000
D2-D3-D4-D6	4	20.0000	180.00	2.000
I1-D3-D4-D5	4	20.0000	180.00	2.000
I1-D3-D4-D6	4	20.0000	180.00	2.000
D3-D4-D5-C9	4	20.0000	180.00	2.000
D3-D4-D5-N2	4	20.0000	180.00	2.000
D6-D4-D5-C9	4	20.0000	180.00	2.000
D6-D4-D5-N2	4	20.0000	180.00	2.000
D3-D4-D6-D0	4	20.0000	180.00	2.000
D3-D4-D6-I2	4	20.0000	180.00	2.000
D5-D4-D6-D0	4	20.0000	180.00	2.000
D5-D4-D6-I2	4	20.0000	180.00	2.000
O1-V1-O4-C2	1	0.2285	349.22	4.000
O1-V1-O4-C4	1	0.2285	349.22	4.000
N1-V1-O4-C2	1	0.2126	250.38	4.000
N2-V1-O4-C4	1	0.2126	250.38	4.000
N1-V1-O4-C4	1	0.1196	198.49	4.000
N2-V1-O4-C2	1	0.1196	198.49	4.000
O4-V1-N1-C9	1	0.1000	340.29	4.000
O4-V1-N2-D5	1	0.1000	340.29	4.000
O4-V1-O2-C1	1	0.2024	262.83	4.000
O4-V1-O5-C3	1	0.2024	262.83	4.000
V1-O4-C2-C1	3	1.1500	0.00	3.000
V1-O4-C4-C3	3	1.1500	0.00	3.000
V1-O4-C2-H2	3	1.1500	0.00	3.000
V1-O4-C4-H4	3	1.1500	0.00	3.000
V1-O4-C4-H3	3	1.1500	0.00	3.000
V1-O4-C2-H1	3	1.1500	0.00	3.000
O5-V1-O4-C4	1	0.2024	262.83	4.000
O2-V1-O4-C2	1	0.2024	262.83	4.000
O2-V1-O4-C4	1	0.2024	262.83	4.000
O5-V1-O4-C2	1	0.2024	262.83	4.000

## NONBONDED

V1	2.7670	1.9040	!
O1	1.6612	0.2100	!
O2	1.6837	0.1700	!
O3	1.6612	0.2100	!
O4	1.6837	0.1700	!
C1	1.9080	0.0860	!
C2	1.9080	0.1094	!
H1	1.3870	0.0157	!
H2	1.3870	0.0157	!
O5	1.6837	0.1700	!
O6	1.6612	0.2100	!
C3	1.9080	0.0860	!
C4	1.9080	0.1094	!
H3	1.3870	0.0157	!
H4	1.3870	0.0157	!

N1	1.8240	0.1700	!
C5	1.9080	0.0860	!
H5	1.4590	0.0150	!
C6	1.9080	0.0860	!
H6	1.4590	0.0150	!
C7	1.9080	0.0860	!
H7	1.4590	0.0150	!
C8	1.9080	0.0860	!
C9	1.9080	0.0860	!
D0	1.9080	0.0860	!
H8	1.4590	0.0150	!
N2	1.8240	0.1700	!
D1	1.9080	0.0860	!
H9	1.4590	0.0150	!
D2	1.9080	0.0860	!
I0	1.4590	0.0150	!
D3	1.9080	0.0860	!
I1	1.4590	0.0150	!
D4	1.9080	0.0860	!
D5	1.9080	0.0860	!
D6	1.9080	0.0860	!
I2	1.4590	0.0150	!
END			

**Table S4** - Atomic charges (RESP) for the vanadium complex [VO(oda)(phen)].

Atom Types	<i>q /e<sup>-</sup></i>
V1	1.107564
O1	-0.492946
O2	-0.599641
O3	-0.599641
O4	-0.254503
C1	0.712157
C2	-0.064250
H1	0.067689
H2	0.067689
O5	-0.599641
O6	-0.599641
C3	0.712157

C4	-0.064250
H3	0.067689
H4	0.067689
N1	-0.149182
C5	0.034732
H5	0.134067
C6	-0.084664
H6	0.134337
C7	-0.147760
H7	0.142578
C8	0.171465
C9	0.052474
D0	-0.209342
H8	0.157235
N2	-0.149182
D1	0.034732
H9	0.134067
D2	-0.084664
I0	0.134337
D3	-0.147760
I1	0.142578
D4	0.171465
D5	0.052474
D6	-0.209342
I2	0.157235

### Section S3

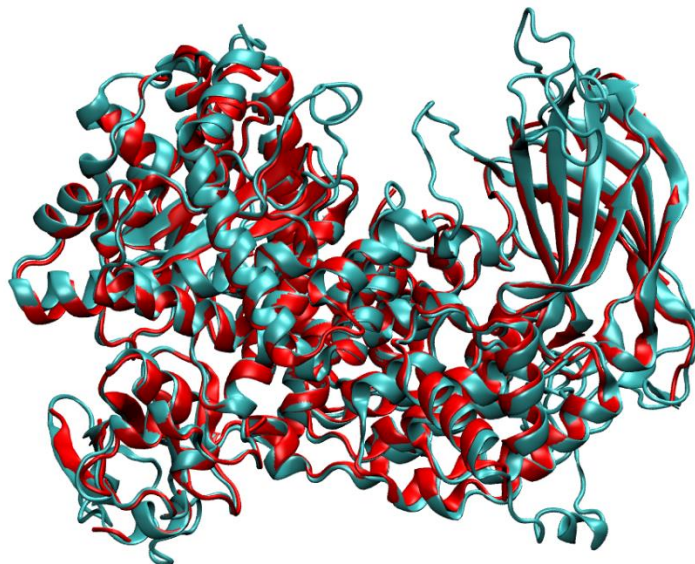


**Figure S1** – Overlay between the original PI3K (in red) and the complete and aligned PI3K (in cyan).

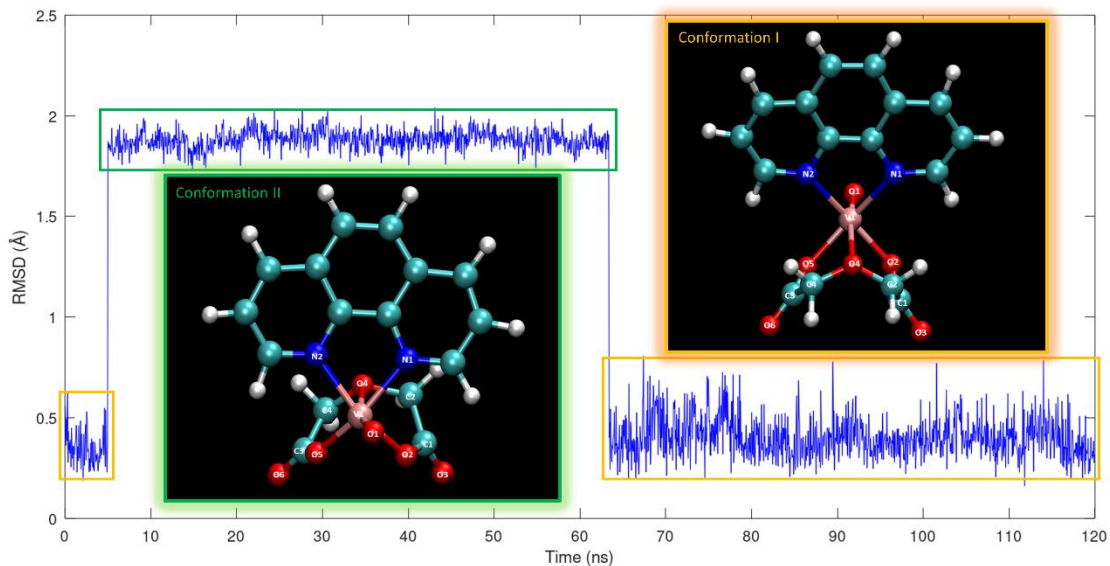


**Figure S2** – Two conformations of the vanadium complex. On the left, the structure outlined in green refers to conformation II and, on the right, the structure outlined in orange refers to conformation I.

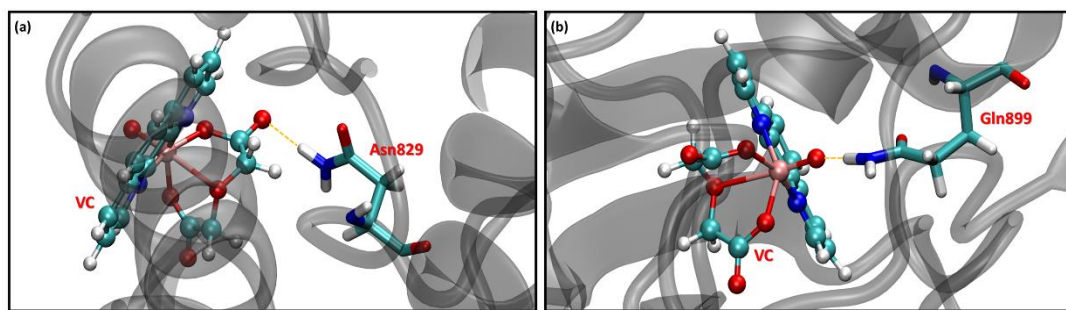


**Figure S3** – (a) H-Bond Asn829@O3(I); (a) H-Bond Gln899@O1(II). Hydrogen bonds in orange.

**Table S1** – Equivalence between the original (795 residues) and complete (945 residues) PI3K. Added residues are represented in bold (PI3K\_complete). Table divided into two columns.

PI3K_original		PI3K_complete	
SER	147	SER	5
GLN	148	GLN	6
ALA	149	ALA	7
PHE	150	PHE	8
GLN	151	GLN	9
ARG	152	ARG	10
GLN	153	GLN	11
LEU	154	LEU	12
THR	155	THR	13
ALA	156	ALA	14
LEU	157	LEU	15
ILE	158	ILE	16
GLY	159	GLY	17
TYR	160	TYR	18
ASP	161	ASP	19
VAL	162	VAL	20
THR	163	THR	21
ASP	164	ASP	22
VAL	165	VAL	23
SER	166	SER	24
ASN	167	ASN	25
VAL	168	VAL	26
HIS	169	HIS	27
ASP	170	ASP	28
ASP	171	ASP	29
GLU	172	GLU	30
LEU	173	LEU	31
GLU	174	GLU	32
PHE	175	PHE	33

THR	176	THR	34
ARG	177	ARG	35
ARG	178	ARG	36
GLY	179	GLY	37
LEU	180	LEU	38
VAL	181	VAL	39
THR	182	THR	40
PRO	183	PRO	41
ARG	184	ARG	42
MET	185	MET	43
ALA	186	ALA	44
GLU	187	GLU	45
VAL	188	VAL	46
ALA	189	ALA	47
SER	190	SER	48
ARG	191	ARG	49
ASP	192	ASP	50
PRO	193	PRO	51
LYS	194	LYS	52
LEU	195	LEU	53
TYR	196	TYR	54
ALA	197	ALA	55
MET	198	MET	56
HIS	199	HIS	57
PRO	200	PRO	58
TRP	201	TRP	59
VAL	202	VAL	60
THR	203	THR	61
SER	204	SER	62
LYS	205	LYS	63
PRO	206	PRO	64

LEU	207	LEU	65
PRO	208	PRO	66
GLU	209	GLU	67
TYR	210	TYR	68
LEU	211	LEU	69
TRP	212	TRP	70
LYS	213	LYS	71
LYS	214	LYS	72
ILE	215	ILE	73
ALA	216	ALA	74
ASN	217	ASN	75
ASN	218	ASN	76
CYS	219	CYS	77
ILE	220	ILE	78
PHE	221	PHE	79
ILE	222	ILE	80
VAL	223	VAL	81
ILE	224	ILE	82
HIS	225	HIS	83
-	-	<b>ARG</b>	<b>84</b>
-	-	<b>SER</b>	<b>85</b>
-	-	<b>THR</b>	<b>86</b>
THR	229	THR	87
SER	230	SER	88
GLN	231	GLN	89
THR	232	THR	90
ILE	233	ILE	91
LYS	234	LYS	92
VAL	235	VAL	93
SER	236	SER	94
PRO	237	PRO	95
ASP	238	ASP	96
ASP	239	ASP	97
THR	240	THR	98
PRO	241	PRO	99
GLY	242	GLY	100
ALA	243	ALA	101
ILE	244	ILE	102
LEU	245	LEU	103
GLN	246	GLN	104
SER	247	SER	105
PHE	248	PHE	106
-	-	<b>PHE</b>	<b>107</b>
-	-	<b>THR</b>	<b>108</b>
-	-	<b>LYS</b>	<b>109</b>
-	-	<b>MET</b>	<b>110</b>
-	-	<b>ALA</b>	<b>111</b>
-	-	<b>LYS</b>	<b>112</b>

-	-	<b>LYS</b>	<b>113</b>
-	-	<b>LYS</b>	<b>114</b>
-	-	<b>SER</b>	<b>115</b>
-	-	<b>LEU</b>	<b>116</b>
-	-	<b>MET</b>	<b>117</b>
-	-	<b>ASP</b>	<b>118</b>
-	-	<b>ILE</b>	<b>119</b>
-	-	<b>PRO</b>	<b>120</b>
-	-	<b>GLU</b>	<b>121</b>
-	-	<b>SER</b>	<b>122</b>
-	-	<b>GLN</b>	<b>123</b>
-	-	<b>SER</b>	<b>124</b>
-	-	<b>GLU</b>	<b>125</b>
-	-	<b>GLN</b>	<b>126</b>
-	-	<b>ASP</b>	<b>127</b>
-	-	<b>PHE</b>	<b>128</b>
VAL	271	VAL	129
LEU	272	LEU	130
ARG	273	ARG	131
VAL	274	VAL	132
CYS	275	CYS	133
GLY	276	GLY	134
ARG	277	ARG	135
ASP	278	ASP	136
GLU	279	GLU	137
TYR	280	TYR	138
LEU	281	LEU	139
VAL	282	VAL	140
GLY	283	GLY	141
GLU	284	GLU	142
THR	285	THR	143
PRO	286	PRO	144
ILE	287	ILE	145
LYS	288	LYS	146
ASN	289	ASN	147
PHE	290	PHE	148
GLN	291	GLN	149
TRP	292	TRP	150
VAL	293	VAL	151
ARG	294	ARG	152
HIS	295	HIS	153
CYS	296	CYS	154
LEU	297	LEU	155
LYS	298	LYS	156
ASN	299	ASN	157
GLY	300	GLY	158
GLU	301	GLU	159
GLU	302	GLU	160

ILE	303	ILE	161
HIS	304	HIS	162
VAL	305	VAL	163
VAL	306	VAL	164
LEU	307	LEU	165
ASP	308	ASP	166
THR	309	THR	167
PRO	310	PRO	168
PRO	311	PRO	169
ASP	312	ASP	170
PRO	313	PRO	171
ALA	314	ALA	172
LEU	315	LEU	173
ASP	316	ASP	174
GLU	317	GLU	175
VAL	318	VAL	176
ARG	319	ARG	177
LYS	320	LYS	178
GLU	321	GLU	179
-	-	<b>GLU</b>	<b>180</b>
-	-	<b>TRP</b>	<b>181</b>
-	-	<b>PRO</b>	<b>182</b>
-	-	<b>LEU</b>	<b>183</b>
-	-	<b>VAL</b>	<b>184</b>
-	-	<b>ASP</b>	<b>185</b>
-	-	<b>ASP</b>	<b>186</b>
-	-	<b>CYS</b>	<b>187</b>
-	-	<b>THR</b>	<b>188</b>
-	-	<b>GLY</b>	<b>189</b>
-	-	<b>VAL</b>	<b>190</b>
-	-	<b>THR</b>	<b>191</b>
-	-	<b>GLY</b>	<b>192</b>
-	-	<b>TYR</b>	<b>193</b>
-	-	<b>HIS</b>	<b>194</b>
-	-	<b>GLU</b>	<b>195</b>
-	-	<b>GLN</b>	<b>196</b>
-	-	<b>LEU</b>	<b>197</b>
-	-	<b>THR</b>	<b>198</b>
-	-	<b>ILE</b>	<b>199</b>
-	-	<b>HIS</b>	<b>200</b>
-	-	<b>GLY</b>	<b>201</b>
-	-	<b>LYS</b>	<b>202</b>
-	-	<b>ASP</b>	<b>203</b>
-	-	<b>HIS</b>	<b>204</b>
-	-	<b>GLU</b>	<b>205</b>
-	-	<b>SER</b>	<b>206</b>
-	-	<b>VAL</b>	<b>207</b>
-	-	<b>PHE</b>	<b>208</b>

-	-	<b>THR</b>	<b>209</b>
-	-	<b>VAL</b>	<b>210</b>
-	-	<b>SER</b>	<b>211</b>
-	-	<b>LEU</b>	<b>212</b>
-	-	<b>TRP</b>	<b>213</b>
ASP	356	ASP	214
CYS	357	CYS	215
ASP	358	ASP	216
ARG	359	ARG	217
LYS	360	LYS	218
PHE	361	PHE	219
ARG	362	ARG	220
VAL	363	VAL	221
LYS	364	LYS	222
ILE	365	ILE	223
ARG	366	ARG	224
GLY	367	GLY	225
ILE	368	ILE	226
ASP	369	ASP	227
ILE	370	ILE	228
PRO	371	PRO	229
VAL	372	VAL	230
-	-	<b>LEU</b>	<b>231</b>
-	-	<b>PRO</b>	<b>232</b>
-	-	<b>ARG</b>	<b>233</b>
-	-	<b>ASN</b>	<b>234</b>
-	-	<b>THR</b>	<b>235</b>
-	-	<b>ASP</b>	<b>236</b>
-	-	<b>LEU</b>	<b>237</b>
THR	380	THR	238
VAL	381	VAL	239
PHE	382	PHE	240
VAL	383	VAL	241
GLU	384	GLU	242
ALA	385	ALA	243
ASN	386	ASN	244
ILE	387	ILE	245
GLN	388	GLN	246
HIS	389	HIS	247
GLY	390	GLY	248
GLN	391	GLN	249
GLN	392	GLN	250
VAL	393	VAL	251
LEU	394	LEU	252
CYS	395	CYS	253
GLN	396	GLN	254
ARG	397	ARG	255
ARG	398	ARG	256

THR	399	THR	257
SER	400	SER	258
PRO	401	PRO	259
LYS	402	LYS	260
PRO	403	PRO	261
PHE	404	PHE	262
THR	405	THR	263
GLU	406	GLU	264
GLU	407	GLU	265
VAL	408	VAL	266
LEU	409	LEU	267
TRP	410	TRP	268
ASN	411	ASN	269
VAL	412	VAL	270
TRP	413	TRP	271
LEU	414	LEU	272
GLU	415	GLU	273
PHE	416	PHE	274
SER	417	SER	275
ILE	418	ILE	276
LYS	419	LYS	277
ILE	420	ILE	278
LYS	421	LYS	279
ASP	422	ASP	280
LEU	423	LEU	281
PRO	424	PRO	282
LYS	425	LYS	283
GLY	426	GLY	284
ALA	427	ALA	285
LEU	428	LEU	286
LEU	429	LEU	287
ASN	430	ASN	288
LEU	431	LEU	289
GLN	432	GLN	290
ILE	433	ILE	291
TYR	434	TYR	292
CYS	435	CYS	293
-	-	GLY	294
-	-	LYS	295
-	-	ALA	296
-	-	PRO	297
-	-	ALA	298
-	-	LEU	299
-	-	SER	300
-	-	SER	301
-	-	LYS	302
-	-	ALA	303
-	-	SER	304

-	-	ALA	305
-	-	GLU	306
-	-	SER	307
-	-	PRO	308
-	-	SER	309
-	-	SER	310
-	-	GLU	311
-	-	SER	312
-	-	LYS	313
-	-	GLY	314
-	-	LYS	315
VAL	458	VAL	316
GLN	459	GLN	317
LEU	460	LEU	318
LEU	461	LEU	319
TYR	462	TYR	320
TYR	463	TYR	321
VAL	464	VAL	322
ASN	465	ASN	323
LEU	466	LEU	324
LEU	467	LEU	325
LEU	468	LEU	326
ILE	469	ILE	327
ASP	470	ASP	328
HIS	471	HIS	329
ARG	472	ARG	330
PHE	473	PHE	331
LEU	474	LEU	332
LEU	475	LEU	333
ARG	476	ARG	334
ARG	477	ARG	335
GLY	478	GLY	336
GLU	479	GLU	337
TYR	480	TYR	338
VAL	481	VAL	339
LEU	482	LEU	340
HIS	483	HIS	341
MET	484	MET	342
TRP	485	TRP	343
GLN	486	GLN	344
ILE	487	ILE	345
-	-	SER	346
-	-	GLY	347
-	-	LYS	348
-	-	GLY	349
-	-	GLU	350
-	-	ASP	351
-	-	GLN	352

-	-	<b>GLY</b>	<b>353</b>
-	-	<b>SER</b>	<b>354</b>
PHE	497	PHE	355
ASN	498	ASN	356
ALA	499	ALA	357
ASP	500	ASP	358
LYS	501	LYS	359
LEU	502	LEU	360
THR	503	THR	361
SER	504	SER	362
ALA	505	ALA	363
THR	506	THR	364
ASN	507	ASN	365
PRO	508	PRO	366
ASP	509	ASP	367
LYS	510	LYS	368
GLU	511	GLU	369
ASN	512	ASN	370
SER	513	SER	371
MET	514	MET	372
SER	515	SER	373
ILE	516	ILE	374
SER	517	SER	375
ILE	518	ILE	376
LEU	519	LEU	377
LEU	520	LEU	378
ASP	521	ASP	379
-	-	<b>ASN</b>	<b>380</b>
-	-	<b>TYR</b>	<b>381</b>
-	-	<b>CYS</b>	<b>382</b>
-	-	<b>HIS</b>	<b>383</b>
-	-	<b>PRO</b>	<b>384</b>
-	-	<b>ILE</b>	<b>385</b>
-	-	<b>ALA</b>	<b>386</b>
-	-	<b>LEU</b>	<b>387</b>
-	-	<b>PRO</b>	<b>388</b>
-	-	<b>LYS</b>	<b>389</b>
-	-	<b>HIS</b>	<b>390</b>
-	-	<b>GLN</b>	<b>391</b>
-	-	<b>PRO</b>	<b>392</b>
-	-	<b>THR</b>	<b>393</b>
-	-	<b>PRO</b>	<b>394</b>
-	-	<b>ASP</b>	<b>395</b>
-	-	<b>PRO</b>	<b>396</b>
-	-	<b>GLU</b>	<b>397</b>
-	-	<b>GLY</b>	<b>398</b>
-	-	<b>ASP</b>	<b>399</b>
-	-	<b>ARG</b>	<b>400</b>

-	-	<b>VAL</b>	<b>401</b>
-	-	<b>ARG</b>	<b>402</b>
-	-	<b>ALA</b>	<b>403</b>
GLU	546	GLU	404
MET	547	MET	405
PRO	548	PRO	406
ASN	549	ASN	407
GLN	550	GLN	408
LEU	551	LEU	409
ARG	552	ARG	410
LYS	553	LYS	411
GLN	554	GLN	412
LEU	555	LEU	413
GLU	556	GLU	414
ALA	557	ALA	415
ILE	558	ILE	416
ILE	559	ILE	417
ALA	560	ALA	418
THR	561	THR	419
ASP	562	ASP	420
PRO	563	PRO	421
LEU	564	LEU	422
ASN	565	ASN	423
PRO	566	PRO	424
LEU	567	LEU	425
THR	568	THR	426
ALA	569	ALA	427
GLU	570	GLU	428
ASP	571	ASP	429
LYS	572	LYS	430
GLU	573	GLU	431
LEU	574	LEU	432
LEU	575	LEU	433
TRP	576	TRP	434
HIS	577	HIS	435
PHE	578	PHE	436
ARG	579	ARG	437
TYR	580	TYR	438
GLU	581	GLU	439
SER	582	SER	440
LEU	583	LEU	441
LYS	584	LYS	442
HIS	585	HIS	443
PRO	586	PRO	444
LYS	587	LYS	445
ALA	588	ALA	446
TYR	589	TYR	447
PRO	590	PRO	448

LYS	591	LYS	449
LEU	592	LEU	450
PHE	593	PHE	451
SER	594	SER	452
SER	595	SER	453
VAL	596	VAL	454
LYS	597	LYS	455
TRP	598	TRP	456
GLY	599	GLY	457
GLN	600	GLN	458
GLN	601	GLN	459
GLU	602	GLU	460
ILE	603	ILE	461
VAL	604	VAL	462
ALA	605	ALA	463
LYS	606	LYS	464
THR	607	THR	465
TYR	608	TYR	466
GLN	609	GLN	467
LEU	610	LEU	468
LEU	611	LEU	469
ALA	612	ALA	470
ARG	613	ARG	471
ARG	614	ARG	472
GLU	615	GLU	473
VAL	616	VAL	474
TRP	617	TRP	475
ASP	618	ASP	476
GLN	619	GLN	477
SER	620	SER	478
ALA	621	ALA	479
LEU	622	LEU	480
ASP	623	ASP	481
VAL	624	VAL	482
GLY	625	GLY	483
LEU	626	LEU	484
THR	627	THR	485
MET	628	MET	486
GLN	629	GLN	487
LEU	630	LEU	488
LEU	631	LEU	489
ASP	632	ASP	490
CYS	633	CYS	491
ASN	634	ASN	492
PHE	635	PHE	493
SER	636	SER	494
ASP	637	ASP	495
GLU	638	GLU	496

ASN	639	ASN	497
VAL	640	VAL	498
ARG	641	ARG	499
ALA	642	ALA	500
ILE	643	ILE	501
ALA	644	ALA	502
VAL	645	VAL	503
GLN	646	GLN	504
LYS	647	LYS	505
LEU	648	LEU	506
GLU	649	GLU	507
SER	650	SER	508
LEU	651	LEU	509
GLU	652	GLU	510
ASP	653	ASP	511
ASP	654	ASP	512
ASP	655	ASP	513
VAL	656	VAL	514
LEU	657	LEU	515
HIS	658	HIS	516
TYR	659	TYR	517
LEU	660	LEU	518
LEU	661	LEU	519
GLN	662	GLN	520
LEU	663	LEU	521
VAL	664	VAL	522
GLN	665	GLN	523
ALA	666	ALA	524
VAL	667	VAL	525
LYS	668	LYS	526
PHE	669	PHE	527
GLU	670	GLU	528
PRO	671	PRO	529
TYR	672	TYR	530
HIS	673	HIS	531
ASP	674	ASP	532
SER	675	SER	533
ALA	676	ALA	534
LEU	677	LEU	535
ALA	678	ALA	536
ARG	679	ARG	537
PHE	680	PHE	538
LEU	681	LEU	539
LEU	682	LEU	540
LYS	683	LYS	541
ARG	684	ARG	542
GLY	685	GLY	543
LEU	686	LEU	544

ARG	687	ARG	545
ASN	688	ASN	546
LYS	689	LYS	547
ARG	690	ARG	548
ILE	691	ILE	549
GLY	692	GLY	550
HIS	693	HIS	551
PHE	694	PHE	552
LEU	695	LEU	553
PHE	696	PHE	554
TRP	697	TRP	555
PHE	698	PHE	556
LEU	699	LEU	557
ARG	700	ARG	558
SER	701	SER	559
GLU	702	GLU	560
ILE	703	ILE	561
ALA	704	ALA	562
GLN	705	GLN	563
SER	706	SER	564
ARG	707	ARG	565
HIS	708	HIS	566
TYR	709	TYR	567
GLN	710	GLN	568
GLN	711	GLN	569
ARG	712	ARG	570
PHE	713	PHE	571
ALA	714	ALA	572
VAL	715	VAL	573
ILE	716	ILE	574
LEU	717	LEU	575
GLU	718	GLU	576
ALA	719	ALA	577
TYR	720	TYR	578
LEU	721	LEU	579
ARG	722	ARG	580
GLY	723	GLY	581
CYS	724	CYS	582
GLY	725	GLY	583
THR	726	THR	584
ALA	727	ALA	585
MET	728	MET	586
LEU	729	LEU	587
HIS	730	HIS	588
ASP	731	ASP	589
PHE	732	PHE	590
THR	733	THR	591
GLN	734	GLN	592

GLN	735	GLN	593
VAL	736	VAL	594
GLN	737	GLN	595
VAL	738	VAL	596
ILE	739	ILE	597
GLU	740	GLU	598
MET	741	MET	599
LEU	742	LEU	600
GLN	743	GLN	601
LYS	744	LYS	602
VAL	745	VAL	603
THR	746	THR	604
LEU	747	LEU	605
ASP	748	ASP	606
ILE	749	ILE	607
LYS	750	LYS	608
SER	751	SER	609
LEU	752	LEU	610
SER	753	SER	611
-	-	ALA	<b>612</b>
-	-	GLU	<b>613</b>
-	-	LYS	<b>614</b>
-	-	TYR	<b>615</b>
ASP	758	ASP	616
VAL	759	VAL	617
SER	760	SER	618
SER	761	SER	619
GLN	762	GLN	620
VAL	763	VAL	621
ILE	764	ILE	622
SER	765	SER	623
GLN	766	GLN	624
LEU	767	LEU	625
LYS	768	LYS	626
GLN	769	GLN	627
LYS	770	LYS	628
LEU	771	LEU	629
GLU	772	GLU	630
ASN	773	ASN	631
LEU	774	LEU	632
GLN	775	GLN	633
ASN	776	ASN	634
-	-	SER	<b>635</b>
-	-	GLN	<b>636</b>
-	-	LEU	<b>637</b>
PRO	780	PRO	638
GLU	781	GLU	639
SER	782	SER	640

PHE	783	PHE	641
ARG	784	ARG	642
VAL	785	VAL	643
PRO	786	PRO	644
TYR	787	TYR	645
ASP	788	ASP	646
PRO	789	PRO	647
GLY	790	GLY	648
LEU	791	LEU	649
LYS	792	LYS	650
ALA	793	ALA	651
GLY	794	GLY	652
ALA	795	ALA	653
LEU	796	LEU	654
ALA	797	ALA	655
ILE	798	ILE	656
GLU	799	GLU	657
LYS	800	LYS	658
CYS	801	CYS	659
LYS	802	LYS	660
VAL	803	VAL	661
MET	804	MET	662
ALA	805	ALA	663
SER	806	SER	664
LYS	807	LYS	665
LYS	808	LYS	666
LYS	809	LYS	667
PRO	810	PRO	668
LEU	811	LEU	669
TRP	812	TRP	670
LEU	813	LEU	671
GLU	814	GLU	672
PHE	815	PHE	673
LYS	816	LYS	674
CYS	817	CYS	675
ALA	818	ALA	676
ASP	819	ASP	677
PRO	820	PRO	678
THR	821	THR	679
ALA	822	ALA	680
LEU	823	LEU	681
SER	824	SER	682
ASN	825	ASN	683
GLU	826	GLU	684
THR	827	THR	685
ILE	828	ILE	686
GLY	829	GLY	687
ILE	830	ILE	688

ILE	831	ILE	689
PHE	832	PHE	690
LYS	833	LYS	691
HIS	834	HIS	692
GLY	835	GLY	693
ASP	836	ASP	694
ASP	837	ASP	695
LEU	838	LEU	696
ARG	839	ARG	697
GLN	840	GLN	698
ASP	841	ASP	699
MET	842	MET	700
LEU	843	LEU	701
ILE	844	ILE	702
LEU	845	LEU	703
GLN	846	GLN	704
ILE	847	ILE	705
LEU	848	LEU	706
ARG	849	ARG	707
ILE	850	ILE	708
MET	851	MET	709
GLU	852	GLU	710
SER	853	SER	711
ILE	854	ILE	712
TRP	855	TRP	713
GLU	856	GLU	714
THR	857	THR	715
GLU	858	GLU	716
SER	859	SER	717
LEU	860	LEU	718
ASP	861	ASP	719
LEU	862	LEU	720
CYS	863	CYS	721
LEU	864	LEU	722
LEU	865	LEU	723
PRO	866	PRO	724
TYR	867	TYR	725
GLY	868	GLY	726
CYS	869	CYS	727
ILE	870	ILE	728
SER	871	SER	729
THR	872	THR	730
GLY	873	GLY	731
ASP	874	ASP	732
LYS	875	LYS	733
ILE	876	ILE	734
GLY	877	GLY	735
MET	878	MET	736

ILE	879	ILE	737
GLU	880	GLU	738
ILE	881	ILE	739
VAL	882	VAL	740
LYS	883	LYS	741
ASP	884	ASP	742
ALA	885	ALA	743
THR	886	THR	744
THR	887	THR	745
ILE	888	ILE	746
ALA	889	ALA	747
LYS	890	LYS	748
ILE	891	ILE	749
GLN	892	GLN	750
GLN	893	GLN	751
SER	894	SER	752
THR	895	THR	753
-	-	<b>VAL</b>	<b>754</b>
-	-	<b>GLY</b>	<b>755</b>
-	-	<b>ASN</b>	<b>756</b>
-	-	<b>THR</b>	<b>757</b>
GLY	900	GLY	758
ALA	901	ALA	759
PHE	902	PHE	760
LYS	903	LYS	761
ASP	904	ASP	762
GLU	905	GLU	763
VAL	906	VAL	764
LEU	907	LEU	765
ASN	908	ASN	766
HIS	909	HIS	767
TRP	910	TRP	768
LEU	911	LEU	769
LYS	912	LYS	770
GLU	913	GLU	771
LYS	914	LYS	772
SER	915	SER	773
PRO	916	PRO	774
THR	917	THR	775
GLU	918	GLU	776
GLU	919	GLU	777
LYS	920	LYS	778
PHE	921	PHE	779
GLN	922	GLN	780
ALA	923	ALA	781
ALA	924	ALA	782
VAL	925	VAL	783
GLU	926	GLU	784

ARG	927	ARG	785
PHE	928	PHE	786
VAL	929	VAL	787
TYR	930	TYR	788
SER	931	SER	789
CYS	932	CYS	790
ALA	933	ALA	791
GLY	934	GLY	792
TYR	935	TYR	793
CYS	936	CYS	794
VAL	937	VAL	795
ALA	938	ALA	796
THR	939	THR	797
PHE	940	PHE	798
VAL	941	VAL	799
LEU	942	LEU	800
GLY	943	GLY	801
ILE	944	ILE	802
GLY	945	GLY	803
ASP	946	ASP	804
ARG	947	ARG	805
HIS	948	HIS	806
ASN	949	ASN	807
ASP	950	ASP	808
ASN	951	ASN	809
ILE	952	ILE	810
MET	953	MET	811
ILE	954	ILE	812
THR	955	THR	813
GLU	956	GLU	814
THR	957	THR	815
GLY	958	GLY	816
ASN	959	ASN	817
LEU	960	LEU	818
PHE	961	PHE	819
HIS	962	HIS	820
ILE	963	ILE	821
ASP	964	ASP	822
PHE	965	PHE	823
GLY	966	GLY	824
HIS	967	HIS	825
-	-	<b>ILE</b>	<b>826</b>
-	-	<b>LEU</b>	<b>827</b>
-	-	<b>GLY</b>	<b>828</b>
-	-	<b>ASN</b>	<b>829</b>
-	-	<b>TYR</b>	<b>830</b>
-	-	<b>LYS</b>	<b>831</b>
-	-	<b>SER</b>	<b>832</b>

-	-	PHE	833
-	-	LEU	834
-	-	GLY	835
-	-	ILE	836
-	-	ASN	837
-	-	LYS	838
GLU	981	GLU	839
ARG	982	ARG	840
VAL	983	VAL	841
PRO	984	PRO	842
PHE	985	PHE	843
VAL	986	VAL	844
LEU	987	LEU	845
THR	988	THR	846
PRO	989	PRO	847
ASP	990	ASP	848
PHE	991	PHE	849
LEU	992	LEU	850
PHE	993	PHE	851
VAL	994	VAL	852
MET	995	MET	853
GLY	996	GLY	854
THR	997	THR	855
SER	998	SER	856
GLY	999	GLY	857
LYS	1000	LYS	858
LYS	1001	LYS	859
THR	1002	THR	860
SER	1003	SER	861
PRO	1004	PRO	862
HIS	1005	HIS	863
PHE	1006	PHE	864
GLN	1007	GLN	865
LYS	1008	LYS	866
PHE	1009	PHE	867
GLN	1010	GLN	868
ASP	1011	ASP	869
ILE	1012	ILE	870
CYS	1013	CYS	871
VAL	1014	VAL	872
LYS	1015	LYS	873
ALA	1016	ALA	874
TYR	1017	TYR	875
LEU	1018	LEU	876
ALA	1019	ALA	877
LEU	1020	LEU	878
ARG	1021	ARG	879
HIS	1022	HIS	880

HIS	1023	HIS	881
THR	1024	THR	882
ASN	1025	ASN	883
LEU	1026	LEU	884
LEU	1027	LEU	885
ILE	1028	ILE	886
ILE	1029	ILE	887
LEU	1030	LEU	888
PHE	1031	PHE	889
SER	1032	SER	890
MET	1033	MET	891
MET	1034	MET	892
LEU	1035	LEU	893
MET	1036	MET	894
THR	1037	THR	895
GLY	1038	GLY	896
MET	1039	MET	897
PRO	1040	PRO	898
-	-	GLN	899
-	-	LEU	900
-	-	THR	901
SER	1044	SER	902
LYS	1045	LYS	903
GLU	1046	GLU	904
ASP	1047	ASP	905
ILE	1048	ILE	906
GLU	1049	GLU	907
TYR	1050	TYR	908
ILE	1051	ILE	909
ARG	1052	ARG	910
ASP	1053	ASP	911
ALA	1054	ALA	912
LEU	1055	LEU	913
THR	1056	THR	914
VAL	1057	VAL	915
GLY	1058	GLY	916
LYS	1059	LYS	917
ASN	1060	ASN	918
GLU	1061	GLU	919
GLU	1062	GLU	920
ASP	1063	ASP	921
ALA	1064	ALA	922
LYS	1065	LYS	923
LYS	1066	LYS	924
TYR	1067	TYR	925
PHE	1068	PHE	926
LEU	1069	LEU	927
ASP	1070	ASP	928

GLN	1071	GLN	929
ILE	1072	ILE	930
GLU	1073	GLU	931
VAL	1074	VAL	932
CYS	1075	CYS	933
ARG	1076	ARG	934
ASP	1077	ASP	935
LYS	1078	LYS	936
GLY	1079	GLY	937
TRP	1080	TRP	938
THR	1081	THR	939
VAL	1082	VAL	940

GLN	1083	GLN	941
PHE	1084	PHE	942
ASN	1085	ASN	943
TRP	1086	TRP	944
PHE	1087	PHE	945
LEU	1088	LEU	946
HIS	1089	HIS	947
-	-	LEU	<b>948</b>
-	-	VAL	<b>949</b>

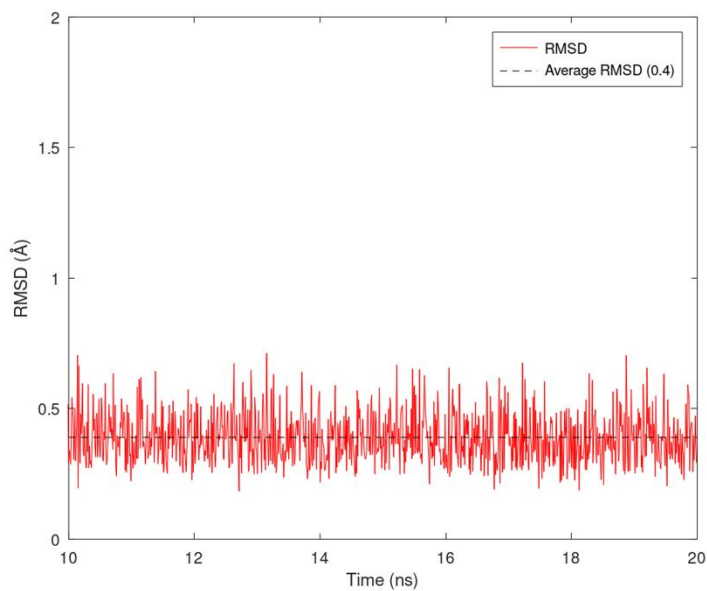


**Figure S4** – RMSD values ( $\text{\AA}$ ) versus time (ns) of MD simulation performed with GAFF in vacuum at 300 K.

**Table S6** – Mean deviation values for the bonds ( $\text{\AA}$ ) and angles ( $^\circ$ ) of New\_FF and GAFF, both with respect to the DFT values.

	[New_FF/DFT]	[GAFF/DFT]
Bonds	0.009	0.022
Angles	1.579	2.514

**Table S7** – Comparative values (%) of selected bond lengths and angles of the vanadium complex. Comparison between experimental values and DFT (*[Exp/QM]*), GAFF (*[Exp/GAFF]*), and New\_FF (*[Exp/MD]*). In addition, the comparison between the values of DFT and New\_FF (*[QM/MD]*).

Bond Lengths	<i>[Exp/QM]</i>	<i>[Exp/GAFF]</i>	<i>[Exp/MD]</i>	<i>[QM/MD]</i>
<b>V1-O1</b>	1.12	1.48	1.46	0.34
<b>V1-O2</b>	0.92	3.29	3.12	2.23
<b>V1-O4</b>	7.96	7.27	8.01	0.049
<b>V1-N1</b>	3.47	3.31	3.81	0.33
<b>O2-C1</b>	1.52	4.43	0.97	0.54
<b>O3-C1</b>	0.18	0.42	0.28	0.10
<b>O4-C2</b>	0.20	1.89	0.72	0.52
<b>C1-C2</b>	1.29	0.47	1.10	0.19
<b>O5-C3</b>	1.52	4.53	0.93	0.58
<b>N1-C5</b>	0.13	5.30	1.06	1.18
Angles	<i>[Exp/QM]</i>	<i>[Exp/GAFF]</i>	<i>[Exp/MD]</i>	<i>[QM/MD]</i>
<b>V1-O4-C2</b>	0.98	5.20	6.17	5.24
<b>V1-N1-C5</b>	1.44	0.01	1.07	2.54
<b>V1-O2-C1</b>	4.27	4.79	3.03	1.18
<b>O1-V1-O2</b>	3.66	6.26	5.19	1.48
<b>O1-V1-O4</b>	0.25	6.09	2.25	2.49
<b>O1-V1-N1</b>	2.64	7.30	7.00	4.48
<b>O2-V1-O4</b>	4.16	6.46	2.58	1.65
<b>O2-V1-O5</b>	8.50	15.97	11.57	2.83
<b>O2-V1-N1</b>	3.77	9.39	6.84	3.19
<b>O2-C1-O3</b>	1.20	2.12	0.63	1.81
<b>C2-O4-C4</b>	1.66	0.04	2.61	0.93
<b>N1-C5-C6</b>	0.06	2.30	0.10	0.04

**Table S8** – Summary of the four comparisons performed. Means of relative errors, means of standard deviation, and the major variation between the relative error percentages of all bonds are shown.

Bonds	<i>[Exp/QM]</i>	<i>[Exp/GAFF]</i>	<i>[Exp/MD]</i>	<i>[QM/MD]</i>
Mean of relative error	4.4%	5.7%	4.8%	0.6%
Mean of Standard deviation	-	0.001%	0.001%	0.001%
Majority variation percentages	0% a 10%	0% a 11%	0% a 10%	0% a 2%

**Table S9** – Means of relative errors, means of standard deviation, and the major variation between the relative error percentages of all angles are shown.

Angles	[Exp/QM]	[Exp/GAFF]	[Exp/MD]	[QM/MD]
Means of relative errors	1.3%	2.7%	2.0%	1.4%
Means of Standard deviation	-	0.128%	0.153%	0.153%
Majority variation percentages	0% a 2%	0% a 4%	0% a 3%	0% a 2%

A useful analysis was performed to investigate the degree of conjugation of this ligand: the Bond Length Alternation (BLA). For a perfectly conjugated system, it is expected that the length of the single bonds is equivalent to the value of the double bonds, that is, that the geometric parameter BLA is equal to zero. Otherwise, a non-zero value is found.

The analyses of this validation step were performed considering the last 10 ns of the MD simulation (total 20 ns), i.e., 1000 frames obtained for each bond length and angle, and therefore an average value of these 1000 frames represented each structural parameter.

Thus, the calculation of BLA is performed by considering the sum of all single bonds (average values), divided by the total number of single bonds in the ligand (9). The same procedure was performed for the double bonds. Thus, the difference between the value obtained for the single bonds and the value obtained for double bonds provided the final value of BLA.

Figure S5 presents BLA values regarding experimental and quantum values, as well as the values obtained from two MD simulations (same conditions) with the newly developed force field and the non-specific GAFF force field. Performing this analysis allowed us to evaluate the performance of the parameter set, proposed by us, to describe the *phen* ligand.

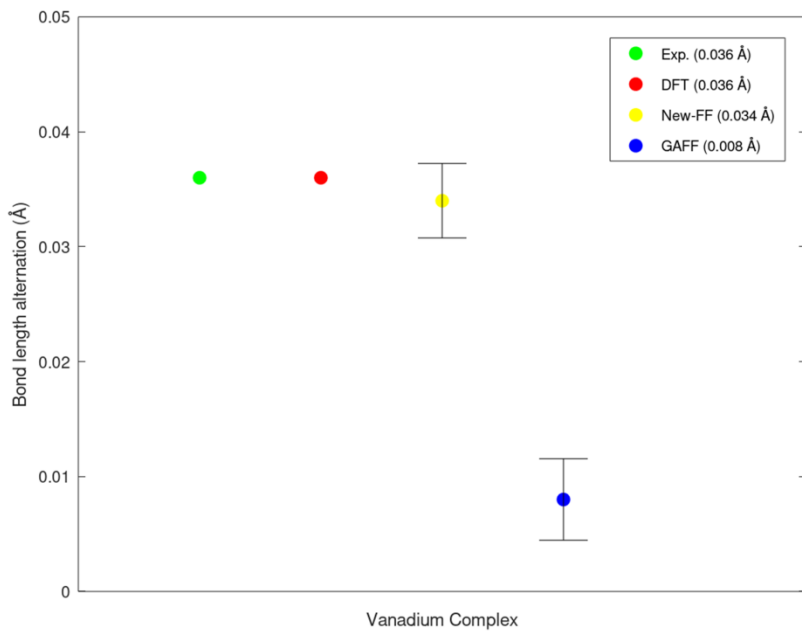


**Figure S5** – BLA values for the four discussed scenarios: experimental values (Exp.); quantum reference (DFT); MD with the developed force field (New\_FF); and MD with the GAFF force field (GAFF).

From the analysis of Figure S5, it can easily be seen how well New\_FF agrees with the experimental and quantum references. The difference in BLA values is appreciably low, with the value provided by the new force field being 0.034 Å, while the experimental and DFT values are both 0.036 Å.

On the other hand, as already expected, GAFF force field, which is not a VC-specific force field, did not reproduce what the experimental data, and neither did the quantum prediction. The value obtained after the MD simulation with the implemented GAFF was 0.008 Å.

**ARTIGO 2**

**Vanadium complex as a potential modulator of the autophagic mechanism through proteins PI3K and ULK1: development, validation and biological implications of a specific force field for [VO(bpy)<sub>2</sub>Cl]**

**Abstract**

The modulation of autophagy has been presented as a very useful strategy in anticancer treatments. In this sense, the vanadium (VC) complex bis(2,2'-bipyridine)chlorooxovanadium(IV), [VO(bpy)<sub>2</sub>Cl], is known for its ability to induce autophagy in triple-negative breast cancer cells (TNBC). An excellent resource to investigate the role of VC in the induction of autophagy is to make use of Molecular Dynamics (MD) simulations. However, until now, the scarcity of force field parameters for the VC prevented a reliable analysis. The autophagy signaling pathway starts with the PI3K protein and ends with ULK1. Therefore, in the first stage of this work we developed a new AMBER force field for the VC (VCFF) from a quantum structure, obtained by DFT calculations. In the second stage, the VCFF was validated through structural analyses. From this, it was possible to investigate, through docking and MD (200 ns), the performance of the PI3K-VC and ULK1-VC systems (third stage). The analyses of this last stage involved RMSD, hydrogen bonds, RMSF and two pathways for the modulation of autophagy. In general, this work fills in the absence of force field parameters (FF) for VC by proposing an efficient and new FF, in addition to investigating, at the molecular level, how VC is able to induce autophagy in TNBC cells. This study encourages new parameterizations of metallic complexes and contributes to the understanding of the duality of autophagic processes.

**Keywords:** autophagy; modulation; vanadium complex; AMBER force field; molecular dynamics.

## 1. Introduction

Breast cancer is considered the leading cause of cancer-related death in women. It is estimated about 2.3 million new cases of female breast cancer, which corresponds to 11.7% of cancer cases worldwide, and almost 685 thousand deaths in 2020, corresponding to 6.9 % of cancer-related deaths worldwide [1]. In addition, a number approaching 15% to 20% of total breast cancer patients can be classified as triple-negative [2].

The name Triple-Negative Breast Cancer (TNBC) comes from the absence of three biomarkers: estrogen receptor (ER), progesterone receptor (PR) and human epidermal growth factor receptor 2 (HER2). In this case, the diagnosis is made by observing the absence of these three biomarkers [3].

Therefore, the drugs developed to treat breast cancer target these three biomarkers, with triple-negative breast cancer being negative for their presence ( $ER^-$ ,  $PR^-$  and  $HER2^-$ ), any treatment with the drugs already developed would be ineffective [4]. Thus, as chemotherapy works by attacking rapidly dividing cells, it is the most effective treatment for this disease [3, 4].

However, chemotherapy not only attacks cancer cells but also healthy cells in the body. Thus, it is important to point out that chemotherapy, as well as radiotherapy, despite being the most traditional treatments, result in serious side effects, which seriously compromises the quality of life of patients [5]. In view of the above, it is clear the need for new combat strategies and, in this case, the modulation of autophagic processes can be a great ally in the fight against cancer [6].

Autophagy (self-eating) is characterized as a homeostatic process that allows the degradation of dysfunctional organelles or proteins [7], where the PI3K/Akt/mTOR pathway is known as the signaling pathway [8, 9]. PI3K and Akt are responsible for activating the mTOR protein which, in turn, negatively regulates the ULK1 protein, another important protein of the autophagic mechanism [10]. As a consequence, deactivated ULK1 indicates no occurrence of autophagy [11].

Thus, the possibility of manipulating autophagy, through positive (induction) or negative (inhibition) regulation of the aforementioned proteins, can be seen as a useful strategy for anticancer treatments [12].

It is reported that autophagy has a dual behavior against cancer, acting both in tumor suppression and disease progression [6, 12]. In other words, when cancer is about to form (carcinogenesis), autophagy works against this process by acting to recycle the damaged materials in the cell [13]. On the other hand, in the scenario where the cancer has already settled and progressed, autophagy acts on behalf of the tumor allowing the tumor cell to survive [14].

Given the reports on the duality of autophagy and the fact that cancer is a disease that occurs in stages, it is possible to use autophagy in favor of anticancer treatments through its manipulation [15]. It is understood that in tumorigenesis the induction of autophagy is suggestive, while in the progression of cancer, inhibition is the most indicated path [6, 12-15].

The manipulation of autophagy (inhibition/induction) can be performed from the interaction of specific modules that are able to interact, at a molecular level, with the proteins presented in the autophagic pathway [16]. In this sense, vanadium complexes are reported in the literature as useful molecules capable of both inducing and inhibiting the autophagy process [17-24].

In this work, we studied the vanadium complex bis(2,2'-bipyridine)chlorooxovanadium(IV), which is known to induce autophagy in triple-negative breast cancer (TNBC) cells [17]. The  $[\text{VO}(\text{bpy})_2\text{Cl}]$  complex is shown in Fig. 1.

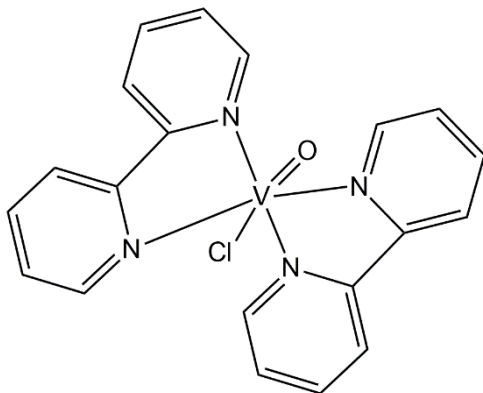


**Fig. 1** Vanadium complex (VC) under study,  $[\text{VO}(\text{bpy})_2\text{Cl}]$

The manipulation of autophagy through metal complexes, activating or deactivating the proteins present in the autophagy signaling pathway, can be investigated from Classical Molecular Dynamics (MD) simulations. However, MD simulations are heavily dependent on the proper choice of force fields (FF) [25].

It is known that force field parameters for molecules with metallic centers are extremely scarce. Also, general force fields may not be effective in describing such molecules [25], as well as not satisfactorily reproducing the structural properties of highly conjugated molecules [26]. Another noteworthy detail is the fact that specific force fields for the vanadium complex (VC) target of this study have not yet been reported in the literature.

Given the clear usefulness of vanadium complexes in the manipulation of autophagy which favors new strategies to fight against cancer, in addition to the advantage of autophagy in relation to chemotherapy treatments (since autophagy acts directly on diseased cells, avoiding possible side effects), the goal of this work is divided in some stage, the first one is the development of AMBER force field parameters for the vanadium complex  $[VO(bpy)_2Cl]$  (Fig. 1), from a lower energy structure optimized with quantum mechanics (DFT). Furthermore, in the second part of the work, we propose the validation of the parameterization performed through a MD simulation in vacuum (20 ns) with the new parameters. To investigate the performance of the new force field, analyses of the structural properties of the complex were performed through comparison with two references: experimental data [27] and quantum mechanics calculations (DFT). Finally, the third stage of this study consisted of investigating, at a molecular level, the interactions between VC and two important proteins present in the autophagy pathway, namely: PI3K (responsible for initiating signaling) and ULK1 (responsible for activating or not autophagy). In this way, two MD simulations (both with 200 ns) were performed in order to provide precious insights into the types of interactions between PI3K-VC and ULK1-VC. In order to perform a reliable MD, the starting structure for both simulations came from molecular docking calculations.

## **2. Preliminary calculations**

### **2.1 Quantum calculations**

To obtain the desired AMBER force field parameters, it was initially necessary to optimize the VC structure that served as a starting point for all other steps. Thus, with the assistance of the Gaussian 09 software [28], the VC was optimized using the DFT (Density Functional Theory) calculation method with the exchange-correlation functional B3LYP and the set of base functions def2-TZVP and LANL2DZ ECP for vanadium. This level of theory has previously been used in purely theoretical work involving vanadium complexes [29, 30].

Optimization calculations were also performed in ORCA 4.0 software [31] to investigate relativistic effects on the vanadium complex. The theory level consisted of the same level used in the Gaussian 09 calculations plus the relativistic ZORA method. The ZORA-def2-TZVP base function set has recently been successfully used for vanadium metal [32].

The calculation of the non-polarizable RESP (Restrained Electrostatic Potential) charges and the Hessian matrix were performed with the same level of theory as the optimization calculation in Gaussian 09. In this way, the initial parameters could be extracted from the calculation of the Hessian matrix through a tool available in the VMD (Visual Molecular Dynamics) software, the Paratool plugin [33].

## 2.2 Biological system preparation (PI3K)

A previous procedure to complete the missing residues in the PI3K protein (PDB code 3QJZ [34]) was carried out using the SWISS-MODEL software [35]. Next, we use the “LovoAlign” protein structural alignment package [36] to align the model generated by SWISS-MODEL with the missing residues added and the original protein (3QJZ). For an analysis of the alignment performed and subsequent test the new model, an RMSD calculation of the structure aligned in relation to the original structure was performed. The superposition of the two structures is available in the Support Information file (Fig. S1, Section S3). It is worth mentioning that it was not necessary to carry out this previous treatment with the ULK1 (PDB code 4WNO [37]) protein, as there were no residues absent in its original file.

## 2.3 Molecular Docking

VC docking simulations with PI3K and ULK1 were performed using the MolDock algorithm present in the Molegro Virtual Docker (MVD) software [38].

**PI3K** – For the simulation of the PI3K-VC system, the binding site determined followed the study of Gurumoorthy and co-workers [39]. According to this work, the ligand present in the VC, bipyridine (bpy), interacts with the PI3K protein through the Arg839 residue. In a radius of 12 Å the residues were considered flexible. The pose that presented the best performance from the conformational and energetic point of view was chosen to start the molecular dynamics stage.

**ULK1** – In the work of Zhang and collaborators [40], the authors highlight some important residues for protein activity. Thus, the binding site was determined taking into account these residues. In addition, flexible residues were assigned with a radius of 12 Å. Likewise, from the docking result, the starting structure for the next step was determined.

## 2.4 Molecular Dynamics

**VC (*vacuum*)** – In order to validate the parameterization performed, a simulation of Classical Molecular Dynamics (MD) with the new force field developed was carried out considering a total simulation time of 20 ns and a temperature of 300 K. In addition, by means of comparison with the developed force field, a simulation with the GAFF force field, under the same conditions as the MD performed in the validation step, was performed. The AMBER 11 software package [41] was used in both MD simulations.

With the assistance of PMEMD software [42], present in the AMBER 20 program package [43], the two MD of the VC with the PI3K and ULK1 proteins could be performed.

**PI3K** – Initially, the PI3K-VC system was minimized in two steps (with restriction of 500 kcal/mol and without restriction) where 500 cycles of steepest descent and 5500 cycles of conjugate gradient methods were performed with constant volume. Then, the system underwent a three-step heating with increment of 100 K, reaching at the end 300 K (restriction of 5 kcal/mol in the three steps of 50 ps). Subsequently, the system was equilibrated at 300 K also at constant volume and in three steps: 50 ps with a force constant of 5 kcal/mol; 50 ps with restriction of 3 kcal/mol; and finally, 100 ps without any restrictions. The last step (production) was performed at 200 ns, with constant pressure and without restrictions.

Following the work of Arba *et al.* [44] and Farrokhzadeh *et al.* [45], in all four steps mentioned, the force field “leaprc.ff14SB” was used to describe the PI3K. To describe the VC, the force field developed in this work was used. A cubic box was added with explicit solvent and TIP3PBOX water model. Eight sodium ions were added to balance the system's charge.

**ULK1** – To the best of our knowledge, MD simulations of the ULK1 protein have not yet been performed in the AMBER software. On the other hand, simulations using the GROMACS software are found [40, 46, 47]. Thus, to choose which force field to use to describe the ULK1 in AMBER, it was chosen to use the most current force field of the software, “leaprc.ff19SB”

[48]. Furthermore, it is recommended to use the OPC water model with this force field. Eight Cl<sup>-</sup> counterions were added. The procedures adopted in the simulations of the PI3K-VC system were also adopted for the four steps (minimization, heating, equilibration and production) of this ULK1-VC system.

### 3. Results and discussion

#### 3.1 How reproducible are force field parameters for vanadium complexes available?

It is important to comment on AMBER and UFF (Universal Force Field) force field parameters that are available, respectively, in the Hyperchem 7.0 and Gaussian 09 software for the [VO(bpy)<sub>2</sub>Cl] complex. However, performing VC optimizations in the mentioned programs is really a viable way? Are the available parameters efficient to describe the geometry of the molecule? To answer these questions, we performed VC optimizations in both programs.

The results of the two optimizations were collected and presented in Table S1, for the selected bond lengths and in Table S2, for the selected bond angles. These results refer to comparisons between experimental values and four levels of theory, namely: Molecular Mechanics (MM) with AMBER force field (FF) (*AMBER/Exp*); MM with UFF (*UFF/Exp*); Quantum Mechanics (QM) with B3LYP/def2-TZVP plus ECP (*ECP/Exp*); and QM with B3LYP/def2-TZVP plus ZORA (*ZORA/Exp*). In addition, a comparison between B3LYP/def2-TZVP plus ECP and B3LYP/def2-TZVP plus ZORA (*ECP/ZORA*) theory levels was performed and presented in both tables in the sixth column.

Comparisons were performed considering the calculation of the relative error (equation (1)). Exceptionally, the comparison performed between *ECP/ZORA* considered the ZORA value to be the truest value.

$$\% = \frac{\text{calculated value} - \text{experimental value}}{\text{experimental value}} \times 100 \quad (1)$$

From the observations in Tables S1 and S2, it can be seen that the MM calculation methods considering the AMBER and UFF force fields are not sufficient to describe the VC geometry by comparing with the experimental values. This observation is based on the analysis of the

relative error percentages, which present higher values. This discussion reinforces the need to develop specific force field parameters for the vanadium complex [VO(bpy)<sub>2</sub>Cl].

On the other hand, the quantum-mechanical methods (columns 4 and 5 of both tables), when compared with the experimental data, provide lower values than the results from the classical methods. All the results provided by the four comparisons, taken together, make it clear that the force fields available to the VC fail to describe their bond lengths and angles, whereas quantum mechanical methods are efficient in describing them.

Another analysis can be observed through Tables S1 and S2. The results shown in the sixth columns of the two tables report the comparison between the VC optimizations performed with the levels of theory B3LYP/def2-TZVP with ECP and B3LYP/def2-TZVP with ZORA (ECP/ZORA). The purpose of making this comparison lies in the fact that some metals in the periodic table have relativistic effects that need to be taken into account in theoretical calculations.

The vanadium atom is a metal present in the fourth period of the periodic table, where relativistic effects are not so pronounced. Expressive relativistic effects are considered to be found from the sixth period of the periodic table on [49]. In this sense, although vanadium does not have significant relativistic effects, we consider viable the comparison between the level of theory used in the calculations of this work (B3LYP/def2-TZVP plus ECP) and the calculation with the same level of theory, but with the relativistic method ZORA (B3LYP/def2-TZVP with ZORA). This last calculation was performed using ORCA 4.0 software [31].

The results show an excellent agreement between the theory level considering the ECP potential and the theory level considering the ZORA relativistic method (sixth column of Tables S1 and S2), with relative errors of less than 0.6% for the bonds and 0.3% for angles. In other words, we can consider that the geometry obtained by the optimization with B3LYP/def2-TZVP plus ECP is a geometry significantly close to that obtained with B3LYP/def2-TZVP with ZORA. In this way, we were able to validate, from the point of view of relativistic effects on vanadium metal, the level of theory used in the calculations of this work, where results obtained with ECP are expressively close to those obtained with ZORA.

## Part I – Development

### 3.2 Labeling the atoms

As a first step, it was necessary to identify and label each atom present in the VC, i.e., all the Atom Types of the molecule were assigned. This is a crucial step for the good development of parameters, since these labels are assigned taking into account the chemical environment of each atom and not just its atomic number.

The topology of the parameter file for simulations in the AMBER software requires Atom Types to be defined from two characters. Thus, in this work we assign the Atom Types using alphanumeric characters, i.e., one letter and one number for each atom. The distribution of Atom Types in the VC under study in this work can be seen in Fig. 2. The Atom Type L1 refers to the chlorine atom; hydrogen atoms are represented by H and I; carbon atoms are expressed by the letters C and D.

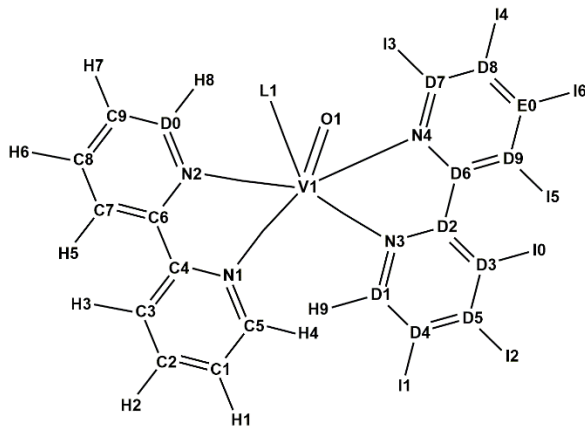


**Fig. 2** Atom Types assigned to the vanadium complex (VC)

### 3.3 Obtaining the parameters for the bonded atoms

The total potential energy ( $V_{\text{Total}}$ ) can be expressed in the form of equation (2), where the potentials referring to the bonded atoms are represented by  $V_L$  (bond stretching),  $V_A$  (angular deformations),  $V_D$  (torsion angles), and the functions that represent atoms that are not bonded are  $V_{\text{LJ}}$  (van der Waals interactions) and  $V_C$  (electrostatic interactions). These terms are further detailed below and are part of a typical force field known as the AMBER force field [25].

$$V_{\text{Total}} = V_L + V_A + V_D + V_{\text{LJ}} + V_C \quad (2)$$

Equations (3) and (4) represent the harmonic potentials  $V_L$  and  $V_A$ , which refer, respectively, to the energy values of stretching of the bonds and angular deformations, each one in relation to the due equilibrium values. These potentials obey Hooke's law and can be represented in the forms

$$V_L = \sum_{bonds} K_b(b - b_0)^2 \quad (3)$$

and

$$V_A = \sum_{angles} K_\theta(\theta - \theta_0)^2 \quad (4)$$

where  $b$  and  $\theta$  correspond to bond lengths and angles, respectively; in addition to  $b_0$  and  $\theta_0$  corresponding to equilibrium values; finally,  $K_b$  and  $K_\theta$  represent the force constants.

The term referring to the energy potential of atoms for a torsion is presented in equation (5), where  $K_\phi$  represents the constant that defines the height of the rotation barrier;  $n$  represents the number of minima; the dihedral angle is represented by  $\phi$ ; and  $\delta$  is the phase angle. The potential energy that describes dihedral angles is usually represented by a periodic function (cosine).

$$V_D = \frac{1}{2} \sum_{dihedral} K_\phi [\cos(n\phi - \delta) + 1] \quad (5)$$

After presenting the equations that make up the intramolecular interactions of the AMBER force field, their respective values could be determined. In this way, the values of the force constants ( $K_b$ ,  $K_\theta$  and  $K_\phi$ ) and the equilibrium values ( $b_0$  and  $\theta_0$ ) could be obtained through the diagonalization of the Hessian matrix, in addition to the values of periodicity ( $n$ ) and phase angle ( $\delta$ ). The procedure for extracting information from the Hessian matrix was performed using the Paratool plugin.

It should be noted that the values of  $b$ ,  $\theta$  and  $\phi$ , which correspond, respectively, to bond lengths, bond angles and dihedral angles, are obtained during molecular dynamics simulations, where the system trajectories are being stored.

### 3.4 Obtaining the parameters for unbonded atoms

The terms referring to the potential functions that represent the unbonded atoms, i.e., the intermolecular interactions, are represented by equations (6) and (7). These equations are responsible for composing the terms referring to the van der Waals interactions (equation (6) –  $V_{LJ}$ ) and the electrostatic interactions (equation (7) –  $V_C$ ) of the AMBER force field.

$$V_{LJ} = \sum_{unbonded} 4\epsilon_{ij} \left[ \frac{\sigma^{12}}{r_{ij}^{12}} - \frac{\sigma^6}{r_{ij}^6} \right] \quad (6)$$

$$V_C = \sum_{unbonded} \left[ \frac{q_i q_j}{4\pi\epsilon_0 r_{ij}} \right] \quad (7)$$

In (6) and (7), the distance between atoms  $i$  and  $j$  is represented by  $r_{ij}$ ; just as the depth of the potential well is represented by  $\epsilon_{ij}$ ;  $\sigma$  corresponds to the distance where the Lennard-Jones potential ( $V_{LJ}$ ) is zero;  $q_i$  and  $q_j$  represent the partial atomic charges; and, finally,  $\epsilon_0$  represents the permittivity in vacuum.

The van der Waals interactions are represented by the Lennard-Jones potential (equation (6)). Thus, the Lennard-Jones parameters  $\sigma$  and  $\epsilon$  were assigned according to the GAFF (General AMBER Force Field) for all atoms except vanadium. Thus, the Lennard-Jones parameters for vanadium ( $\sigma = 2,767$  and  $\epsilon = 1,904$ ) were assigned according to the literature [50], since the parameterization of the GAFF [51] was performed targeting organic molecules. And, finally, the partial atomic charges,  $q_i$  and  $q_j$ , referring to the Coulomb interactions (equation (7)), were obtained by calculating the non-polarizable RESP.

The complete parameter file, obtained from the Atom Types assignment (Fig. 2) discussed in Subsection 3.2 and containing all the information described in Subsections 3.3 and 3.4 can be found in the Supporting Information (SI) file made available by the authors (Section S2). In addition, the respective values referring to the RESP charges can also be found in the SI file (Table S3).

## Part II - Validation

### 3.5 Structural validation

The first stage of this work consisted in the development of the parameters of the AMBER force field. Thus, the second stage is carried out by the validation of the parameterization performed in the first stage. Validation by structural bias is described in this section.

A Classical Molecular Dynamics (MD) simulation with the new parameters implemented, in vacuum, with a total temperature of 300 K, a total simulation time of 20 ns and an interval of 1 fs, acted as a basis to carry out the validation of the new field of developed force, here called “VCFF” (Vanadium Complex Force Field). It is important to note that only the last 10 ns of simulation were considered for analysis, which is equivalent to the last thousand frames. This procedure was adopted to ensure that the system has reached equilibrium.

The first analysis performed in this work to test the effectiveness of the VCFF is the calculation of the RMSD (*root mean square deviation*). Firstly, analyzing the RMSD is an extremely suggestive choice, since the RMSD calculation is able to provide an understanding of the difference in the x, y and z coordinates of each atom of the molecule compared to the x, y and z coordinates of each atom of a reference (in this case, the quantum reference – DFT).

The RMSD calculation is performed using equations (8) and (9), where two molecules (the molecule under analysis and the reference molecule) are considered, represented by the sets  $a$  and  $b$ . N represents the total number of atoms that must be, without fail, equal in the two molecules.

$$RMSD(a, b) = \sqrt{\frac{1}{N} \sum_{i=1}^N \|a_i - b_i\|^2} \quad (8)$$

$$RMSD(a, b) = \sqrt{\frac{1}{N} \left[ \sum_{i=1}^N (a_{i,x} - b_{i,x})^2 + (a_{i,y} - b_{i,y})^2 + (a_{i,z} - b_{i,z})^2 \right]} \quad (9)$$

Behind the scenes of the RMSD calculation, the two geometries are superimposed, in order to find the best fit between the two molecules. For this, it is possible that the second molecule

(MD with the VCFF) undergoes translations and rotations to provide the best positions between each pair of atoms in the two molecules (being an atom of the quantum reference and an atom of a frame of the MD simulation) [52]. The result of the RMSD calculation is shown in Fig. 3.

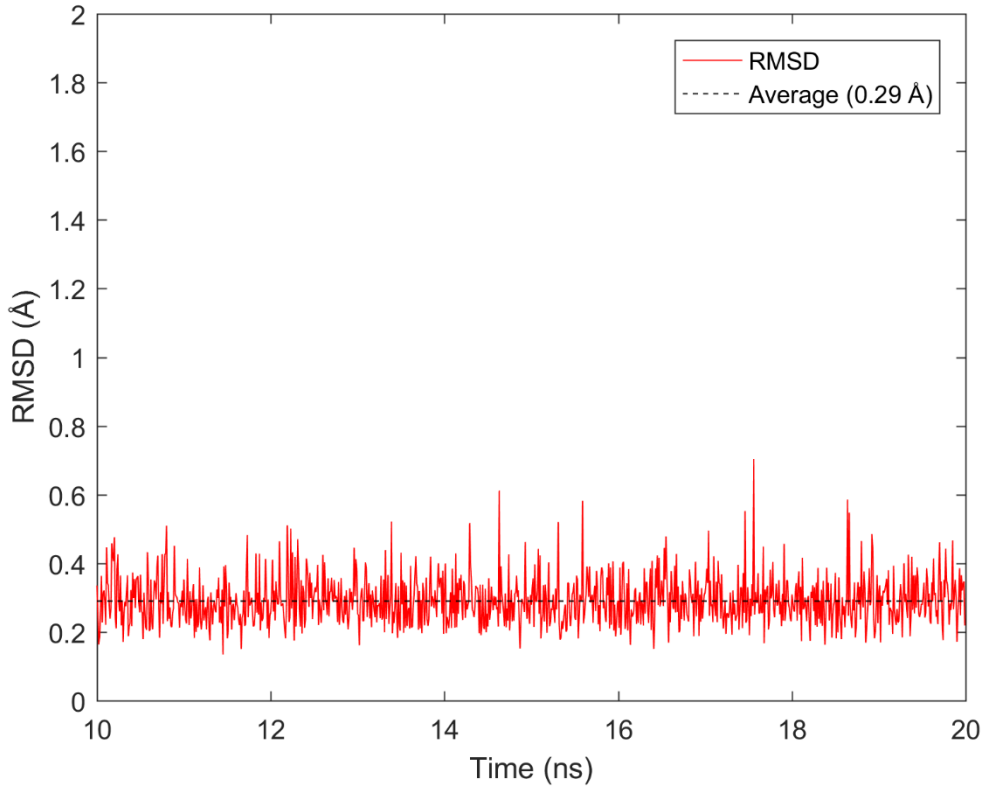


**Fig. 3** RMSD values ( $\text{\AA}$ ) *versus* time (ns) of MD simulation performed in vacuum at 300 K

The RMSD values shown in the graph of Fig. 3 together provide an average variation of  $0.29 \text{ \AA} \pm 0.002 \text{ \AA}$ . Furthermore, by subtracting the highest value of RMSD ( $0.7039 \text{ \AA}$ ) and the lowest value ( $0.1253 \text{ \AA}$ ), we have an oscillation amplitude of only  $0.6 \text{ \AA}$ .

Observing these results, it can be clearly understood that the spatial coordinates of the atoms presented in the VC are extremely close to the quantum reference coordinates, due to the lower value of the RMSD. Another noteworthy detail is that even though the VC was simulated in vacuum, without the possibility of any molecules that prevent its movements, we obtained an excellent result of the RMSD calculation, showing that the oscillation of the cartesian coordinates of the VC, in comparison with the quantum reference had oscillations around  $0.29 \text{ \AA}$ , i.e., oscillations close to zero.

Regarding the MD simulation with VCFF and GAFF, where system trajectories are considered, an arithmetic average of the bond length values of the last thousand frames (last 10

ns) of the simulation was calculated, resulting in a single value that was compared with the experimental result [27] and the quantum reference. That is, to perform the data analysis, percentages of relative errors were considered (equation (1)).

In this way, we performed four types of comparisons, namely:

1. *[QM/Exp]*, quantum values compared to experimental values;
2. *[GAFF/Exp]*, MD simulation values using GAFF compared to experimental values;
3. *[VCFF/Exp]*, MD simulation values using VCFF compared to experimental values;
4. *[VCFF/QM]*, MD simulation values using VCFF compared to quantum reference values (DFT).

The first comparison (*QM/Exp*) was useful to certify that the level of theory used in this work was reliable. The second comparison (*GAFF/Exp*) was made in order to analyze whether the GAFF force field, often used, is able to efficiently describe the structural parameters of the VC. Although its development was carried out targeting organic molecules[51], we believe it is valid to test whether its parameters satisfactorily describe the structural parameters of the VC. Furthermore, the vanadium complex ( $[\text{VO}(\text{bpy})_2\text{Cl}]$ ), the target of this study, has two organic ligands (equal molecules), bipyridine.

In this same perspective, the last two comparisons (*VCFF/Exp* and *VCFF/QM*) sought to analyze the performance of the parameterization proposed in this work by comparing it with the two sets of reference values (experimental and quantum values). The summary of all these comparisons can be seen in Table 1. In view of the results presented, it is possible to highlight three observations.

First, the level of theory adopted in this work (B3LYP/def2-TZVP plus ECP for the vanadium atom) is efficient to describe the structural properties of VC, as it provides excellent agreement with the experimental data (Table 1, column 2). The average of all relative errors from the comparison (*QM/Exp*) provided an extremely low value, around 1.3%. In addition, about 90.6% of the bonds varied their relative errors between 0% and 2% only. This certainly allows us to validate the level of theory used.

The second observation is easily understood when looking at the results provided by GAFF force field, where force field fails to describe the VC geometry, even in the presence of two

organic ligands (both being bipyridines). The summary of the results obtained by GAFF can be found in Table 1 (column 3).

Finally, it is noted that the VCFF presents mean of relative error of 1.2% when compared to the experimental data (VCFF/Exp) and 87.5% of the bonds vary from 0% to 2% only. The validation of the VCFF compared to the quantum reference (VCFF/QM) provides even more encouraging results, where the mean of relative error was only 0.8% and the majority variation (89.6%) between the relative error percentages was between 0% and 1% only.

**Table 1** – Summary of the four comparisons performed. Means of relative errors, means of standard deviation, and the major variation between the relative error percentages of all bonds are shown.

Bonds	[QM/Exp]	[GAFF/Exp]	[VCFF/Exp]	[VCFF/QM]
Mean of relative error	1.3%	4.5%	1.2%	0.8%
Means of Standard deviation	-	0.001%	0.001%	0.001%
Majority variation percentages	0% a 2%	1% a 7%	0% a 2%	0% a 1%

Regarding the analysis of bond angles, it is expected that the angular deformations are more pronounced than the stretching of the bonds. This can be confirmed from the values referring to the force constants for the bonds ( $K_b$ ) and the angles ( $K_\theta$ ), where it is observed that the  $K_\theta$  values are appreciably smaller than the  $K_b$  values (see Section S2). In other words, it is understood that larger force constants ( $K_b$ ) make it more difficult to stretch the bonds, while smaller force constants do not so accurately prevent angular deformations ( $K_\theta$ ).

With respect to the bonds, the final result of the comparison between the experimental and quantum references (Table 2, column 2) is considered low, compared to the other percentage values. Most angles (81.8%) have relative errors from 0% to 5% only, with an average of 8.0%. This allows us, again, to validate the use of the quantum results in the comparison and evaluation of the VCFF. By the way, excellent values are found from the comparison between the VCFF and the quantum reference values (Table 2, column 5).

Overall, the results of four types of comparisons, summarized in Table 2, allow us to infer that, as expected, GAFF force field also fails to describe the bond angles. Different from the

new force field proposed by us. All results of the angular deformations, taken together, allow us to validate the set of parameters that were developed.

**Table 2** – Means of relative errors, means of standard deviation, and the major variation between the relative error percentages of all angles are shown.

Angles	[QM/Exp]	[GAFF/Exp]	[VCFF/Exp]	[VCFF/QM]
Means of relative errors	8.0%	9.8%	8.4%	1.5%
Means of Standard deviation	-	0.124%	0.128%	0.128%
Majority variation percentages	0% a 5%	0% a 19%	0% a 6%	0% a 3%

### ***Part III – Biological Implications and application***

#### **3.6 Static analysis - Docking**

After completing the PI3K protein through the SWISS-MODEL software, 150 residues were recovered, leaving the protein with a total of 945 residues. This new model was aligned with the original protein through the LovoAlign program. To analyze the quality of the new model, an RMSD was performed using the coordinates of the original protein as a reference. The superposition of the two proteins can be seen in Fig. S1, where the excellent value of RMSD (0.8 Å) was obtained.

As new residues were added to the PDB of the protein, we provide the parallel between the residues of the original protein and the residues of the new model (Table S4). In this way, it is possible to follow the new nomenclature used from now on, for example, the residue Arg839 became Arg697 (Table S4).

Carrying out the previous step provides greater reliability for the biomolecular studies to follow. Otherwise, if this pre-treatment had not been carried out, there could be a low confidence in the information provided, in addition to being less realistic information. Thus, the complete and aligned protein was reliably used to perform the docking and MD simulations.

The results of the two docking simulations (PI3K-VC and ULK1-VC) are presented below.

### **PI3K-VC**

As predicted by Gurumoorthy *et al.*[39], the VC bipyridine ligand actually interacts with the amino group of the Arginine 839 residue, which, in the new nomenclature, is the Arg697 residue. Furthermore, as a result of the simulation, we found two new interactions of VC with the amino acid Lysine (Lys526). These three interactions are shown in Fig. 4.

In addition, the pose shown in Fig. 4 has the most favorable conformation and orientation from an energetic point of view, i.e., it has the lowest energy value of the entire simulation ( $-131.3 \text{ kcal/mol}$ ). Thus, from the structural and energetic criteria, the pose illustrated in Fig. 4 served as a starting point for the molecular dynamics simulation.

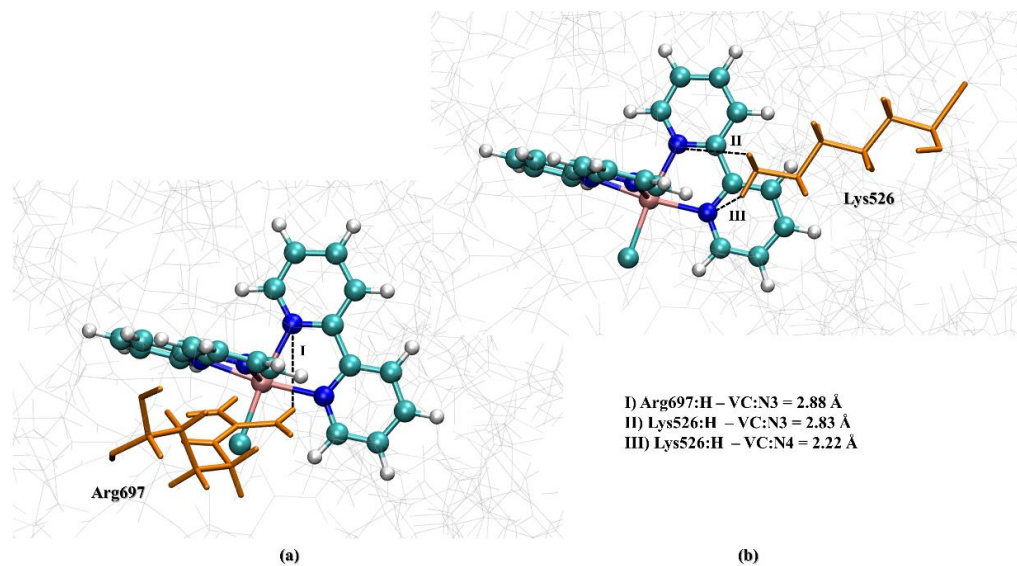


**Fig. 4** Hydrogen bonds resulting from the docking simulation. **(a)** Arg697:H–VC:N3; **(b)** Lys526:H–VC:N3 and Lys526:H–VC:N4. The bonds lengths are pointed out

### **ULK1-VC**

As mentioned before by Zhang and co-workers[40], three important residues for the activity of the ULK1 protein were indicated, namely: Glu93, Cys95 and Asp165. The result of the

docking simulation showed a hydrogen bond between the Cysteine 95 residue and the oxygen of the VC, as can be seen in Fig. 5.

To choose which result of the docking simulation to use in the molecular dynamics simulation, we consider the conformational criterion as the main one and, in the sequence, the energetic criterion. Thus, after selecting the poses that presented interactions with the key residues for protein activity, we proceeded to the energetic criterion, where the pose presented in Fig. 5 indicates an energy of – 123.6 kcal/mol.

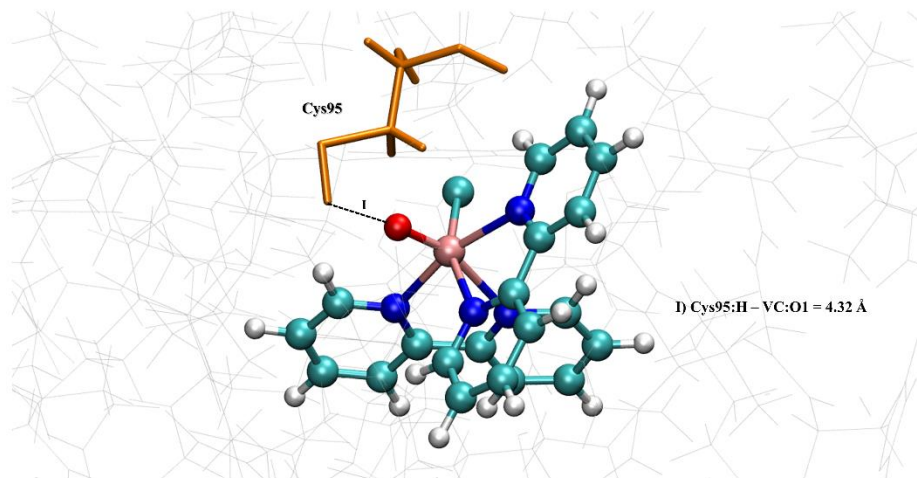


**Fig. 5** Hydrogen bond found after docking simulation (Cys95:H–VC:O1). The bonds lengths are pointed out

### 3.7 Analysis over time – Molecular Dynamics

#### 3.7.1 The behavior of PI3K-VC and ULK1-VC systems

The analyzes of the two MDs, i.e., the behavior over time of the two PI3K-VC and ULK1-VC systems, are discussed below.

#### **PI3K-VC**

The RMSD calculation (equation 9) was performed to evaluate the behavior of the protein-ligand system with reference to the structure obtained from the docking study. From the analysis

of the graph presented in Fig. 6, it is possible to understand the behavior of the vanadium complex inside the PI3K protein.

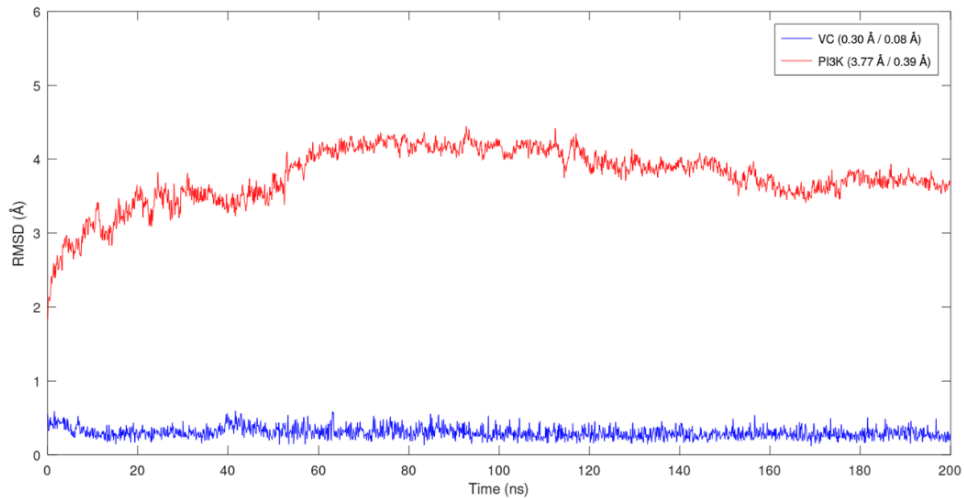


**Fig. 6** Result of RMSD vs. Time performed after the MD simulation. In blue is the behavior of the VC and, in red, of the PI3K

As can be seen, the vanadium complex presents an excellent performance during all 200 ns of simulation, with an average oscillation of only 0.30 Å and standard deviation of 0.08 Å. Although this stage of the work does not aim to evaluate the parameterization performed, we believe that it is extremely valid to understand that such a good result corresponds to the excellent parameterization performed in the first stage of this study.

Regarding the behavior of the PI3K protein, the RMSD graph suggests an oscillation greater than that of the VC (average of 3.77 Å), as expected. However, furtherly analyzing, it is possible to notice that the standard deviation considering the entire simulation was only 0.39 Å, which shows stability during the calculation. Moreover, one must consider that proteins are large systems with high degrees of freedom.

In addition, it is possible to monitor which residues contributed to the greatest degree to the behavior observed in Fig. 6. Therefore, with the assistance of the PyMOL software [53], an analysis of the regions that had greater fluctuations was performed by calculating of RMSF (*root mean square fluctuation*).

Thus, a sausage representation was prepared and presented in Fig. 7. The regions with greater thickness indicate greater oscillations, while the blue and red colors indicate smaller and

larger fluctuations, respectively [54]. Furthermore, the residues responsible for the regions with the greatest fluctuations are shown in Fig. 7, where the regions that most contributed to the PI3K oscillations follow the order *a*, *b*, *c* and *d*.

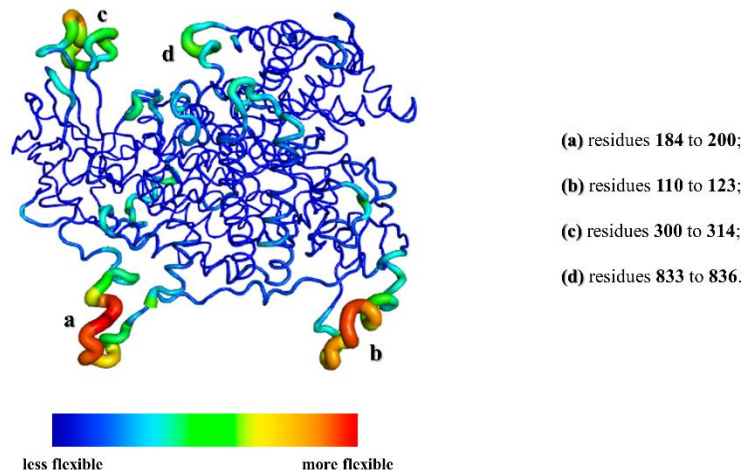


**Fig. 7** Sausage representation of PI3K

### ***ULK1-VC***

In a similar way to the previous system, the result of the RMSD calculation for the ULK1-VC, presented in Fig. 8, was performed with reference to the structure resulting from the docking calculation result.

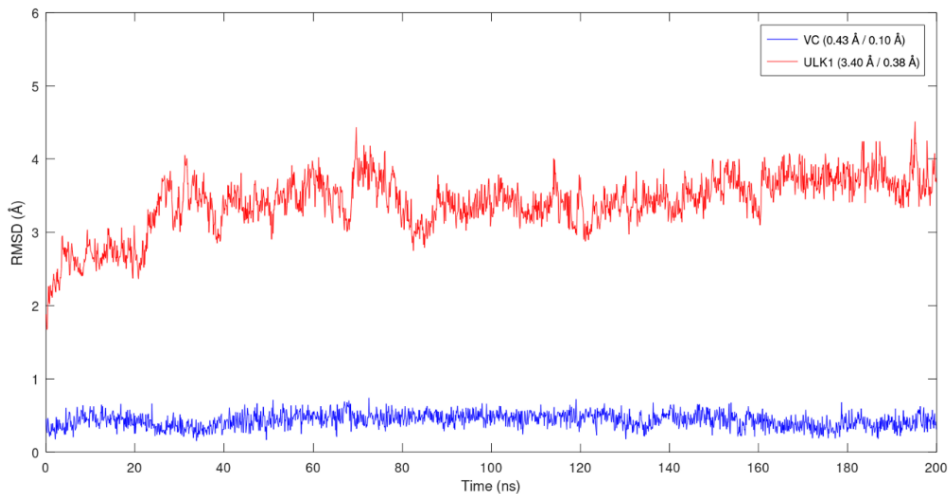


**Fig. 8** RMSD vs. Time. The behavior of the VC during the entire simulation is shown in blue, while the evolution of the ULK1 protein is shown in red

Again, we obtained satisfactory results. As can be seen in the graph of Fig. 8, the variation of the VC was minimal, with an average oscillation of 0.43 Å and standard deviation of 0.10 Å. This is the third RMSD result that we present in relation to VC (Fig. 3, 6 and 8). In both results, we attest to the excellent performance of VCFF, both for structure in vacuum and in the protein cavity.

Through Fig. 8, it is also possible to analyze the behavior of the ULK1 protein during the 200 ns simulation. As can be seen, the biomolecule undergoes greater oscillations until the 90 ns of the simulation. After that, it remains stable within its oscillation range. The average of oscillation is 3.40 Å, however, the standard deviation is only 0.38 Å.

Similar to the previous system, we were able to perform the RMSF calculation on the ULK1 protein and propose a sausage representation (Fig. 9) that would provide a clearer understanding of which regions and protein residues contributed most to the oscillation shown in the graph of Fig. 8.

It is possible to notice, through Fig. 9, that there are regions where greater oscillations occur. Thus, it is possible to suggest that these regions, mainly region *a*, are the most responsible for the oscillations observed in the graph of Fig. 8. The residues that make up this region are described in Fig. 9.

All four of these regions correspond to protein loops, which is in agreement with the literature, as it is already known that these loops are the regions that most contribute to the fluctuations of biomolecules because they are more flexible [55].

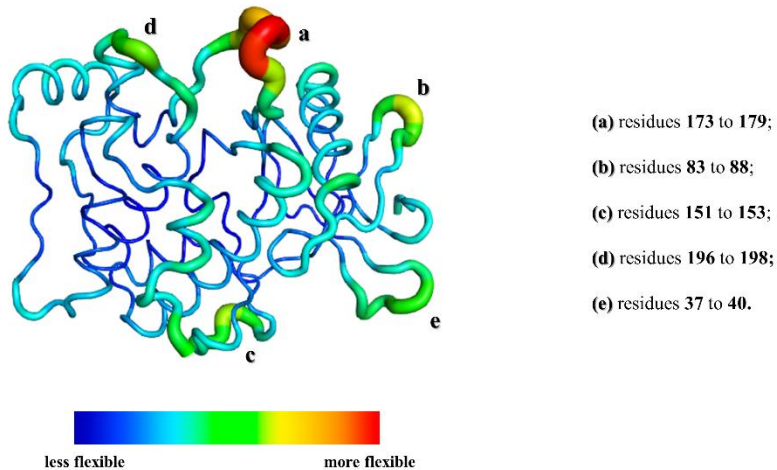


**Fig. 9** Sausage representation of ULK1

### 3.7.2 Intermolecular interactions (H-Bonds)

Hydrogen bonds (H-Bonds) formed between the two systems studied in this work were investigated using the VMD (Visual Molecular Dynamics) software [33] over 200 ns of simulation. Such analyses are commented below.

#### **PI3K-VC**

Fig. 4 shows the result of the docking simulation performed between the PI3K protein and the VC. As mentioned before, it is pointed out in the literature that the bipyridine ligand interacts with the Arg697 residue [39], through its amino group. Furthermore, in our docking study, we pointed out two new interactions formed between the bipyridine nitrogen atoms and the Lys526 residue.

Two of the relevant results found in the MD simulation point to an interaction formed between Arg697 and the N1 from VC, in addition to a bond between Lys526 and N4 from VC. These two results are shown in Fig. 10.

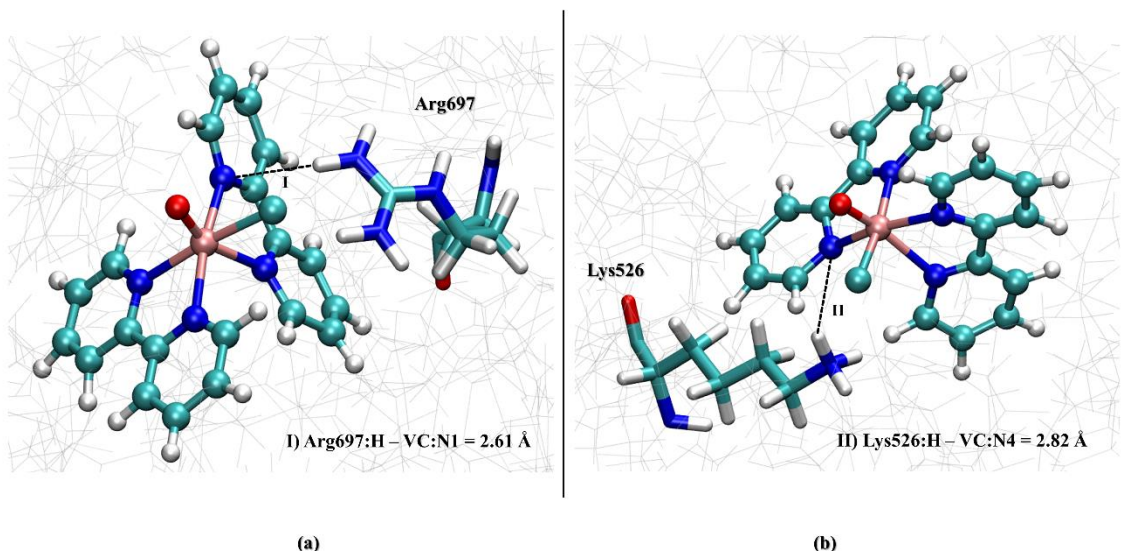


**Fig. 10** MD results. **(a)** Interaction between Arg697 and VC (I) and **(b)** interaction between Lys526 and VC (II).  
The bonds lengths are pointed out

The comparison between the results of Fig. 4a and 10a and Fig. 4b and 10b shows excellent convergence. In the first comparison (Fig. 4a and 10a) there was only the difference between the nitrogen atoms participating in the interactions (N3 and N1, respectively). However, considering that they are the same ligands (both bpy), this difference becomes irrelevant.

In the second comparison (Fig. 4b and 10b), due to the position of the Lys526 residue in the MD, the interaction with the VC type N3 atom was not identified. However, after the simulation, a bond between Lysine 526 and N4 was found, as shown in the docking (Fig. 4b).

It is important to mention that the docking study portrays a static docking scenario. Thus, it is suggestive that an MD simulation completes the interpretations presented in the docking, since it investigates the fitting between protein-ligand over time and this leads to a deeper investigation of the interactions. Therefore, we consider the comparison between the results found in docking (Fig. 4) and those found in MD to be satisfactory (Fig. 10).

Another relevant result pointed out through the MD is presented in Fig. 11. The interactions presented are the H-Bonds with the highest occurrence during the entire simulation. The three bonds shown in Fig. 11 are formed with the residue Gly353 and the atom types O1, N4 and N3 of the VC. The order of highest occurrence is presented by the sequence Gly353:H-VC:O1 (Fig. 11a), Gly353:H-VC:N4 (Fig. 11b) and Gly353:H-VC:N3 (Fig. 11c).

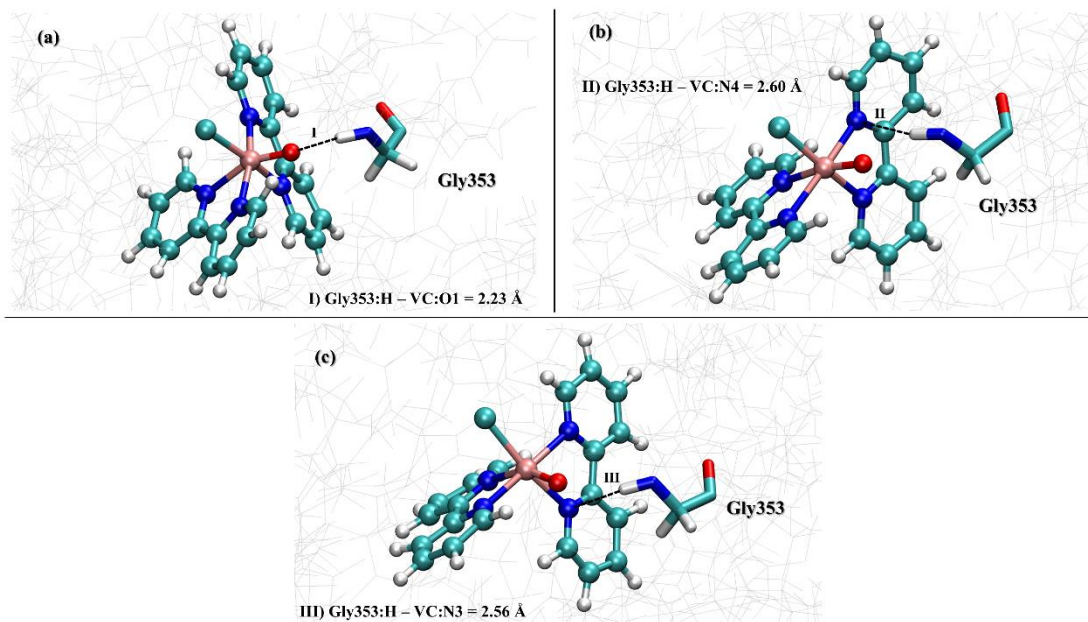


**Fig. 11** Results of interactions pointed out in the MD simulation of the PI3K-VC system between the residue Gly353 and the VC atom types (a) O1 (b) N4 and (c) N3. The lengths of the bonds are pointed out

The MD simulation also showed H-Bonds formed between the atom types O1, N4 and N3 and the amino acid Glutamine (Gln352 residue), however, these interactions had a low occurrence during the 200 ns. For this reason, these bonds were not shown.

In fact, these new residues (Gly353 and Gln352) were not identified in the docking study. However, it is important to note that molecular dynamics simulations take into account the thermal effect, in addition to the solvent effect [56]. This allows energy barriers to be overcome and new regions to be probed. This fact may explain the presence of new residues.

Something important to note is the fact that both the Gly353 residue (Fig. 11) and the Gln352 residue were not present in the original PI3K file. It is possible to confirm this information by looking at Table S4 in the SI file. After completing the protein with the SWISS-MODEL software these residues (and many others) were recovered. This reinforces the importance of being careful in advance with the systems that will be worked on, because, as we have seen, these interactions would never have been pointed out if a previous treatment with the PI3K protein had not been carried out.

### **ULK1-VC**

For this second system, the hydrogen bond shown in Fig. 5 corresponds to an interaction between the H attached to the sulfur atom of the Cys95 residue and the atom type O1 of the VC. This bond was indicated by the docking study to have a length of 4.32 Å, i.e., a relatively large bond. This suggests less stability for the presented bond [57].

In fact, when simulating the ULK1-VC system over 200 ns, this interaction was not observed. On the other hand, a bond involving the same atom type (O1) and the same residue (Cys95) was observed, with the difference that the H involved in the bond is bound to the Cysteine nitrogen and not to the sulfur (Fig. 12a).

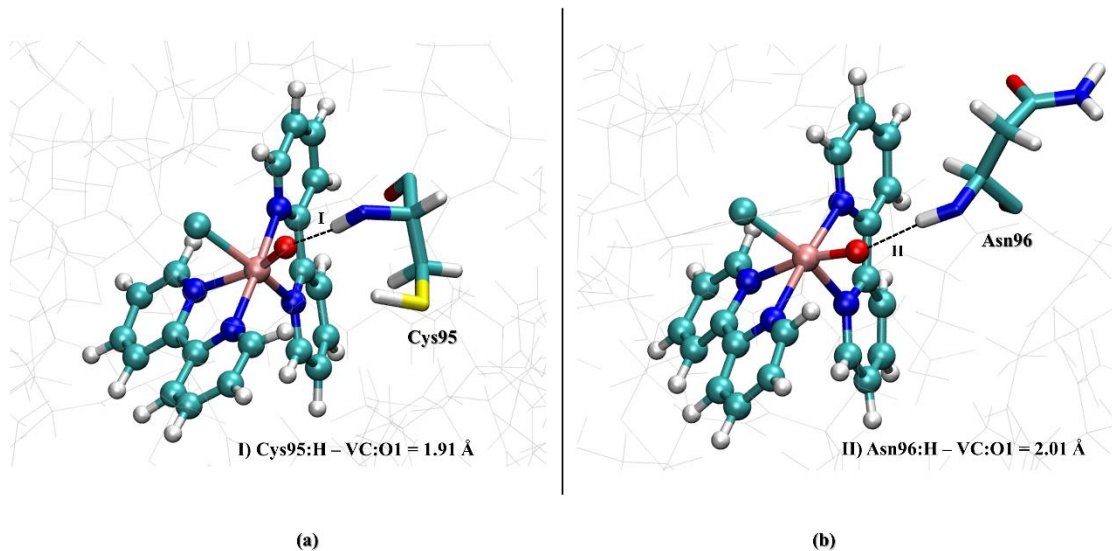


**Fig. 12** ULK1-VC system MD Results. **(a)** H-Bond formed between Cys95:H-VC:O1 and **(b)** Asn96:H-VC:O1.  
The bonds lengths are pointed out

The newly-reported bond shown in Fig. 12a had length of only 1.91 Å, suggesting greater stability than that reported by the docking study (Fig. 5). This reinforces, once again, the need to unite the two methodologies (docking and MD) to investigate protein-ligand systems. The combination of the two studies provides a more detailed and reliable interpretation of the systems of interest.

It is important to mention that the interaction shown in Fig. 12a, in addition to having a connection with the docking result, was also identified as the H-Bond with the highest

frequency of occurrence during the entire MD simulation. All our findings, taken together, point to the Cys95 residue occupying the most prominent place in relation to other residues.

The amino acid Asparagine 96 also appeared among the hydrogen bonds pointed out in the MD study (although with a lower frequency of occurrence). The interaction occurred between the nitrogen bound H of Asparagine with the atom type O1 of the vanadium complex. The bond shown in Fig. 12b presented length of 2.01 Å.

### 3.8 Two pathways for autophagy modulation

As mentioned previously, the autophagy signaling pathway is composed of the PI3K/Akt/mTOR proteins that precede the ULK1 protein [8-11]. This pathway is known as the negative regulatory pathway of autophagy and starts with the PI3K protein, which is responsible for activating Akt and, subsequently, activating mTOR. When mTOR is activated, it down-regulates the ULK1 protein. Therefore, with ULK1 inhibited, autophagy does not occur [10, 11]. This sequence can be seen in Fig. 13.

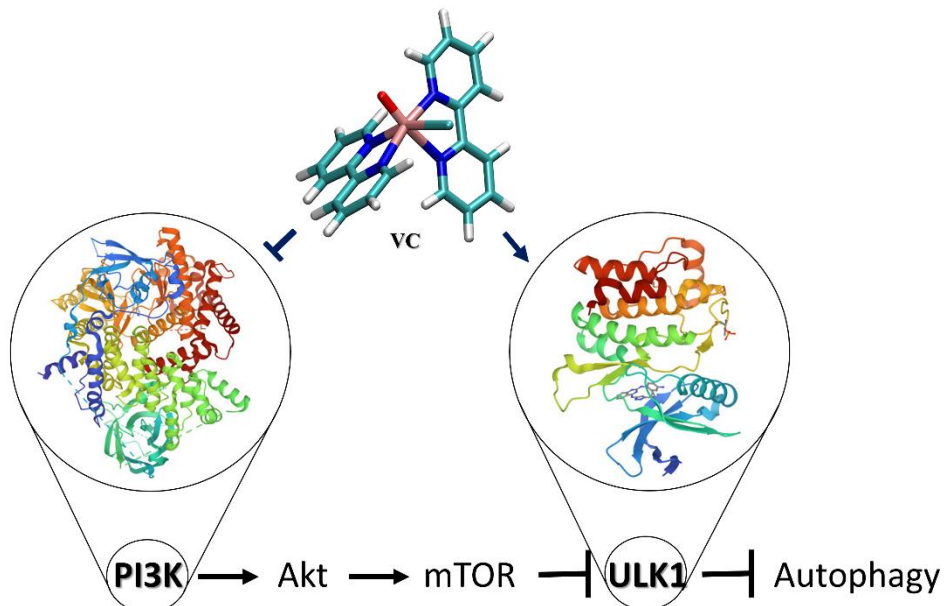


**Fig. 13** Negative regulatory pathway of autophagy. Action of the vanadium complex on PI3K and ULK1 proteins in a scenario in which autophagy would be induced

The VC (Fig. 1) for which we developed a new force field so that it could be studied with proteins at the beginning and end of the autophagy pathway, is known for its ability to induce

autophagy in triple-negative breast cancer cells (TNBC) [17]. Thus, interpreting the pathway shown in Fig. 13, it is possible to understand that the role of the VC would be to reverse the activation/deactivation sequence of proteins, since this complex is known to induce autophagy.

Therefore, the role of VC acting with the protein that initiates the pathway (PI3K) would be to inhibit this protein, which would lead to the opposite sequence of that observed in Fig. 13 and, therefore, the final result would be the induction of autophagy. Aligned with this, the action of the VC with the protein that is on the verge of autophagy to occur or not (ULK1), would activate this protein, since its induction would lead to the occurrence of autophagy. For further clarification, this reasoning has been summarized in Scheme S1 (Section S3) and can be seen in conjunction with Fig. 13.

It is very well established that the possibility of manipulating autophagy, either by inducing or inhibiting pathway proteins, is interpreted as a useful strategy for anticancer treatments [12]. This interpretation becomes quite clear when one understands the duality of autophagy (commented on in Section 1) and that cancer happens in stages. Thus, it is understood that in the initial stage of the disease, the induction of autophagy is suggested, and in the advanced stage, the inhibition of autophagy is suggested so that it does not act in favor of cancer [6, 12-15].

In the previous Section (3.7.2), the hydrogen bond analyses for the two systems PI3K-VC and ULK1-VC were presented. The analysis of the first system highlighted the occurrence of the Gly353:H-VC:O1 bond as the majority. The analysis performed in the second system pointed out the Cys95:H-VC:O1 bond as having the highest frequency of occurrence during the MD simulation. It is worth mentioning the common point between the two mentioned H-Bonds, both were formed through the atom type O1 of the VC.

Thus, it is possible to suggest that the activations of PI3K and ULK1 proteins through the VC are carried out mainly by the formation of these two H-Bonds (Gly353:H-VC:O1 and Cys95:H-VC:O1, respectively). From the point of view of the role of the VC with ULK1, the interpretation is simple, since, as mentioned, the activation of this protein through the VC occurs through the interaction with the amino acid Cysteine.

Another scenario is presented in the performance of VC with PI3K, as the complex has the role of deactivating this protein so that autophagy is induced. In this sense, we suggest that the

way to inactivate PI3K is to prevent the interaction with the Gly353 residue from happening. A possible way to do this would be to propose changes in the VC structure, such as the occupation of the oxygen electron pair used in the formation of the Gly353:H–VC:O1 bond.

Expanding the analysis and thinking about the suggestive context of manipulation of autophagy, in a scenario where the complex [VO(bpy)<sub>2</sub>Cl] acted as an agent capable of, this time, inhibiting autophagy, the VC would have the role of activating PI3K and disable ULK1.

In this sense, as PI3K initiates a process that leads to the non-occurrence of autophagy, the VC's action would be to activate it through interaction with the residue Gly353 (Gly353:H–VC:O1) so that the cascade naturally leads to the inhibition of autophagy. On the other hand, with ULK1, VC would act as an inhibitor to prevent autophagy from occurring. This could be suggested by preventing binding to the Cys95 residue (Cys95:H–VC:O1).

#### **4. Conclusion**

In the first stage of this work, we developed a new and efficient AMBER force field (FF) for the bis(2,2'-bipyridine)chlorooxovanadium(IV) (Fig. 1), from a quantum structure optimized with DFT. This VC is known for its ability to induce autophagy in triple-negative breast cancer cells.

In the sequence (second step), we validated this new FF (VCFF) by implementing it in a MD simulation in vacuum (20 ns), in which an RMSD calculation and analyses of its bond lengths and angles were performed, having experimental and quantum data as reference. In addition, a comparison of the VCFF with the GAFF was performed.

In the third and last step, a docking calculation was performed to obtain a reliable starting structure for the evaluation over time of the two systems studied in this work. On this basis, we performed two MD simulations (both with 200 ns) of the VC with the PI3K and ULK1 proteins, respectively known as the protein that initiates the autophagy signaling pathway and the protein that is on the verge of autophagy to occur or not. To evaluate the evolution of the PI3K-VC and ULK1-VC systems over 200 ns, several analyses were performed, namely: RMSD; H-Bonds; RMSF; and modulation of autophagy.

This last analysis allowed this work to contribute to the understanding of the autophagic machinery complex, as well as the well-known duality of autophagy. From the interactions with the highest frequency of occurrence between the VC and the two proteins PI3K (Gly353:H–VC:O1) and ULK1 (Cys95:H–VC:O1), it was possible to propose two ways for the VC to induce the autophagy.

In general terms, we believe that this work contemplates, at least, two important paths in chemical science. We propose new efficient AMBER force field parameters for the vanadium complex, filling the gap left by the absence of parameters for this compound and, in addition, we propose an important application in the context of autophagy, which can lead to an interesting contribution to anticancer treatments. In other words, this work contributes to both the theoretical chemistry bias and the medicinal chemistry bias.

## **Declarations**

### **Competing Interests**

The authors declare no conflict of interest.

### **Funding**

This work was carried out with the financial support of the Conselho Nacional de Desenvolvimento Científico e Tecnológico (CNPq, 307837/2014-9) and the Fundação de Amparo à Pesquisa do Estado de Minas Gerais (FAPEMIG, PPM-00831-15).

### **Ethics approval**

Not applicable.

### **Consent for publication**

All authors fully agree with the content of this work and are aware of the publication.

### **Data availability**

The authors provide a Supporting Information (SI) file to complement the results and discussions presented in this manuscript.

## Acknowledgements

The authors thank the Brazilian agencies CNPq, FAPEMIG and CAPES for the financial support.

## References

1. Sung, H., et al., *Global cancer statistics 2020: GLOBOCAN estimates of incidence and mortality worldwide for 36 cancers in 185 countries*. Ca-a Cancer Journal for Clinicians, 2021. **71**(3): p. 209-249.
2. Lee, K.L., et al., *Triple-Negative Breast Cancer: Current Understanding and Future Therapeutic Breakthrough Targeting Cancer Stemness*. Cancers, 2019. **11**(9).
3. Kalimutho, M., et al., *Targeted Therapies for Triple-Negative Breast Cancer: Combating a Stubborn Disease*. Trends in Pharmacological Sciences, 2015. **36**(12): p. 822-846.
4. Mahmoud, R., P. Ordonez-Moran, and C. Allegrucci, *Challenges for Triple Negative Breast Cancer Treatment: Defeating Heterogeneity and Cancer Stemness*. Cancers, 2022. **14**(17).
5. Mbugua, S.N., et al., *Beyond DNA-targeting in Cancer Chemotherapy. Emerging Frontiers - A Review*. Current Topics in Medicinal Chemistry, 2021. **21**(1): p. 28-47.
6. Nam, H.J., *Autophagy Modulators in Cancer: Focus on Cancer Treatment*. Life-Basel, 2021. **11**(8).
7. Chun, Y. and J. Kim, *Autophagy: An Essential Degradation Program for Cellular Homeostasis and Life*. Cells, 2018. **7**(12).
8. Su, K.J., et al., *Particulate matter exposure induces the autophagy of macrophages via oxidative stress-mediated PI3K/AKT/mTOR pathway*. Chemosphere, 2017. **167**: p. 444-453.
9. Kocak, M., et al., *Targeting autophagy in disease: established and new strategies*. Autophagy, 2022. **18**(3): p. 473-495.
10. Kaleagasioglu, F., D.M. Ali, and M.R. Berger, *Multiple Facets of Autophagy and the Emerging Role of Alkylphosphocholines as Autophagy Modulators*. Frontiers in Pharmacology, 2020. **11**.
11. Zhang, Y., et al., *M(6)A demethylase fat mass and obesity-associated protein regulates cisplatin resistance of gastric cancer by modulating autophagy activation through ULK1*. Cancer Science, 2022. **113**(9): p. 3085-3096.
12. Dikic, I. and Z. Lazar, *Mechanism and medical implications of mammalian autophagy*. Nature Reviews Molecular Cell Biology, 2018. **19**(6): p. 349-364.
13. Bishop, E. and T.D. Bradshaw, *Autophagy modulation: a prudent approach in cancer treatment?* Cancer Chemotherapy and Pharmacology, 2018. **82**(6): p. 913-922.
14. Yun, C.W. and S.H. Lee, *The Roles of Autophagy in Cancer*. International Journal of Molecular Sciences, 2018. **19**(11).
15. Mishra, P., V. Ammanathan, and R. Manjithaya, *Chemical Biology Strategies to Study Autophagy*. Frontiers in Cell and Developmental Biology, 2018. **6**.
16. Cai, B.C., et al., *Identification of Gossypol Acetate as an Autophagy Modulator with Potent Anti-tumor Effect against Cancer Cells*. Journal of Agricultural and Food Chemistry, 2022. **70**(8): p. 2589-2599.
17. El-Shafey, E.S. and E.S. Elsherbiny, *Possible Selective Cytotoxicity of Vanadium Complex on Breast Cancer Cells Involving Pathophysiological Pathways*. Anti-Cancer Agents in Medicinal Chemistry, 2019. **19**(17): p. 2130-2139.

18. Sutradhar, M., et al., *Antiproliferative activity of heterometallic sodium and potassium-dioxidovanadium(V) polymers*. Journal of Inorganic Biochemistry, 2019. **200**.
19. Kowalski, S., I. Inkielewicz-Stepniak, and D. Wyrzykowski, *New oxidovanadium(IV) coordination complex containing 2-methylnitrilotriacetate ligands induces cell cycle arrest and autophagy in human pancreatic ductal adenocarcinoma cell lines*. Febs Open Bio, 2019. **9**: p. 346-346.
20. Kowalski, S., et al., *Selective cytotoxicity of vanadium complexes on human pancreatic ductal adenocarcinoma cell line by inducing necroptosis, apoptosis and mitotic catastrophe process*. Oncotarget, 2017. **8**(36): p. 60324-60341.
21. Huang, Y., et al., *Vanadium(IV)-chlorodipicolinate alleviates hepatic lipid accumulation by inducing autophagy via the LKB1/AMPK signaling pathway in vitro and in vivo*. Journal of Inorganic Biochemistry, 2018. **183**: p. 66-76.
22. Machado, P.D., et al., *VOSalophen: a vanadium complex with a stilbene derivative-induction of apoptosis, autophagy, and efficiency in experimental cutaneous leishmaniasis*. Journal of Biological Inorganic Chemistry, 2017. **22**(6): p. 929-939.
23. Walker, C.L., et al., *Systemic Bisperoxovanadium Activates Akt/mTOR, Reduces Autophagy, and Enhances Recovery following Cervical Spinal Cord Injury*. Plos One, 2012. **7**(1): p. 315-326.
24. Wu, Y.H., et al., *Sodium orthovanadate inhibits growth of human hepatocellular carcinoma cells in vitro and in an orthotopic model in vivo*. Cancer Letters, 2014. **351**(1): p. 108-116.
25. Pereira, A.F., I.G. Prandi, and T.C. Ramalho, *Parameterization and validation of a new force field for Pt(II) complexes of 2-(4'-amino-2'-hydroxyphenyl)benzothiazole*. International Journal of Quantum Chemistry, 2021. **121**(6).
26. Prandi, I.G., et al., *Combining Classical Molecular Dynamics and Quantum Mechanical Methods for the Description of Electronic Excitations: The Case of Carotenoids*. Journal of Computational Chemistry, 2016. **37**(11): p. 981-991.
27. Brand, S.G., et al., *AN OXO-BRIDGED BINUCLEAR VANADIUM(III) 2,2'-BIPYRIDINE COMPLEX AND ITS VANADIUM(IV) AND VANADIUM(V) OXIDATION-PRODUCTS*. Inorganic Chemistry, 1990. **29**(3): p. 434-438.
28. FRISCH, M.J., et al., *Gaussian 09, Revision A.02*. 2016: Gaussian, Inc., Wallingford CT.
29. Kaur, N., et al., *Spin Inversion Phenomenon and Two-State Reactivity Mechanism for Direct Benzene Hydroxylation by V4O10 Cluster*. Journal of Physical Chemistry A, 2016. **120**(48): p. 9588-9597.
30. Kaur, N., S. Gupta, and N. Goel, *Enantioselective synthesis of sulfoxide using an SBA-15 supported vanadia catalyst: a computational elucidation using a QM/MM approach*. Physical Chemistry Chemical Physics, 2017. **19**(36): p. 25059-25070.
31. Neese, F., *Software update: the ORCA program system, version 4.0*. Wiley Interdisciplinary Reviews-Computational Molecular Science, 2018. **8**(1).
32. Cardenas, G., et al., *A Force Field for a Manganese-Vanadium Water Oxidation Catalyst: Redox Potentials in Solution as Showcase*. Catalysts, 2021. **11**(4).
33. Humphrey, W., A. Dalke, and K. Schulten, *VMD: Visual molecular dynamics*. Journal of Molecular Graphics & Modelling, 1996. **14**(1): p. 33-38.
34. D'Angelo, N.D., et al., *Discovery and Optimization of a Series of Benzothiazole Phosphoinositide 3-Kinase (PI3K)/Mammalian Target of Rapamycin (mTOR) Dual Inhibitors*. Journal of Medicinal Chemistry, 2011. **54**(6): p. 1789-1811.
35. Waterhouse, A., et al., *SWISS-MODEL: homology modelling of protein structures and complexes*. Nucleic Acids Research, 2018. **46**(W1): p. W296-W303.

36. Martinez, L., R. Andreani, and J.M. Martinez, *Convergent algorithms for protein structural alignment*. Bmc Bioinformatics, 2007. **8**.
37. Lazarus, M.B., C.J. Novotny, and K.M. Shokat, *Structure of the Human Autophagy Initiating Kinase ULK1 in Complex with Potent Inhibitors*. Acs Chemical Biology, 2015. **10**(1): p. 257-261.
38. Thomsen, R. and M.H. Christensen, *MolDock: A new technique for high-accuracy molecular docking*. Journal of Medicinal Chemistry, 2006. **49**(11): p. 3315-3321.
39. Gurumoorthy, P., D. Mahendiran, and A.K. Rahiman, *Theoretical calculations, DNA interaction, topoisomerase I and phosphatidylinositol-3-kinase studies of water soluble mixed-ligand nickel(II) complexes*. Chemico-Biological Interactions, 2016. **248**: p. 21-35.
40. Zhang, H.R., et al., *Homology modeling, virtual screening and MD simulations for the identification of NUAK1 and ULK1 potential dual inhibitors*. New Journal of Chemistry, 2022. **46**(9): p. 4103-4113.
41. CASE, D.A., et al., *AMBER 11*. 2010: University of California, San Francisco.
42. Case, D.A., et al., *The Amber biomolecular simulation programs*. Journal of Computational Chemistry, 2005. **26**(16): p. 1668-1688.
43. CASE, D.A., et al., *AMBER 2020*. 2020: University of California, San Francisco.
44. Arba, M., M. Sufriadin, and D.H. Tjahjono, *Identification of Phosphatidylinositol 3-Kinase delta (PI3K delta) Inhibitor: Pharmacophore-based Virtual Screening and Molecular Dynamics Simulation*. Indonesian Journal of Chemistry, 2020. **20**(5): p. 1070-1079.
45. Farrokhzadeh, A., F.B. Akher, and T.J. Egan, *Molecular Mechanism Exploration of Potent Fluorinated PI3K Inhibitors with a Triazine Scaffold: Unveiling the Unusual Synergistic Effect of Pyridine-to-Pyrimidine Ring Interconversion and CF3 Defluorination*. Journal of Physical Chemistry B, 2021. **125**(36): p. 10072-10084.
46. Mu, P. and R. Karuppasamy, *Discovery of human autophagy initiation kinase ULK1 inhibitors by multi-directional in silico screening strategies*. Journal of Receptors and Signal Transduction, 2019. **39**(2): p. 122-133.
47. Kumar, M. and E. Papaleo, *A pan-cancer assessment of alterations of the kinase domain of ULK1, an upstream regulator of autophagy*. Scientific Reports, 2020. **10**(1).
48. Tian, C., et al., *ff19SB: Amino-Acid-Specific Protein Backbone Parameters Trained against Quantum Mechanics Energy Surfaces in Solution*. Journal of Chemical Theory and Computation, 2020. **16**(1): p. 528-552.
49. Pyper, N.C., *Relativity and the periodic table*. Philosophical Transactions of the Royal Society a-Mathematical Physical and Engineering Sciences, 2020. **378**(2180).
50. Sebesta, F., et al., *Estimation of Transition-Metal Empirical Parameters for Molecular Mechanical Force Fields*. Journal of Chemical Theory and Computation, 2016. **12**(8): p. 3681-3688.
51. Wang, J.M., et al., *Development and testing of a general amber force field*. Journal of Computational Chemistry, 2004. **25**(9): p. 1157-1174.
52. Sargsyan, K., C. Grauffel, and C. Lim, *How Molecular Size Impacts RMSD Applications in Molecular Dynamics Simulations*. Journal of Chemical Theory and Computation, 2017. **13**(4): p. 1518-1524.
53. Schrödinger, L., *The PyMOL Molecular Graphics System*. 2015.
54. Sun, Z.T., et al., *Utility of B-Factors in Protein Science: Interpreting Rigidity, Flexibility, and Internal Motion and Engineering Thermostability*. Chemical Reviews, 2019. **119**(3): p. 1626-1665.
55. Subramani, A. and C.A. Floudas, *Structure Prediction of Loops with Fixed and Flexible Stems*. Journal of Physical Chemistry B, 2012. **116**(23): p. 6670-6682.

56. Alonso, H., A.A. Bliznyuk, and J.E. Gready, *Combining docking and molecular dynamic simulations in drug design*. Medicinal Research Reviews, 2006. **26**(5): p. 531-568.
57. Kaupp, M., B. Metz, and H. Stoll, *Breakdown of bond length-bond strength correlation: A case study*. Angewandte Chemie-International Edition, 2000. **39**(24): p. 4607-+.

## SUPPORTING INFORMATION

Of

**Vanadium complex as a potential modulator of the autophagic mechanism through proteins PI3K and ULK1: development, validation and biological implications of a specific force field for [VO(bpy)<sub>2</sub>Cl]**

### Section S1

**Table S1** – Comparative values (%) of selected bond lengths of the vanadium complex (VC), [VO(bpy)<sub>2</sub>Cl]. Comparison between experimental values and four levels of theory: MM (with AMBER and UFF force fields) and QM (B3LYP/def2-TZVP plus ECP and B3LYP/def2-TZVP plus ZORA). In addition, a comparison between B3LYP/def2-TZVP plus ECP and B3LYP/def2-TZVP plus ZORA theory levels.

Bonds	[AMBER/Exp] (%)	[UFF/Exp] (%)	[ECP/Exp] (%)	[ZORA/Exp] (%)	[ECP/ZORA] (%)
V1-O1	16.406	8.550	-3.080	-2.542	-0.553
V1-L1	-4.609	0.976	-1.312	-1.281	-0.031
V1-N2	-13.205	-3.003	11.526	11.078	0.403
V1-N4	-12.460	-3.199	1.098	0.971	0.125
N1-V1	-13.017	-2.839	2.086	1.646	0.432
V1-N3	-19.276	-9.197	-4.368	-4.472	0.109
C4-N1	0.711	6.007	-0.451	-0.392	-0.059
C4-C6	-5.775	0.658	1.036	0.957	0.078
C6-N2	0.287	5.653	-1.383	-1.314	-0.070
D0-N2	1.594	-2.420	-0.336	-0.273	-0.063

**Table S2** – Comparative values (%) of selected bond angles of the vanadium complex (VC), [VO(bpy)<sub>2</sub>Cl]. Comparison between experimental values and four levels of theory: MM (with AMBER and UFF force fields) and QM (B3LYP/def2-TZVP plus ECP and B3LYP/def2-TZVP plus ZORA). Furthermore, a comparison between B3LYP/def2-TZVP plus ECP and B3LYP/def2-TZVP plus ZORA theory levels.

Angles	[AMBER/Exp] (%)	[UFF/Exp] (%)	[ECP/Exp] (%)	[ZORA/Exp] (%)	[ECP/ZORA] (%)
L1-V1-O1	-14.231	-20.860	4.050	4.005	0.043
N2-V1-N1	13.097	5.618	-7.262	-7.005	-0.276
N3-V1-N4	13.566	11.640	3.348	3.349	-0.001
N1-V1-N3	27.297	16.493	23.793	24.003	-0.169
N2-V1-N4	-14.813	-40.466	-41.205	-41.346	0.240
V1-N3-D1	-0.765	-1.023	-1.513	-1.484	-0.029
N1-V1-O1	-30.846	-3.112	-2.085	-2.178	0.094
N4-V1-L1	-10.831	6.374	3.198	3.142	0.055
C4-N1-C5	-0.087	2.273	0.215	0.103	0.112
C6-N2-D0	-0.370	2.042	-0.119	-0.193	0.075

## Section S2

Parameter file for the vanadium complex [VO(bpy)<sub>2</sub>Cl]:

```
MASS
C1 12.01 0.0
C2 12.01 0.0
C3 12.01 0.0
C4 12.01 0.0
C5 12.01 0.0
N1 14.01 0.0
C6 12.01 0.0
C7 12.01 0.0
C8 12.01 0.0
C9 12.01 0.0
D0 12.01 0.0
N2 14.01 0.0
V1 50.94 0.0
D1 12.01 0.0
N3 14.01 0.0
D2 12.01 0.0
D3 12.01 0.0
D4 12.01 0.0
D5 12.01 0.0
D6 12.01 0.0
N4 14.01 0.0
```

D7 12.01 0.0  
 D8 12.01 0.0  
 D9 12.01 0.0  
 E0 12.01 0.0  
 L1 35.45 0.0  
 O1 16.00 0.0  
 H1 1.008 0.0  
 H2 1.008 0.0  
 H3 1.008 0.0  
 H4 1.008 0.0  
 H5 1.008 0.0  
 H6 1.008 0.0  
 H7 1.008 0.0  
 H8 1.008 0.0  
 H9 1.008 0.0  
 I0 1.008 0.0  
 I1 1.008 0.0  
 I2 1.008 0.0  
 I3 1.008 0.0  
 I4 1.008 0.0  
 I5 1.008 0.0  
 I6 1.008 0.0

## BONDS

C1	C2	419.913	1.3869
C1	C5	413.085	1.3850
C1	H1	377.541	1.0807
C2	C3	420.403	1.3861
C2	H2	374.587	1.0820
C3	C4	397.660	1.3929
C3	H3	380.709	1.0792
C4	N1	406.094	1.3485
C4	C6	320.830	1.4797
C5	N1	444.189	1.3370
C5	H4	377.312	1.0810
N1	V1	79.684	2.1802
C6	C7	397.690	1.3926
C6	N2	378.308	1.3474
C7	C8	420.047	1.3869
C7	H5	380.452	1.0793
C8	C9	421.896	1.3864
C8	H6	374.441	1.0820
C9	D0	409.544	1.3866
C9	H7	377.364	1.0808
D0	N2	448.265	1.3350
D0	H8	374.114	1.0819
V1	N3	79.684	2.1802
V1	N4	89.316	2.1665
V1	N2	89.316	2.1665
V1	L1	107.047	2.2974

V1	O1	559.189	1.5691
D1	N3	444.189	1.3370
D1	D4	413.085	1.3850
D1	H9	377.312	1.0810
N3	D2	406.094	1.3485
D2	D3	397.660	1.3929
D2	D6	320.830	1.4797
D3	D5	419.273	1.3861
D3	I0	380.709	1.0793
D4	D5	419.913	1.3869
D4	I1	377.541	1.0807
D5	I2	374.587	1.0820
D6	N4	378.308	1.3474
D6	D9	397.690	1.3926
N4	D7	448.265	1.3350
D7	D8	409.544	1.3866
D7	I3	374.114	1.0819
D8	E0	421.896	1.3864
D8	I4	377.364	1.0808
D9	E0	420.047	1.3869
D9	I5	380.452	1.0793
E0	I6	374.441	1.0820

#### ANGLES

C2	C1	C5	24.745	118.42
C2	C1	H1	23.653	121.64
C5	C1	H1	23.709	119.95
C1	C2	C3	23.934	119.07
C1	C2	H2	23.980	120.76
C3	C2	H2	24.007	120.18
C2	C3	C4	26.334	119.62
C2	C3	H3	25.349	119.74
C4	C3	H3	24.375	120.64
C3	C4	N1	29.032	120.75
C3	C4	C6	98.504	123.23
N1	C4	C6	128.329	116.03
C1	C5	N1	27.577	122.64
C1	C5	H4	25.646	121.32
N1	C5	H4	28.634	116.06
C4	N1	C5	25.222	119.52
C4	N1	V1	90.274	118.68
C5	N1	V1	71.053	121.50
C4	C6	C7	67.554	123.18
C4	C6	N2	84.494	115.78
C7	C6	N2	30.565	121.04
C6	C7	C8	25.665	119.41
C6	C7	H5	24.229	120.86
C8	C7	H5	25.176	119.73
C7	C8	C9	24.124	119.08
C7	C8	H6	24.041	120.16

C9	C8	H6	23.012	120.77
C8	C9	D0	24.843	118.42
C8	C9	H7	23.709	121.60
D0	C9	H7	23.767	119.98
C9	D0	N2	27.991	122.68
C9	D0	H8	25.882	121.32
N2	D0	H8	28.698	116.01
C6	N2	D0	37.955	119.38
N1	V1	N3	8.955	97.55
N1	V1	L1	8.828	90.10
N1	V1	O1	8.148	92.92
N3	V1	N4	6.763	75.13
N3	V1	L1	4.063	159.17
N3	V1	O1	3.346	92.86
N4	V1	L1	7.676	92.78
N4	V1	O1	5.016	100.23
L1	V1	O1	4.332	106.13
N3	D1	D4	27.577	122.64
N3	D1	H9	28.634	116.06
D4	D1	H9	25.646	121.32
V1	N3	D1	71.053	121.50
V1	N3	D2	90.274	118.68
D1	N3	D2	25.222	119.52
N3	D2	D3	29.032	120.75
N3	D2	D6	128.329	116.03
D3	D2	D6	98.504	123.23
D2	D3	D5	26.334	119.62
D2	D3	I0	24.375	120.64
D5	D3	I0	25.349	119.74
D1	D4	D5	24.745	118.42
D1	D4	I1	23.709	119.95
D5	D4	I1	23.653	121.64
D3	D5	D4	23.934	119.07
D3	D5	I2	24.007	120.18
D4	D5	I2	23.980	120.76
D2	D6	N4	84.494	115.78
D2	D6	D9	67.554	123.18
N4	D6	D9	30.565	121.04
V1	N4	D6	14.758	115.62
V1	N4	D7	23.082	124.53
D6	N4	D7	37.955	119.38
N4	D7	D8	27.991	122.68
N4	D7	I3	28.698	116.01
D8	D7	I3	25.882	121.32
D7	D8	E0	24.843	118.42
D7	D8	I4	23.767	119.98
E0	D8	I4	23.709	121.60
D6	D9	E0	25.665	119.41
D6	D9	I5	24.229	120.86
E0	D9	I5	25.176	119.73

D8	E0	D9	24.124	119.08
D8	E0	I6	23.012	120.77
D9	E0	I6	24.041	120.16
N1	V1	N4	3.741	166.84
N2	V1	N4	8.780	94.42
N2	V1	L1	7.676	83.90
N2	V1	O1	5.016	161.68
N2	V1	N3	3.741	80.28
N2	V1	N1	6.763	71.41
V1	N2	D0	23.082	124.53
V1	N2	C6	14.758	115.62

## DIHEDRALS

C5-C1-C2-C3	4	16.0000	180.00	2.000
C5-C1-C2-H2	4	16.0000	180.00	2.000
H1-C1-C2-C3	4	16.0000	180.00	2.000
H1-C1-C2-H2	4	16.0000	180.00	2.000
C2-C1-C5-N1	4	16.0000	180.00	2.000
C2-C1-C5-H4	4	16.0000	180.00	2.000
H1-C1-C5-N1	4	16.0000	180.00	2.000
H1-C1-C5-H4	4	16.0000	180.00	2.000
C1-C2-C3-C4	4	16.0000	180.00	2.000
C1-C2-C3-H3	4	16.0000	180.00	2.000
H2-C2-C3-C4	4	16.0000	180.00	2.000
H2-C2-C3-H3	4	16.0000	180.00	2.000
C2-C3-C4-N1	4	16.0000	180.00	2.000
C2-C3-C4-C6	4	16.0000	180.00	2.000
H3-C3-C4-N1	4	16.0000	180.00	2.000
H3-C3-C4-C6	4	16.0000	180.00	2.000
C3-C4-N1-C5	4	6.8000	180.00	2.000
C3-C4-N1-V1	4	6.8000	180.00	2.000
C6-C4-N1-C5	4	6.8000	180.00	2.000
C6-C4-N1-V1	4	6.8000	180.00	2.000
C3-C4-C6-C7	4	16.0000	180.00	2.000
C3-C4-C6-N2	4	16.0000	180.00	2.000
N1-C4-C6-C7	4	16.0000	180.00	2.000
N1-C4-C6-N2	4	16.0000	180.00	2.000
C1-C5-N1-C4	4	6.8000	180.00	2.000
C1-C5-N1-V1	4	6.8000	180.00	2.000
H4-C5-N1-C4	4	6.8000	180.00	2.000
H4-C5-N1-V1	4	6.8000	180.00	2.000
C4-N1-V1-N3	1	0.1414	352.86	4.000
C4-N1-V1-L1	1	0.1780	256.68	4.000
C4-N1-V1-O1	1	0.1184	180.00	4.000
C5-N1-V1-N3	1	0.1633	282.96	4.000
C5-N1-V1-L1	1	0.2212	83.53	4.000
C5-N1-V1-O1	1	0.1494	260.20	4.000
C4-C6-C7-C8	4	16.0000	180.00	2.000
C4-C6-C7-H5	4	16.0000	180.00	2.000
N2-C6-C7-C8	4	16.0000	180.00	2.000

N2-C6-C7-H5	4	16.0000	180.00	2.000
C4-C6-N2-D0	4	6.8000	180.00	2.000
C7-C6-N2-D0	4	6.8000	180.00	2.000
C6-C7-C8-C9	4	16.0000	180.00	2.000
C6-C7-C8-H6	4	16.0000	180.00	2.000
H5-C7-C8-C9	4	16.0000	180.00	2.000
H5-C7-C8-H6	4	16.0000	180.00	2.000
C7-C8-C9-D0	4	16.0000	180.00	2.000
C7-C8-C9-H7	4	16.0000	180.00	2.000
H6-C8-C9-D0	4	16.0000	180.00	2.000
H6-C8-C9-H7	4	16.0000	180.00	2.000
C8-C9-D0-N2	4	16.0000	180.00	2.000
C8-C9-D0-H8	4	16.0000	180.00	2.000
H7-C9-D0-N2	4	16.0000	180.00	2.000
H7-C9-D0-H8	4	16.0000	180.00	2.000
C9-D0-N2-C6	4	6.8000	180.00	2.000
H8-D0-N2-C6	4	6.8000	180.00	2.000
N1-V1-N3-D1	1	0.1792	282.96	4.000
N1-V1-N3-D2	1	0.1791	352.86	4.000
N4-V1-N3-D1	1	0.0689	180.00	4.000
N4-V1-N3-D2	1	0.0442	180.00	4.000
L1-V1-N3-D1	1	0.1491	83.53	4.000
L1-V1-N3-D2	1	0.1445	256.68	4.000
O1-V1-N3-D1	1	0.2288	260.20	4.000
O1-V1-N3-D2	1	0.2389	180.00	4.000
N3-V1-N4-D6	1	0.0492	173.29	4.000
N3-V1-N4-D7	1	0.0756	180.00	4.000
L1-V1-N4-D6	1	0.1028	10.49	4.000
L1-V1-N4-D7	1	0.1215	198.29	4.000
O1-V1-N4-D6	1	0.1313	180.00	4.000
O1-V1-N4-D7	1	0.1334	180.00	4.000
D4-D1-N3-V1	4	6.8000	180.00	2.000
D4-D1-N3-D2	4	6.8000	180.00	2.000
H9-D1-N3-V1	4	6.8000	180.00	2.000
H9-D1-N3-D2	4	6.8000	180.00	2.000
N3-D1-D4-D5	4	16.0000	180.00	2.000
N3-D1-D4-I1	4	16.0000	180.00	2.000
H9-D1-D4-D5	4	16.0000	180.00	2.000
H9-D1-D4-I1	4	16.0000	180.00	2.000
V1-N3-D2-D3	4	6.8000	180.00	2.000
V1-N3-D2-D6	4	6.8000	180.00	2.000
D1-N3-D2-D3	4	6.8000	180.00	2.000
D1-N3-D2-D6	4	6.8000	180.00	2.000
N3-D2-D3-D5	4	16.0000	180.00	2.000
N3-D2-D3-I0	4	16.0000	180.00	2.000
D6-D2-D3-D5	4	16.0000	180.00	2.000
D6-D2-D3-I0	4	16.0000	180.00	2.000
N3-D2-D6-N4	4	16.0000	180.00	2.000
N3-D2-D6-D9	4	16.0000	180.00	2.000
D3-D2-D6-N4	4	16.0000	180.00	2.000

D3-D2-D6-D9	4	16.0000	180.00	2.000
D2-D3-D5-D4	4	16.0000	180.00	2.000
D2-D3-D5-I2	4	16.0000	180.00	2.000
I0-D3-D5-D4	4	16.0000	180.00	2.000
I0-D3-D5-I2	4	16.0000	180.00	2.000
D1-D4-D5-D3	4	16.0000	180.00	2.000
D1-D4-D5-I2	4	16.0000	180.00	2.000
I1-D4-D5-D3	4	16.0000	180.00	2.000
I1-D4-D5-I2	4	16.0000	180.00	2.000
D2-D6-N4-V1	4	6.8000	180.00	2.000
D2-D6-N4-D7	4	6.8000	180.00	2.000
D9-D6-N4-V1	4	6.8000	180.00	2.000
D9-D6-N4-D7	4	6.8000	180.00	2.000
D2-D6-D9-E0	4	16.0000	180.00	2.000
D2-D6-D9-I5	4	16.0000	180.00	2.000
N4-D6-D9-E0	4	16.0000	180.00	2.000
N4-D6-D9-I5	4	16.0000	180.00	2.000
V1-N4-D7-D8	4	6.8000	180.00	2.000
V1-N4-D7-I3	4	6.8000	180.00	2.000
D6-N4-D7-D8	4	6.8000	180.00	2.000
D6-N4-D7-I3	4	6.8000	180.00	2.000
N4-D7-D8-E0	4	16.0000	180.00	2.000
N4-D7-D8-I4	4	16.0000	180.00	2.000
I3-D7-D8-E0	4	16.0000	180.00	2.000
I3-D7-D8-I4	4	16.0000	180.00	2.000
D7-D8-E0-D9	4	16.0000	180.00	2.000
D7-D8-E0-I6	4	16.0000	180.00	2.000
I4-D8-E0-D9	4	16.0000	180.00	2.000
I4-D8-E0-I6	4	16.0000	180.00	2.000
D6-D9-E0-D8	4	16.0000	180.00	2.000
D6-D9-E0-I6	4	16.0000	180.00	2.000
I5-D9-E0-D8	4	16.0000	180.00	2.000
I5-D9-E0-I6	4	16.0000	180.00	2.000
C4-N1-V1-N4	1	0.1603	180.00	4.000
N2-V1-N3-D2	1	0.1603	180.00	4.000
C4-N1-V1-N2	1	0.0442	180.00	4.000
C4-C6-N2-V1	4	6.8000	180.00	2.000
C5-N1-V1-N4	1	0.1713	180.00	4.000
N2-V1-N3-D1	1	0.1713	180.00	4.000
C5-N1-V1-N2	1	0.0689	180.00	4.000
N1-V1-N4-D6	1	0.1063	180.00	4.000
C6-N2-V1-N3	1	0.1063	180.00	4.000
N1-V1-N4-D7	1	0.1195	180.00	4.000
D0-N2-V1-N3	1	0.1195	180.00	4.000
N1-V1-N2-C6	1	0.0492	173.29	4.000
N1-V1-N2-D0	1	0.0756	180.00	4.000
C6-N2-V1-O1	1	0.1313	180.00	4.000
C6-N2-V1-N4	1	0.1063	180.00	4.000
N2-V1-N4-D6	1	0.1063	180.00	4.000
C6-N2-V1-L1	1	0.1028	10.49	4.000

C7-C6-N2-V1 4 6.8000 180.00 2.000  
 C9-D0-N2-V1 4 6.8000 180.00 2.000  
 D0-N2-V1-O1 1 0.1334 180.00 4.000  
 D0-N2-V1-N4 1 0.1195 180.00 4.000  
 N2-V1-N4-D7 1 0.1195 180.00 4.000  
 D0-N2-V1-L1 1 0.1215 198.29 4.000  
 V1-N2-D0-H8 4 6.8000 180.00 2.000

## NONBONDED

C1 1.9080 0.0860 !  
 C2 1.9080 0.0860 !  
 C3 1.9080 0.0860 !  
 C4 1.9080 0.0860 !  
 C5 1.9080 0.0860 !  
 N1 1.8240 0.1700 !  
 C6 1.9080 0.0860 !  
 C7 1.9080 0.0860 !  
 C8 1.9080 0.0860 !  
 C9 1.9080 0.0860 !  
 D0 1.9080 0.0860 !  
 N2 1.8240 0.1700 !  
 V1 2.7670 1.9040 !  
 D1 1.9080 0.0860 !  
 N3 1.8240 0.1700 !  
 D2 1.9080 0.0860 !  
 D3 1.9080 0.0860 !  
 D4 1.9080 0.0860 !  
 D5 1.9080 0.0860 !  
 D6 1.9080 0.0860 !  
 N4 1.8240 0.1700 !  
 D7 1.9080 0.0860 !  
 D8 1.9080 0.0860 !  
 D9 1.9080 0.0860 !  
 E0 1.9080 0.0860 !  
 L1 1.9480 0.2650 !  
 O1 1.6612 0.2100 !  
 H1 1.4590 0.0150 !  
 H2 1.4590 0.0150 !  
 H3 1.4590 0.0150 !  
 H4 1.4590 0.0150 !  
 H5 1.4590 0.0150 !  
 H6 1.4590 0.0150 !  
 H7 1.4590 0.0150 !  
 H8 1.4590 0.0150 !  
 H9 1.4590 0.0150 !  
 I0 1.4590 0.0150 !  
 I1 1.4590 0.0150 !  
 I2 1.4590 0.0150 !  
 I3 1.4590 0.0150 !  
 I4 1.4590 0.0150 !

I5        1.4590    0.0150    !  
 I6        1.4590    0.0150    !  
 END

**Table S3** – Atomic Charges (RESP) for the vanadium complex [VO(bpy)<sub>2</sub>Cl].

Atom Types	<i>q /e<sup>-</sup></i>
C1	-0.059204
C2	-0.074306
C3	-0.093892
C4	0.106746
C5	-0.014492
N1	-0.196015
C6	0.106746
C7	-0.093892
C8	-0.074306
C9	-0.059204
D0	-0.014492
N2	-0.196015
V1	0.969414
D1	-0.014492
N3	-0.196015
D2	0.106746
D3	-0.093892
D4	-0.059204
D5	-0.074306
D6	0.106746
N4	-0.196015
D7	-0.014492
D8	-0.059204

D9	-0.093892
E0	-0.074306
L1	-0.402956
O1	-0.402302
H1	0.138363
H2	0.150839
H3	0.128669
H4	0.122253
H5	0.128669
H6	0.150839
H7	0.138363
H8	0.122253
H9	0.122253
I0	0.128669
I1	0.138363
I2	0.150839
I3	0.122253
I4	0.138363
I5	0.128669
I6	0.150839

## Section S3

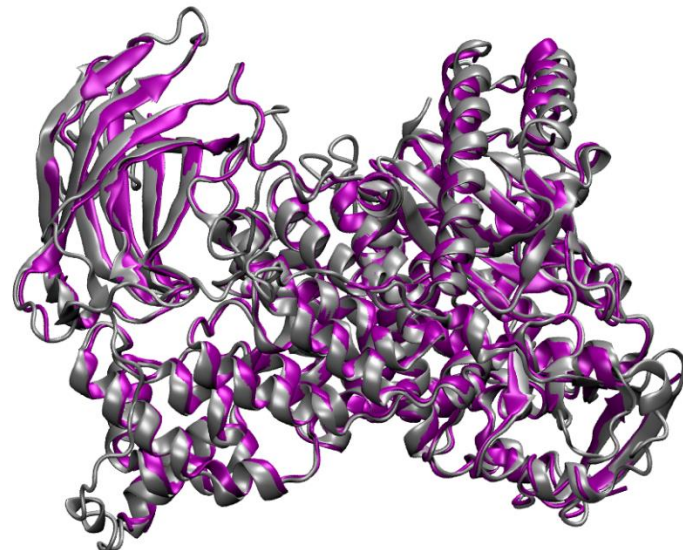
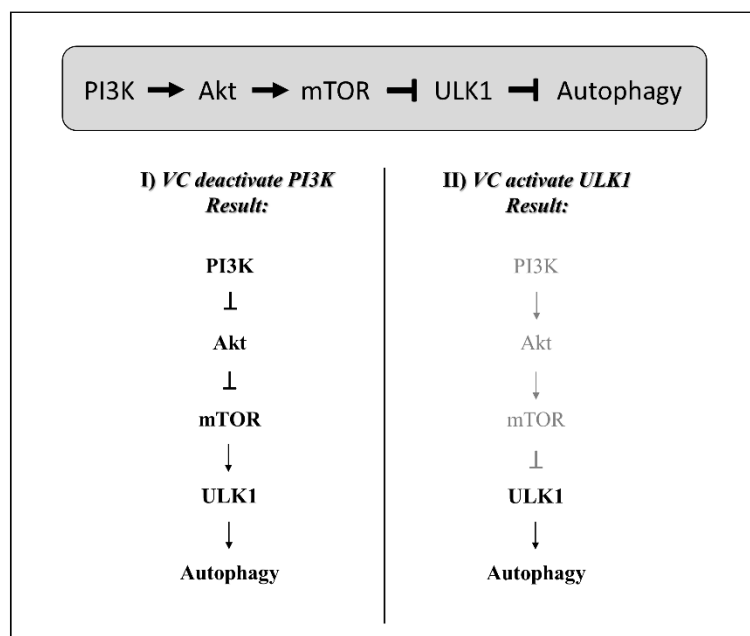


**Fig. S1** Superposition between the original PI3K (purple) and the new model (silver)



**Scheme S1** Summary of what would lead to the action of the vanadium complex on PI3K and ULK1 proteins

**Table S4** – Parallel between the original protein residues and the new model residues. Recovered residues are highlighted in bold.

PI3K_original		PI3K_complete	
SER	147	SER	5
GLN	148	GLN	6
ALA	149	ALA	7
PHE	150	PHE	8
GLN	151	GLN	9
ARG	152	ARG	10
GLN	153	GLN	11
LEU	154	LEU	12
THR	155	THR	13
ALA	156	ALA	14
LEU	157	LEU	15
ILE	158	ILE	16
GLY	159	GLY	17
TYR	160	TYR	18
ASP	161	ASP	19
VAL	162	VAL	20
THR	163	THR	21
ASP	164	ASP	22
VAL	165	VAL	23
SER	166	SER	24
ASN	167	ASN	25
VAL	168	VAL	26
HIS	169	HIS	27
ASP	170	ASP	28
ASP	171	ASP	29
GLU	172	GLU	30
LEU	173	LEU	31
GLU	174	GLU	32
PHE	175	PHE	33
THR	176	THR	34
ARG	177	ARG	35
ARG	178	ARG	36
GLY	179	GLY	37
LEU	180	LEU	38
VAL	181	VAL	39
THR	182	THR	40
PRO	183	PRO	41
ARG	184	ARG	42
MET	185	MET	43
ALA	186	ALA	44
GLU	187	GLU	45
VAL	188	VAL	46
ALA	189	ALA	47
SER	190	SER	48

ARG	191	ARG	49
ASP	192	ASP	50
PRO	193	PRO	51
LYS	194	LYS	52
LEU	195	LEU	53
TYR	196	TYR	54
ALA	197	ALA	55
MET	198	MET	56
HIS	199	HIS	57
PRO	200	PRO	58
TRP	201	TRP	59
VAL	202	VAL	60
THR	203	THR	61
SER	204	SER	62
LYS	205	LYS	63
PRO	206	PRO	64
LEU	207	LEU	65
PRO	208	PRO	66
GLU	209	GLU	67
TYR	210	TYR	68
LEU	211	LEU	69
TRP	212	TRP	70
LYS	213	LYS	71
LYS	214	LYS	72
ILE	215	ILE	73
ALA	216	ALA	74
ASN	217	ASN	75
ASN	218	ASN	76
CYS	219	CYS	77
ILE	220	ILE	78
PHE	221	PHE	79
ILE	222	ILE	80
VAL	223	VAL	81
ILE	224	ILE	82
HIS	225	HIS	83
-	-	<b>ARG</b>	<b>84</b>
-	-	<b>SER</b>	<b>85</b>
-	-	<b>THR</b>	<b>86</b>
THR	229	THR	87
SER	230	SER	88
GLN	231	GLN	89
THR	232	THR	90
ILE	233	ILE	91
LYS	234	LYS	92
VAL	235	VAL	93
SER	236	SER	94

PRO	237	PRO	95
ASP	238	ASP	96
ASP	239	ASP	97
THR	240	THR	98
PRO	241	PRO	99
GLY	242	GLY	100
ALA	243	ALA	101
ILE	244	ILE	102
LEU	245	LEU	103
GLN	246	GLN	104
SER	247	SER	105
PHE	248	PHE	106
-	-	<b>PHE</b>	<b>107</b>
-	-	<b>THR</b>	<b>108</b>
-	-	<b>LYS</b>	<b>109</b>
-	-	<b>MET</b>	<b>110</b>
-	-	<b>ALA</b>	<b>111</b>
-	-	<b>LYS</b>	<b>112</b>
-	-	<b>LYS</b>	<b>113</b>
-	-	<b>LYS</b>	<b>114</b>
-	-	<b>SER</b>	<b>115</b>
-	-	<b>LEU</b>	<b>116</b>
-	-	<b>MET</b>	<b>117</b>
-	-	<b>ASP</b>	<b>118</b>
-	-	<b>ILE</b>	<b>119</b>
-	-	<b>PRO</b>	<b>120</b>
-	-	<b>GLU</b>	<b>121</b>
-	-	<b>SER</b>	<b>122</b>
-	-	<b>GLN</b>	<b>123</b>
-	-	<b>SER</b>	<b>124</b>
-	-	<b>GLU</b>	<b>125</b>
-	-	<b>GLN</b>	<b>126</b>
-	-	<b>ASP</b>	<b>127</b>
-	-	<b>PHE</b>	<b>128</b>
VAL	271	VAL	129
LEU	272	LEU	130
ARG	273	ARG	131
VAL	274	VAL	132
CYS	275	CYS	133
GLY	276	GLY	134
ARG	277	ARG	135
ASP	278	ASP	136
GLU	279	GLU	137
TYR	280	TYR	138
LEU	281	LEU	139
VAL	282	VAL	140
GLY	283	GLY	141
GLU	284	GLU	142

THR	285	THR	143
PRO	286	PRO	144
ILE	287	ILE	145
LYS	288	LYS	146
ASN	289	ASN	147
PHE	290	PHE	148
GLN	291	GLN	149
TRP	292	TRP	150
VAL	293	VAL	151
ARG	294	ARG	152
HIS	295	HIS	153
CYS	296	CYS	154
LEU	297	LEU	155
LYS	298	LYS	156
ASN	299	ASN	157
GLY	300	GLY	158
GLU	301	GLU	159
GLU	302	GLU	160
ILE	303	ILE	161
HIS	304	HIS	162
VAL	305	VAL	163
VAL	306	VAL	164
LEU	307	LEU	165
ASP	308	ASP	166
THR	309	THR	167
PRO	310	PRO	168
PRO	311	PRO	169
ASP	312	ASP	170
PRO	313	PRO	171
ALA	314	ALA	172
LEU	315	LEU	173
ASP	316	ASP	174
GLU	317	GLU	175
VAL	318	VAL	176
ARG	319	ARG	177
LYS	320	LYS	178
GLU	321	GLU	179
-	-	<b>GLU</b>	<b>180</b>
-	-	<b>TRP</b>	<b>181</b>
-	-	<b>PRO</b>	<b>182</b>
-	-	<b>LEU</b>	<b>183</b>
-	-	<b>VAL</b>	<b>184</b>
-	-	<b>ASP</b>	<b>185</b>
-	-	<b>ASP</b>	<b>186</b>
-	-	<b>CYS</b>	<b>187</b>
-	-	<b>THR</b>	<b>188</b>
-	-	<b>GLY</b>	<b>189</b>
-	-	<b>VAL</b>	<b>190</b>

-	-	<b>THR</b>	<b>191</b>
-	-	<b>GLY</b>	<b>192</b>
-	-	<b>TYR</b>	<b>193</b>
-	-	<b>HIS</b>	<b>194</b>
-	-	<b>GLU</b>	<b>195</b>
-	-	<b>GLN</b>	<b>196</b>
-	-	<b>LEU</b>	<b>197</b>
-	-	<b>THR</b>	<b>198</b>
-	-	<b>ILE</b>	<b>199</b>
-	-	<b>HIS</b>	<b>200</b>
-	-	<b>GLY</b>	<b>201</b>
-	-	<b>LYS</b>	<b>202</b>
-	-	<b>ASP</b>	<b>203</b>
-	-	<b>HIS</b>	<b>204</b>
-	-	<b>GLU</b>	<b>205</b>
-	-	<b>SER</b>	<b>206</b>
-	-	<b>VAL</b>	<b>207</b>
-	-	<b>PHE</b>	<b>208</b>
-	-	<b>THR</b>	<b>209</b>
-	-	<b>VAL</b>	<b>210</b>
-	-	<b>SER</b>	<b>211</b>
-	-	<b>LEU</b>	<b>212</b>
-	-	<b>TRP</b>	<b>213</b>
ASP	356	ASP	214
CYS	357	CYS	215
ASP	358	ASP	216
ARG	359	ARG	217
LYS	360	LYS	218
PHE	361	PHE	219
ARG	362	ARG	220
VAL	363	VAL	221
LYS	364	LYS	222
ILE	365	ILE	223
ARG	366	ARG	224
GLY	367	GLY	225
ILE	368	ILE	226
ASP	369	ASP	227
ILE	370	ILE	228
PRO	371	PRO	229
VAL	372	VAL	230
-	-	<b>LEU</b>	<b>231</b>
-	-	<b>PRO</b>	<b>232</b>
-	-	<b>ARG</b>	<b>233</b>
-	-	<b>ASN</b>	<b>234</b>
-	-	<b>THR</b>	<b>235</b>
-	-	<b>ASP</b>	<b>236</b>
-	-	<b>LEU</b>	<b>237</b>
THR	380	THR	238

VAL	381	VAL	239
PHE	382	PHE	240
VAL	383	VAL	241
GLU	384	GLU	242
ALA	385	ALA	243
ASN	386	ASN	244
ILE	387	ILE	245
GLN	388	GLN	246
HIS	389	HIS	247
GLY	390	GLY	248
GLN	391	GLN	249
GLN	392	GLN	250
VAL	393	VAL	251
LEU	394	LEU	252
CYS	395	CYS	253
GLN	396	GLN	254
ARG	397	ARG	255
ARG	398	ARG	256
THR	399	THR	257
SER	400	SER	258
PRO	401	PRO	259
LYS	402	LYS	260
PRO	403	PRO	261
PHE	404	PHE	262
THR	405	THR	263
GLU	406	GLU	264
GLU	407	GLU	265
VAL	408	VAL	266
LEU	409	LEU	267
TRP	410	TRP	268
ASN	411	ASN	269
VAL	412	VAL	270
TRP	413	TRP	271
LEU	414	LEU	272
GLU	415	GLU	273
PHE	416	PHE	274
SER	417	SER	275
ILE	418	ILE	276
LYS	419	LYS	277
ILE	420	ILE	278
LYS	421	LYS	279
ASP	422	ASP	280
LEU	423	LEU	281
PRO	424	PRO	282
LYS	425	LYS	283
GLY	426	GLY	284
ALA	427	ALA	285
LEU	428	LEU	286

LEU	429	LEU	287
ASN	430	ASN	288
LEU	431	LEU	289
GLN	432	GLN	290
ILE	433	ILE	291
TYR	434	TYR	292
CYS	435	CYS	293
-	-	<b>GLY</b>	<b>294</b>
-	-	<b>LYS</b>	<b>295</b>
-	-	<b>ALA</b>	<b>296</b>
-	-	<b>PRO</b>	<b>297</b>
-	-	<b>ALA</b>	<b>298</b>
-	-	<b>LEU</b>	<b>299</b>
-	-	<b>SER</b>	<b>300</b>
-	-	<b>SER</b>	<b>301</b>
-	-	<b>LYS</b>	<b>302</b>
-	-	<b>ALA</b>	<b>303</b>
-	-	<b>SER</b>	<b>304</b>
-	-	<b>ALA</b>	<b>305</b>
-	-	<b>GLU</b>	<b>306</b>
-	-	<b>SER</b>	<b>307</b>
-	-	<b>PRO</b>	<b>308</b>
-	-	<b>SER</b>	<b>309</b>
-	-	<b>SER</b>	<b>310</b>
-	-	<b>GLU</b>	<b>311</b>
-	-	<b>SER</b>	<b>312</b>
-	-	<b>LYS</b>	<b>313</b>
-	-	<b>GLY</b>	<b>314</b>
-	-	<b>LYS</b>	<b>315</b>
VAL	458	VAL	316
GLN	459	GLN	317
LEU	460	LEU	318
LEU	461	LEU	319
TYR	462	TYR	320
TYR	463	TYR	321
VAL	464	VAL	322
ASN	465	ASN	323
LEU	466	LEU	324
LEU	467	LEU	325
LEU	468	LEU	326
ILE	469	ILE	327
ASP	470	ASP	328
HIS	471	HIS	329
ARG	472	ARG	330
PHE	473	PHE	331
LEU	474	LEU	332
LEU	475	LEU	333
ARG	476	ARG	334

ARG	477	ARG	335
GLY	478	GLY	336
GLU	479	GLU	337
TYR	480	TYR	338
VAL	481	VAL	339
LEU	482	LEU	340
HIS	483	HIS	341
MET	484	MET	342
TRP	485	TRP	343
GLN	486	GLN	344
ILE	487	ILE	345
-	-	<b>SER</b>	<b>346</b>
-	-	<b>GLY</b>	<b>347</b>
-	-	<b>LYS</b>	<b>348</b>
-	-	<b>GLY</b>	<b>349</b>
-	-	<b>GLU</b>	<b>350</b>
-	-	<b>ASP</b>	<b>351</b>
-	-	<b>GLN</b>	<b>352</b>
-	-	<b>GLY</b>	<b>353</b>
-	-	<b>SER</b>	<b>354</b>
PHE	497	PHE	355
ASN	498	ASN	356
ALA	499	ALA	357
ASP	500	ASP	358
LYS	501	LYS	359
LEU	502	LEU	360
THR	503	THR	361
SER	504	SER	362
ALA	505	ALA	363
THR	506	THR	364
ASN	507	ASN	365
PRO	508	PRO	366
ASP	509	ASP	367
LYS	510	LYS	368
GLU	511	GLU	369
ASN	512	ASN	370
SER	513	SER	371
MET	514	MET	372
SER	515	SER	373
ILE	516	ILE	374
SER	517	SER	375
ILE	518	ILE	376
LEU	519	LEU	377
LEU	520	LEU	378
ASP	521	ASP	379
-	-	<b>ASN</b>	<b>380</b>
-	-	<b>TYR</b>	<b>381</b>
-	-	<b>CYS</b>	<b>382</b>

-	-	<b>HIS</b>	<b>383</b>
-	-	<b>PRO</b>	<b>384</b>
-	-	<b>ILE</b>	<b>385</b>
-	-	<b>ALA</b>	<b>386</b>
-	-	<b>LEU</b>	<b>387</b>
-	-	<b>PRO</b>	<b>388</b>
-	-	<b>LYS</b>	<b>389</b>
-	-	<b>HIS</b>	<b>390</b>
-	-	<b>GLN</b>	<b>391</b>
-	-	<b>PRO</b>	<b>392</b>
-	-	<b>THR</b>	<b>393</b>
-	-	<b>PRO</b>	<b>394</b>
-	-	<b>ASP</b>	<b>395</b>
-	-	<b>PRO</b>	<b>396</b>
-	-	<b>GLU</b>	<b>397</b>
-	-	<b>GLY</b>	<b>398</b>
-	-	<b>ASP</b>	<b>399</b>
-	-	<b>ARG</b>	<b>400</b>
-	-	<b>VAL</b>	<b>401</b>
-	-	<b>ARG</b>	<b>402</b>
-	-	<b>ALA</b>	<b>403</b>
GLU	546	GLU	404
MET	547	MET	405
PRO	548	PRO	406
ASN	549	ASN	407
GLN	550	GLN	408
LEU	551	LEU	409
ARG	552	ARG	410
LYS	553	LYS	411
GLN	554	GLN	412
LEU	555	LEU	413
GLU	556	GLU	414
ALA	557	ALA	415
ILE	558	ILE	416
ILE	559	ILE	417
ALA	560	ALA	418
THR	561	THR	419
ASP	562	ASP	420
PRO	563	PRO	421
LEU	564	LEU	422
ASN	565	ASN	423
PRO	566	PRO	424
LEU	567	LEU	425
THR	568	THR	426
ALA	569	ALA	427
GLU	570	GLU	428
ASP	571	ASP	429
LYS	572	LYS	430

GLU	573	GLU	431
LEU	574	LEU	432
LEU	575	LEU	433
TRP	576	TRP	434
HIS	577	HIS	435
PHE	578	PHE	436
ARG	579	ARG	437
TYR	580	TYR	438
GLU	581	GLU	439
SER	582	SER	440
LEU	583	LEU	441
LYS	584	LYS	442
HIS	585	HIS	443
PRO	586	PRO	444
LYS	587	LYS	445
ALA	588	ALA	446
TYR	589	TYR	447
PRO	590	PRO	448
LYS	591	LYS	449
LEU	592	LEU	450
PHE	593	PHE	451
SER	594	SER	452
SER	595	SER	453
VAL	596	VAL	454
LYS	597	LYS	455
TRP	598	TRP	456
GLY	599	GLY	457
GLN	600	GLN	458
GLN	601	GLN	459
GLU	602	GLU	460
ILE	603	ILE	461
VAL	604	VAL	462
ALA	605	ALA	463
LYS	606	LYS	464
THR	607	THR	465
TYR	608	TYR	466
GLN	609	GLN	467
LEU	610	LEU	468
LEU	611	LEU	469
ALA	612	ALA	470
ARG	613	ARG	471
ARG	614	ARG	472
GLU	615	GLU	473
VAL	616	VAL	474
TRP	617	TRP	475
ASP	618	ASP	476
GLN	619	GLN	477
SER	620	SER	478

ALA	621	ALA	479
LEU	622	LEU	480
ASP	623	ASP	481
VAL	624	VAL	482
GLY	625	GLY	483
LEU	626	LEU	484
THR	627	THR	485
MET	628	MET	486
GLN	629	GLN	487
LEU	630	LEU	488
LEU	631	LEU	489
ASP	632	ASP	490
CYS	633	CYS	491
ASN	634	ASN	492
PHE	635	PHE	493
SER	636	SER	494
ASP	637	ASP	495
GLU	638	GLU	496
ASN	639	ASN	497
VAL	640	VAL	498
ARG	641	ARG	499
ALA	642	ALA	500
ILE	643	ILE	501
ALA	644	ALA	502
VAL	645	VAL	503
GLN	646	GLN	504
LYS	647	LYS	505
LEU	648	LEU	506
GLU	649	GLU	507
SER	650	SER	508
LEU	651	LEU	509
GLU	652	GLU	510
ASP	653	ASP	511
ASP	654	ASP	512
ASP	655	ASP	513
VAL	656	VAL	514
LEU	657	LEU	515
HIS	658	HIS	516
TYR	659	TYR	517
LEU	660	LEU	518
LEU	661	LEU	519
GLN	662	GLN	520
LEU	663	LEU	521
VAL	664	VAL	522
GLN	665	GLN	523
ALA	666	ALA	524
VAL	667	VAL	525
LYS	668	LYS	526

PHE	669	PHE	527
GLU	670	GLU	528
PRO	671	PRO	529
TYR	672	TYR	530
HIS	673	HIS	531
ASP	674	ASP	532
SER	675	SER	533
ALA	676	ALA	534
LEU	677	LEU	535
ALA	678	ALA	536
ARG	679	ARG	537
PHE	680	PHE	538
LEU	681	LEU	539
LEU	682	LEU	540
LYS	683	LYS	541
ARG	684	ARG	542
GLY	685	GLY	543
LEU	686	LEU	544
ARG	687	ARG	545
ASN	688	ASN	546
LYS	689	LYS	547
ARG	690	ARG	548
ILE	691	ILE	549
GLY	692	GLY	550
HIS	693	HIS	551
PHE	694	PHE	552
LEU	695	LEU	553
PHE	696	PHE	554
TRP	697	TRP	555
PHE	698	PHE	556
LEU	699	LEU	557
ARG	700	ARG	558
SER	701	SER	559
GLU	702	GLU	560
ILE	703	ILE	561
ALA	704	ALA	562
GLN	705	GLN	563
SER	706	SER	564
ARG	707	ARG	565
HIS	708	HIS	566
TYR	709	TYR	567
GLN	710	GLN	568
GLN	711	GLN	569
ARG	712	ARG	570
PHE	713	PHE	571
ALA	714	ALA	572
VAL	715	VAL	573
ILE	716	ILE	574

LEU	717	LEU	575
GLU	718	GLU	576
ALA	719	ALA	577
TYR	720	TYR	578
LEU	721	LEU	579
ARG	722	ARG	580
GLY	723	GLY	581
CYS	724	CYS	582
GLY	725	GLY	583
THR	726	THR	584
ALA	727	ALA	585
MET	728	MET	586
LEU	729	LEU	587
HIS	730	HIS	588
ASP	731	ASP	589
PHE	732	PHE	590
THR	733	THR	591
GLN	734	GLN	592
GLN	735	GLN	593
VAL	736	VAL	594
GLN	737	GLN	595
VAL	738	VAL	596
ILE	739	ILE	597
GLU	740	GLU	598
MET	741	MET	599
LEU	742	LEU	600
GLN	743	GLN	601
LYS	744	LYS	602
VAL	745	VAL	603
THR	746	THR	604
LEU	747	LEU	605
ASP	748	ASP	606
ILE	749	ILE	607
LYS	750	LYS	608
SER	751	SER	609
LEU	752	LEU	610
SER	753	SER	611
-	-	<b>ALA</b>	<b>612</b>
-	-	<b>GLU</b>	<b>613</b>
-	-	<b>LYS</b>	<b>614</b>
-	-	<b>TYR</b>	<b>615</b>
ASP	758	ASP	616
VAL	759	VAL	617
SER	760	SER	618
SER	761	SER	619
GLN	762	GLN	620
VAL	763	VAL	621
ILE	764	ILE	622

SER	765	SER	623
GLN	766	GLN	624
LEU	767	LEU	625
LYS	768	LYS	626
GLN	769	GLN	627
LYS	770	LYS	628
LEU	771	LEU	629
GLU	772	GLU	630
ASN	773	ASN	631
LEU	774	LEU	632
GLN	775	GLN	633
ASN	776	ASN	634
-	-	<b>SER</b>	<b>635</b>
-	-	<b>GLN</b>	<b>636</b>
-	-	<b>LEU</b>	<b>637</b>
PRO	780	PRO	638
GLU	781	GLU	639
SER	782	SER	640
PHE	783	PHE	641
ARG	784	ARG	642
VAL	785	VAL	643
PRO	786	PRO	644
TYR	787	TYR	645
ASP	788	ASP	646
PRO	789	PRO	647
GLY	790	GLY	648
LEU	791	LEU	649
LYS	792	LYS	650
ALA	793	ALA	651
GLY	794	GLY	652
ALA	795	ALA	653
LEU	796	LEU	654
ALA	797	ALA	655
ILE	798	ILE	656
GLU	799	GLU	657
LYS	800	LYS	658
CYS	801	CYS	659
LYS	802	LYS	660
VAL	803	VAL	661
MET	804	MET	662
ALA	805	ALA	663
SER	806	SER	664
LYS	807	LYS	665
LYS	808	LYS	666
LYS	809	LYS	667
PRO	810	PRO	668
LEU	811	LEU	669
TRP	812	TRP	670

LEU	813	LEU	671
GLU	814	GLU	672
PHE	815	PHE	673
LYS	816	LYS	674
CYS	817	CYS	675
ALA	818	ALA	676
ASP	819	ASP	677
PRO	820	PRO	678
THR	821	THR	679
ALA	822	ALA	680
LEU	823	LEU	681
SER	824	SER	682
ASN	825	ASN	683
GLU	826	GLU	684
THR	827	THR	685
ILE	828	ILE	686
GLY	829	GLY	687
ILE	830	ILE	688
ILE	831	ILE	689
PHE	832	PHE	690
LYS	833	LYS	691
HIS	834	HIS	692
GLY	835	GLY	693
ASP	836	ASP	694
ASP	837	ASP	695
LEU	838	LEU	696
ARG	839	ARG	697
GLN	840	GLN	698
ASP	841	ASP	699
MET	842	MET	700
LEU	843	LEU	701
ILE	844	ILE	702
LEU	845	LEU	703
GLN	846	GLN	704
ILE	847	ILE	705
LEU	848	LEU	706
ARG	849	ARG	707
ILE	850	ILE	708
MET	851	MET	709
GLU	852	GLU	710
SER	853	SER	711
ILE	854	ILE	712
TRP	855	TRP	713
GLU	856	GLU	714
THR	857	THR	715
GLU	858	GLU	716
SER	859	SER	717
LEU	860	LEU	718

ASP	861	ASP	719
LEU	862	LEU	720
CYS	863	CYS	721
LEU	864	LEU	722
LEU	865	LEU	723
PRO	866	PRO	724
TYR	867	TYR	725
GLY	868	GLY	726
CYS	869	CYS	727
ILE	870	ILE	728
SER	871	SER	729
THR	872	THR	730
GLY	873	GLY	731
ASP	874	ASP	732
LYS	875	LYS	733
ILE	876	ILE	734
GLY	877	GLY	735
MET	878	MET	736
ILE	879	ILE	737
GLU	880	GLU	738
ILE	881	ILE	739
VAL	882	VAL	740
LYS	883	LYS	741
ASP	884	ASP	742
ALA	885	ALA	743
THR	886	THR	744
THR	887	THR	745
ILE	888	ILE	746
ALA	889	ALA	747
LYS	890	LYS	748
ILE	891	ILE	749
GLN	892	GLN	750
GLN	893	GLN	751
SER	894	SER	752
THR	895	THR	753
-	-	VAL	754
-	-	GLY	755
-	-	ASN	756
-	-	THR	757
GLY	900	GLY	758
ALA	901	ALA	759
PHE	902	PHE	760
LYS	903	LYS	761
ASP	904	ASP	762
GLU	905	GLU	763
VAL	906	VAL	764
LEU	907	LEU	765
ASN	908	ASN	766

HIS	909	HIS	767
TRP	910	TRP	768
LEU	911	LEU	769
LYS	912	LYS	770
GLU	913	GLU	771
LYS	914	LYS	772
SER	915	SER	773
PRO	916	PRO	774
THR	917	THR	775
GLU	918	GLU	776
GLU	919	GLU	777
LYS	920	LYS	778
PHE	921	PHE	779
GLN	922	GLN	780
ALA	923	ALA	781
ALA	924	ALA	782
VAL	925	VAL	783
GLU	926	GLU	784
ARG	927	ARG	785
PHE	928	PHE	786
VAL	929	VAL	787
TYR	930	TYR	788
SER	931	SER	789
CYS	932	CYS	790
ALA	933	ALA	791
GLY	934	GLY	792
TYR	935	TYR	793
CYS	936	CYS	794
VAL	937	VAL	795
ALA	938	ALA	796
THR	939	THR	797
PHE	940	PHE	798
VAL	941	VAL	799
LEU	942	LEU	800
GLY	943	GLY	801
ILE	944	ILE	802
GLY	945	GLY	803
ASP	946	ASP	804
ARG	947	ARG	805
HIS	948	HIS	806
ASN	949	ASN	807
ASP	950	ASP	808
ASN	951	ASN	809
ILE	952	ILE	810
MET	953	MET	811
ILE	954	ILE	812
THR	955	THR	813
GLU	956	GLU	814

THR	957	THR	815
GLY	958	GLY	816
ASN	959	ASN	817
LEU	960	LEU	818
PHE	961	PHE	819
HIS	962	HIS	820
ILE	963	ILE	821
ASP	964	ASP	822
PHE	965	PHE	823
GLY	966	GLY	824
HIS	967	HIS	825
-	-	ILE	<b>826</b>
-	-	LEU	<b>827</b>
-	-	GLY	<b>828</b>
-	-	ASN	<b>829</b>
-	-	TYR	<b>830</b>
-	-	LYS	<b>831</b>
-	-	SER	<b>832</b>
-	-	PHE	<b>833</b>
-	-	LEU	<b>834</b>
-	-	GLY	<b>835</b>
-	-	ILE	<b>836</b>
-	-	ASN	<b>837</b>
-	-	LYS	<b>838</b>
GLU	981	GLU	839
ARG	982	ARG	840
VAL	983	VAL	841
PRO	984	PRO	842
PHE	985	PHE	843
VAL	986	VAL	844
LEU	987	LEU	845
THR	988	THR	846
PRO	989	PRO	847
ASP	990	ASP	848
PHE	991	PHE	849
LEU	992	LEU	850
PHE	993	PHE	851
VAL	994	VAL	852
MET	995	MET	853
GLY	996	GLY	854
THR	997	THR	855
SER	998	SER	856
GLY	999	GLY	857
LYS	1000	LYS	858
LYS	1001	LYS	859
THR	1002	THR	860
SER	1003	SER	861
PRO	1004	PRO	862

HIS	1005	HIS	863
PHE	1006	PHE	864
GLN	1007	GLN	865
LYS	1008	LYS	866
PHE	1009	PHE	867
GLN	1010	GLN	868
ASP	1011	ASP	869
ILE	1012	ILE	870
CYS	1013	CYS	871
VAL	1014	VAL	872
LYS	1015	LYS	873
ALA	1016	ALA	874
TYR	1017	TYR	875
LEU	1018	LEU	876
ALA	1019	ALA	877
LEU	1020	LEU	878
ARG	1021	ARG	879
HIS	1022	HIS	880
HIS	1023	HIS	881
THR	1024	THR	882
ASN	1025	ASN	883
LEU	1026	LEU	884
LEU	1027	LEU	885
ILE	1028	ILE	886
ILE	1029	ILE	887
LEU	1030	LEU	888
PHE	1031	PHE	889
SER	1032	SER	890
MET	1033	MET	891
MET	1034	MET	892
LEU	1035	LEU	893
MET	1036	MET	894
THR	1037	THR	895
GLY	1038	GLY	896
MET	1039	MET	897
PRO	1040	PRO	898
-	-	GLN	<b>899</b>
-	-	LEU	<b>900</b>
-	-	THR	<b>901</b>
SER	1044	SER	902
LYS	1045	LYS	903
GLU	1046	GLU	904
ASP	1047	ASP	905
ILE	1048	ILE	906
GLU	1049	GLU	907
TYR	1050	TYR	908
ILE	1051	ILE	909

ARG	1052	ARG	910
ASP	1053	ASP	911
ALA	1054	ALA	912
LEU	1055	LEU	913
THR	1056	THR	914
VAL	1057	VAL	915
GLY	1058	GLY	916
LYS	1059	LYS	917
ASN	1060	ASN	918
GLU	1061	GLU	919
GLU	1062	GLU	920
ASP	1063	ASP	921
ALA	1064	ALA	922
LYS	1065	LYS	923
LYS	1066	LYS	924
TYR	1067	TYR	925
PHE	1068	PHE	926
LEU	1069	LEU	927
ASP	1070	ASP	928
GLN	1071	GLN	929
ILE	1072	ILE	930
GLU	1073	GLU	931
VAL	1074	VAL	932
CYS	1075	CYS	933
ARG	1076	ARG	934
ASP	1077	ASP	935
LYS	1078	LYS	936
GLY	1079	GLY	937
TRP	1080	TRP	938
THR	1081	THR	939
VAL	1082	VAL	940
GLN	1083	GLN	941
PHE	1084	PHE	942
ASN	1085	ASN	943
TRP	1086	TRP	944
PHE	1087	PHE	945
LEU	1088	LEU	946
HIS	1089	HIS	947
-	-	LEU	<b>948</b>
-	-	VAL	<b>949</b>

## ANEXO

Trabalhos desenvolvidos no período do Doutorado:

- **Value of Contrast-enhanced Magnetic Resonance Imaging (MRI) in the Diagnosis of Breast Cancer**

Mateus A. Gonçalves, Bruna T. L. Pereira, Camila A. Tavares, Taináh M. R. Santos, Elaine F. F. da Cunha, and Teodorico C. Ramalho

(Artigo publicado na *Mini-Reviews in Medicinal Chemistry*)

<https://doi.org/10.2174/138955752166210521113155>

- **Molecular Dynamics-Assisted Interaction of Vanadium Complex–AMPK: From Force Field Development to Biological Application for Alzheimer’s Treatment**

Camila A. Tavares, Taináh M. R. Santos, Elaine F. F. da Cunha, and Teodorico C. Ramalho

(Artigo publicado na *The Journal of Physical Chemistry B*)

<https://doi.org/10.1021/acs.jpcb.2c07147>

- **Improving the path to obtain spectroscopic parameters for the PI3K–(platinum complex) system: Theoretical Evidences for Using  $^{195}\text{Pt}$  NMR as a Probe**

Taináh M. R. Santos, Gustavo A. Andolpho, Camila A. Tavares, Mateus A. Gonçalves, and Teodorico C. Ramalho

(Artigo publicado na *Magnetochemistry*)

<https://doi.org/10.3390/magnetochemistry9040089>

- **Evaluation of autophagy inhibition to combat cancer: (vanadium complex)–protein interactions, parameterization, and validation of a new force field**

Taináh M. R. Santos, Camila A. Tavares, Ander F. Pereira, Elaine F. F. da Cunha and Teodorico C. Ramalho

(Artigo publicado na *Journal of Molecular Modeling*)

<https://doi.org/10.1007/s00894-023-05530-7>

- **Vanadium complex as a potential modulator of the autophagic mechanism through proteins PI3K and ULK1: development, validation and biological implications of a specific force field for  $[\text{VO}(\text{bpy})_2\text{Cl}]$**

Taináh M. R. Santos, Camila A. Tavares, Elaine F. F. da Cunha and Teodorico C. Ramalho

(Artigo submetido na *Journal of Computer-Aided Molecular Design*)

- **Parameterization and validation of a new AMBER force field for an oxovanadium (IV) complex with therapeutic potential implications in Alzheimer's Disease**

Camila A. Tavares, Taináh M. R. Santos, Elaine F. F. da Cunha, and Teodorico C. Ramalho

(Artigo submetido na *Journal of Molecular Graphics and Modelling*)

- **Enhanced Sampling in Molecular Dynamics (MD) simulations: how many MD snapshots can be needed to reproduce the biological behavior?**

Camila A. Tavares, Taináh M. R. Santos, Mateus A. Gonçalves, Elaine F. F. Cunha and Teodorico C.

Ramalho

(Artigo submetido na *Mini-Reviews in Medicinal Chemistry*)

- **Smoothing and differentiation of data by Tikhonov and fractional derivative tools, applied to surface-enhanced Raman scattering (SERS) spectra of crystal violet dye**

Nelson H. T. Lemes, Taináh M. R. Santos, Camila A. Tavares, Luciano S. Virtuoso, Kelly A. S. Souza,

and Teodorico C. Ramalho

(Artigo submetido na *Computational and Applied Mathematics*)

Trabalhos desenvolvidos no período do Mestrado:

- **Improving a Tikhonov regularization method with a fractional-order differential operator for the inverse black body radiation problem**

Taináh M. R. Santos, Camila A. Tavares, Nelson H. T. Lemes, José P. C. dos Santos, and João P. Braga

(Artigo publicado na *Inverse Problems in Science and Engineering*)

<https://doi.org/10.1080/17415977.2020.1732957>

- **Solving ill-posed problems faster using fractional-order Hopfield neural network**

Camila A. Tavares, Taináh M. R. Santos, Nelson H. T. Lemes, José P. C. dos Santos, José C. Ferreira,

and João P. Braga

(Artigo publicado na *Journal of Computational and Applied Mathematics*)

<https://doi.org/10.1016/j.cam.2020.112984>

Trabalho desenvolvido no período da Iniciação Científica (Graduação):

- **Host-guest intermolecular hydrogen bonds and stability in aqueous media: the benzaldehyde/β-CD case study**

Cleber P. A. Anconi, Taináh M. R. Santos, Amanda C. Souza, Willian M. S. Borges, and Alice L. R.

Sales

(Artigo publicado na *Journal of Inclusion Phenomena and Macrocyclic Chemistry*)

<https://doi.org/10.1007/s10847-017-0734-4>